

NASA-CR-173,829

NASA-CR-173829
19840021782

DISPLAY 01/2/1
84N29851*# ISSUE 20 PAGE 3125 CATEGORY 2
RPT#: NASA-CR-173829 NAS 1.26:173829 CNT#: NCC1-65 84/08/00 152 PAGES
UNCLASSIFIED DOCUMENT

UTTL: Implementation of uniform perturbation method for potential flow past axisymmetric and two-dimensional bodies TLSP: Progress Report, period ending 31 May 1984

AUTH: A/WONG, T. C.; B/TIWARI, S. N.

CORP: Old Dominion Univ., Norfolk, VA. CSS: (Dept. of Mechanical Engineering and Mechanics.) AVAIL.CASI

SAP: Avail: CASI HC A08/MF A02

CIO: UNITED STATES

MAJS: /*AERODYNAMIC CHARACTERISTICS/*AIRFOIL PROFILES/*AXISYMMETRIC BODIES/*
PERTURBATION THEORY/*POTENTIAL FLOW

MINS: / INTEGRAL EQUATIONS/ LINEAR EQUATIONS/ PANEL METHOD (FLUID DYNAMICS)/
PRESSURE DISTRIBUTION/ SUPERPOSITION (MATHEMATICS)

ABA: Author

ABS: The aerodynamic characteristics of potential flow past an axisymmetric slender body and a thin airfoil are calculated using a uniform perturbation analysis method. The method is based on the superposition of potentials of point singularities distributed inside the body. The strength distribution satisfies a linear integral equation by enforcing the flow tangency condition on the surface of the body. The complete

ENTER:

MOPE

LIBRARY COPY

JAN 17 1984

LANGLEY RESEARCH CENTER
LANGLEY AFB
HAMPTON, VIRGINIA

N84-29851#

ABSTRACT

IMPLEMENTATION OF UNIFORM PERTURBATION METHOD FOR POTENTIAL FLOW PAST AXISYMMETRIC AND TWO-DIMENSIONAL BODIES

Tin Chee Wong
Old Dominion University, 1984
Director: Dr. Surendra N. Tiwari
Dr. Chen-Huei Liu

The aerodynamic characteristics of potential flow past an axisymmetric slender body and a thin airfoil are calculated by using a uniform perturbation analysis method. The method is based on the superposition of potentials of point singularities distributed inside the body. The strength distribution satisfies a linear integral equation by enforcing the flow tangency condition on the surface of the body. The complete uniform asymptotic expansion of its solution is obtained with respect to the slenderness ratio by modifying and adapting an existing technique. Results calculated by the perturbation analysis method are compared with the existing surface-singularity-panel method and some available analytical solutions for a number of cases under identical conditions. From these comparisons, it is found that the perturbation analysis method can provide quite accurate results for bodies with small slenderness ratio. The present method is much simpler and requires less memory and computation time than an existing surface-singularity-panel method of comparable accuracy.

IMPLEMENTATION OF UNIFORM PERTURBATION METHOD FOR POTENTIAL
FLOW PAST AXISYMMETRIC AND TWO-DIMENSIONAL BODIES

by


Tin Chee Wong
B.S. (Mechanical Engineering) June 1982, National Taiwan
University, Taiwan, R.O.C.

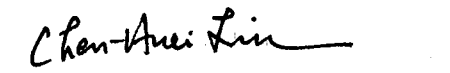
A Thesis Submitted to the Faculty of
Old Dominion University in Partial Fulfillment
of the Requirements for the Degree of

MASTER OF ENGINEERING
MECHANICAL ENGINEERING

OLD DOMINION UNIVERSITY
August 1984

Approved by:


Surendra N. Tiwari (Director)


Chen-Huei Liu (Co-Director)


John M. Kuhlman


Jeffrey J. Kelly

Acknowledgments

I am deeply indebted to the co-directors of my masters program, Dr. Chen-Huei Liu (NASA Langley Research Center) and Dr. Surendra N. Tiwari (Old Dominion University) in directing this dissertation. Thanks are also extended to Dr. John M. Kuhlman and Dr. Jeffrey J. Kelly, who served as the members of the thesis committee.

My sincere thanks are extended to Dr. James F. Geer (State University of New York, Binghamton) for offering technical assistance during the course of this research. My sincere appreciation is due to Mr. Scott O. Kjelgaard, Analytical Methods Branch at the NASA Langley Research Center for assisting in the solutions of the panel method used in this study; Mr. Richard J. Margason and his branch staff for their encouragement and support of this research.

This work was supported by the NASA Langley Research Center under Cooperative Agreement NCC1-65.

I also wish to thank Ms. Jacqueline Smith for her diligent and timely typing of the manuscript.

Last but not least, it is an honor and a privilege to extend my deepest gratitude to my parents and brother for their never-ending moral and financial support during my entire academic career.

TABLE OF CONTENTS

	PAGE
LIST OF TABLES.....	v
LIST OF FIGURES.....	vi
LIST OF SYMBOLS.....	xi
Chapter	
1. INTRODUCTION	1
2. THEORETICAL FORMULATION.....	6
2.1 Perturbation Analysis Technique	7
2.1.1 Axially Distributed Singularity Method for an Axisymmetric Body	8
2.1.2 Line Distribution of Singularities Inside a Two-dimensional Airfoil	19
2.1.3 Second Order Joukowski Airfoil	32
2.2 Other Solution Techniques	38
2.2.1 Some Exact Solutions	38
2.2.2 Panel Method	40
3. APPLICATION OF PERTURBATION METHOD	44
3.1 Perturbation Technique for Slender Bodies of Revolution.....	44
3.2 Perturbation Technique for Thin Airfoils.....	46
4. RESULTS AND DISCUSSION.....	55
4.1 Axisymmetric Bodies	55
4.2 Two-dimensional Airfoils.....	56
5. CONCLUDING REMARKS.....	115
REFERENCES.....	117

APPENDICES

A.	Determination of the Coefficients of $\alpha(\epsilon)$ and $\beta(\epsilon)$ for Axisymmetric Bodies.....	119
B.	Boundary Conditions in Complex Plane.....	123
C.	Expressions for Two-dimensional airfoils.....	125
1.	Linear Operators of the Integral Equation.....	125
2.	Determination of the Coefficients of $\alpha(\epsilon)$ and $\beta(\epsilon)$	125
D.	Elliptical Coordinate System.....	128
E.	Simplified Expressions for Axisymmetric Bodies and Two-dimensional Airfoils.....	132
1.	Axisymmetric Bodies.....	132
1.1	Ellipsoidal Body.....	132
1.2	Dumbbell Shaped Body.....	133
2.	Two-dimensional Airfoils.....	133
2.1	Elliptic Airfoil.....	133
2.2	General Joukowski Airfoil.....	134

LIST OF TABLES

TABLE	PAGE
4.1 Comparison of lift coefficients of the perturbation, panel and exact solutions for the symmetrical Joukowski airfoils.....	101
4.2 Comparison of lift coefficients of the perturbation, panel and exact solutions for the cambered Joukowski airfoils.....	114

LIST OF FIGURES

FIGURE		PAGE
2.1	Axially symmetric body immersed in a uniform stream.....	9
2.2	Uniform stream past a two-dimensional airfoil with an arbitrary angle of attack.....	20
2.3	Illustrating the derivation of an arbitrary Joukowski airfoil.....	33
2.4	Body immersed in a bounded flowfield.....	42
3.1	Ellipsoidal body geometry with $\epsilon = 0.05$	47
3.2	Dumbbell shaped body geometry with $\epsilon = 0.05$; $b = 3$	48
3.3	Elliptic airfoil of 10% thickness.....	52
3.4	Symmetrical Joukowski airfoil of 6.5% thickness.....	53
3.5	Cambered Joukowski airfoil of 6.5% thickness.....	54
4.1	Comparison of pressure distributions from the perturbation analysis method with the analytical solution for ellipsoidal body	
	(a) $\epsilon = 0.1$; ϕ expanded up to ϵ^2	59
	(b) $\epsilon = 0.1$; ϕ expanded up to ϵ^4	60
	(c) $\epsilon = 0.1$; ϕ expanded up to ϵ^6	61
4.2	Comparison of pressure distributions from the perturbation analysis method with the analytical solution for ellipsoidal body	
	(a) $\epsilon = 0.2$; ϕ expanded up to ϵ^2	62
	(b) $\epsilon = 0.2$; ϕ expanded up to ϵ^4	63
	(c) $\epsilon = 0.2$; ϕ expanded up to ϵ^6	64
4.3	Comparison of the perturbation and exact solutions with the panel method for ellipsoidal body	

	(a)	$\epsilon = 0.1$; ϕ expanded up to ϵ^6 ; 60 panels with cosine spacing.....	65
	(b)	$\epsilon = 0.1$; ϕ expanded up to ϵ^6 ; 180 panels with cosine spacing.....	66
	(c)	$\epsilon = 0.1$; ϕ expanded up to ϵ^6 ; 300 panels with cosine spacing.....	67
4.4		Pressure distributions from the perturbation analysis and the panel methods are compared with the exact solution for ellipsoidal body	
	(a)	$\epsilon = 0.05$; ϕ expanded up to ϵ^6 ; 300 panels with cosine spacing.....	68
	(b)	$\epsilon = 0.10$; ϕ expanded up to ϵ^6 ; 300 panels with cosine spacing.....	69
	(c)	$\epsilon = 0.20$; ϕ expanded up to ϵ^6 ; 300 panels with cosine spacing.....	70
	(d)	$\epsilon = 0.25$; ϕ expanded up to ϵ^6 ; 300 panels with cosine spacing.....	71
4.5		Comparison of pressure distributions from the perturbation analysis method with the panel method for dumbbell shaped body	
	(a)	$\epsilon = 0.03$; $b = 2$; ϕ expanded up to ϵ^4 ; 300 panels with cosine spacing.....	72
	(b)	$\epsilon = 0.07$; $b = 2$; ϕ expanded up to ϵ^4 ; 300 panels with cosine spacing.....	73
4.6		Comparison of pressure distributions from the perturbation analysis method with the panel method for dumbbell shaped body	
	(a)	$\epsilon = 0.03$; $b = 3$; ϕ expanded up to ϵ^4 ; 300 panels with cosine spacing.....	74
	(b)	$\epsilon = 0.07$; $b = 3$; ϕ expanded up to ϵ^4 ; 300 panels with cosine spacing.....	75
4.7		Comparison of pressure distributions from the perturbation analysis method with the exact solution for elliptic airfoil	
	(a)	$\epsilon = 0.1$; ϕ expanded up to ϵ^2 ; $t/C = 20\%$	76
	(b)	$\epsilon = 0.1$; ϕ expanded up to ϵ^3 ; $t/C = 20\%$	77

4.8	Comparison of pressure distributions from the perturbation analysis method with the exact solution for elliptic airfoil	
(a)	$\epsilon = 0.15$; ϕ expanded up to ϵ^2 ; $t/C = 30\%$	78
(b)	$\epsilon = 0.15$; ϕ expanded up to ϵ^3 ; $t/C = 30\%$	79
4.9	Comparison of pressure distributions from the perturbation analysis method with the exact solution for elliptic airfoil	
(a)	$\epsilon = 0.05$; ϕ expanded up to ϵ^3 ; $t/C = 10\%$	80
(b)	$\epsilon = 0.10$; ϕ expanded up to ϵ^3 ; $t/C = 20\%$	81
(c)	$\epsilon = 0.15$; ϕ expanded up to ϵ^3 ; $t/C = 30\%$	82
4.10	Comparison of pressure distributions from the perturbation analysis method with the panel method for symmetrical Joukowski airfoil	
(a)	$\epsilon = 0.03248$; $\gamma = 0^0$; ϕ expanded up to ϵ^2 ; $t/C = 6.5\%$; 10 panels with cosine spacing.....	83
(b)	$\epsilon = 0.03248$; $\gamma = 0^0$; ϕ expanded up to ϵ^2 ; $t/C = 6.5\%$; 30 panels with cosine spacing.....	84
(c)	$\epsilon = 0.03248$; $\gamma = 0^0$; ϕ expanded up to ϵ^2 ; $t/C = 6.5\%$; 50 panels with cosine spacing.....	85
4.11	Comparison of pressure distributions from the perturbation analysis method with the panel method for symmetrical Joukowski airfoil	
(a)	$\epsilon = 0.03248$; $\gamma = 6^0$; ϕ expanded up to ϵ^2 ; $t/C = 6.5\%$; 10 panels with cosine spacing.....	86
(b)	$\epsilon = 0.03248$; $\gamma = 6^0$; ϕ expanded up to ϵ^2 ; $t/C = 6.5\%$; 30 panels with cosine spacing.....	87
(c)	$\epsilon = 0.03248$; $\gamma = 6^0$; ϕ expanded up to ϵ^2 ; $t/C = 6.5\%$; 50 panels with cosine spacing.....	88
4.12	Comparison of pressure distributions from the perturbation analysis method with the panel method for symmetrical Joukowski airfoil	
(a)	$\epsilon = 0.01624$; $\gamma = 0^0$; ϕ expanded up to ϵ^2 ; $t/C = 3.25\%$; 50 panels with cosine spacing.....	89
(b)	$\epsilon = 0.01624$; $\gamma = 6^0$; ϕ expanded up to ϵ^2 ; $t/C = 3.25\%$; 50 panels with cosine spacing.....	90

	(c)	$\epsilon = 0.01624$; $\gamma = 12^0$; ϕ expanded up to ϵ^2 ; t/C = 3.25%; 50 panels with cosine spacing.....	91
4.13	Comparison of pressure distributions from the perturbation analysis method with the panel method for symmetrical Joukowski airfoil		
	(a)	$\epsilon = 0.03248$; $\gamma = 0^0$; ϕ expanded up to ϵ^2 ; t/C = 6.5%; 50 panels with cosine spacing.....	92
	(b)	$\epsilon = 0.03248$; $\gamma = 6^0$; ϕ expanded up to ϵ^2 ; t/C = 6.5%; 50 panels with cosine spacing.....	93
	(c)	$\epsilon = 0.03248$; $\gamma = 12^0$; ϕ expanded up to ϵ^2 ; t/C = 6.5%; 50 panels with cosine spacing.....	94
4.14	Comparison of pressure distributions from the perturbation analysis method with the panel method for symmetrical Joukowski airfoil		
	(a)	$\epsilon = 0.04872$; $\gamma = 0^0$; ϕ expanded up to ϵ^2 ; t/C = 9.75%; 50 panels with cosine spacing.....	95
	(b)	$\epsilon = 0.04872$; $\gamma = 6^0$; ϕ expanded up to ϵ^2 ; t/C = 9.75%; 50 panels with cosine spacing.....	96
	(c)	$\epsilon = 0.04872$; $\gamma = 12^0$; ϕ expanded up to ϵ^2 ; t/C = 9.75%; 50 panels with cosine spacing.....	97
4.15	Comparison of pressure distributions from the perturbation analysis method with the panel method for symmetrical Joukowski airfoil		
	(a)	$\epsilon = 0.06496$; $\gamma = 0^0$; ϕ expanded up to ϵ^2 ; t/C = 13%; 50 panels with cosine spacing.....	98
	(b)	$\epsilon = 0.06496$; $\gamma = 6^0$; ϕ expanded up to ϵ^2 ; t/C = 13%; 50 panels with cosine spacing.....	99
	(c)	$\epsilon = 0.06496$; $\gamma = 12^0$; ϕ expanded up to ϵ^2 ; t/C = 13%; 50 panels with cosine spacing.....	100
4.16	Comparison of pressure distributions from the perturbation analysis method with the panel method for cambered Joukowski airfoil		
	(a)	$\epsilon = 0.02688$; $\gamma = 0^0$; ϕ expanded up to ϵ^2 ; t/C = 3.25%; 50 panels with cosine spacing.....	102
	(b)	$\epsilon = 0.02688$; $\gamma = 6^0$; ϕ expanded up to ϵ^2 ; t/C = 3.25%; 50 panels with cosine spacing.....	103
	(c)	$\epsilon = 0.02688$; $\gamma = 12^0$; ϕ expanded up to ϵ^2 ; t/C = 3.25%; 50 panels with cosine spacing.....	104

4.17	Comparison of pressure distributions from the perturbation analysis method with the panel method for cambered Joukowski airfoil	
(a)	$\epsilon = 0.05376$; $\gamma = 0^0$; ϕ expanded up to ϵ^2 ; t/C = 6.5%; 50 panels with cosine spacing.....	105
(b)	$\epsilon = 0.05376$; $\gamma = 6^0$; ϕ expanded up to ϵ^2 ; t/C = 6.5%; 50 panels with cosine spacing.....	106
(c)	$\epsilon = 0.05376$; $\gamma = 12^0$; ϕ expanded up to ϵ^2 ; t/C = 6.5%; 50 panels with cosine spacing.....	107
4.18	Comparison of pressure distributions from the perturbation analysis method with the panel method for cambered Joukowski airfoil	
(a)	$\epsilon = 0.08064$; $\gamma = 0^0$; ϕ expanded up to ϵ^2 ; t/C = 9.75%; 50 panels with cosine spacing.....	108
(b)	$\epsilon = 0.08064$; $\gamma = 6^0$; ϕ expanded up to ϵ^2 ; t/C = 9.75%; 50 panels with cosine spacing.....	109
(c)	$\epsilon = 0.08064$; $\gamma = 12^0$; ϕ expanded up to ϵ^2 ; t/C = 9.75%; 50 panels with cosine spacing.....	110
4.19	Comparison of pressure distributions from the perturbation analysis method with the panel method for cambered Joukowski airfoil	
(a)	$\epsilon = 0.10752$; $\gamma = 0^0$; ϕ expanded up to ϵ^2 ; t/C = 13%; 50 panels with cosine spacing	111
(b)	$\epsilon = 0.10752$; $\gamma = 6^0$; ϕ expanded up to ϵ^2 ; t/C = 13%; 50 panels with cosine spacing.....	112
(c)	$\epsilon = 0.10752$; $\gamma = 12^0$; ϕ expanded up to ϵ^2 ; t/C = 13%; 50 panels with cosine spacing.....	113
D.	Two families of elliptical and hyperbolic curves with different values of ξ and η	129

LIST OF SYMBOLS

a	radius of a circle in ζ -plane; major semi-axis length of an ellipse
a_j	coefficients of a binomial expansion
A	constant determines the curvature of a camber line
b	minor semi-axis length of an ellipse; profile parameter of a dumbbell shaped body
$c_n, \tilde{c}_n, d_n, \tilde{d}_n$	coefficients of power series expansions
C	chord
C(x)	camber distribution
$C^{(n)}(x)$	nth derivative of C(x) with respect to x
$C_{\ell,ex}, C_{\ell,pn}, C_{\ell,pt}$	lift coefficients from the exact, panel and perturbation analysis methods respectively
C_p	pressure coefficient
d	diameter of an axisymmetric body
dS	differential surface area
$\bar{e}_\xi, \bar{e}_\eta, \bar{e}_\beta$	unit vectors in elliptical coordinate system
$f(x,e), f(x,\epsilon)$	singularity strength
$f_n(x), f_{mn}(x)$	functions in singularity strength expansions
G_j, L_j, L_j^P	linear operators, (p = 0,1)
(h,k)	coordinates of a point in ζ -plane
h_ξ, h_η, h_β	scale factors of the elliptical coordinate system
$I(x,\epsilon), I^P(x,\epsilon)$	integral operators, (p = 0,1)
Im [F(x)]	imaginary part of a function F(x)

k	ratio of b to a
L	body length
$L(\epsilon)$	lift force
\bar{n}	unit outward normal vector
P	pressure
P_∞	static pressure
(r, θ, x)	cylindrical coordinate system
$\text{Re} [F(x)]$	real part of a function $F(x)$
$S(x)$	thickness distribution
$S^{(n)}(x)$	n th derivative of $S(x)$ with respect to x
t	maximum thickness of an airfoil
U_s	surface velocity
U_∞	uniform free-stream velocity
V	flow velocity
(x_1, x_2, x_3)	Cartesian coordinate system
$Z(\zeta)$	transformed point in Z -plane
$\alpha(\epsilon), \beta(\epsilon)$	constants determine the extent of the singularity distribution
α_k, β_k	coefficients of expansions for $\alpha(\epsilon)$ and $\beta(\epsilon)$ respectively
Γ	strength of circulation
γ	angle of attack
δ	camber line parameter
ϵ	slenderness ratio
ϵ_1	perturbation parameter
μ	doublet strength per unit area
(ξ, η, β)	elliptical coordinate system
ρ	fluid density

σ	source strength per unit area
ϕ	velocity potential
ϕ_I	velocity potential in the imaginary internal flowfield
ϕ^b	perturbation velocity potential
ϕ^o	incident velocity potential
ψ	stream function
ψ_j	coefficients of ψ^o expansion
ψ^o	incident stream function

SUBSCRIPTS

s	boundary surface
T	trailing edge
∞	free-stream condition

Chapter 1

INTRODUCTION

In recent years, applications of powerful and sophisticated computers are being made extensively to analyze and solve important aerodynamic problems. Computer codes are now being developed to simulate the flowfield over entire aircraft configurations by considering the boundary-layer and full-potential formulations. For realistic physical applications, it would be desirable to work with the full Navier-Stokes equations. However, this requires large computer resources (memory and execution time) which makes the computational costs prohibitive for many applications. For this reason, the former method is highly desirable for solving many important aerodynamic problems. Thus, potential solutions become essential in analyzing many flow problems. Although it would be desirable to obtain potential solutions for the complete aerodynamic configurations, it is usually convenient to analyze different basic components of the system separately. In analyzing the flowfield over an airplane, it is customary to divide the entire problem into the three separate problems of fuselage, wing, and tail. Thus, separate programs are developed to analyze the flow over the fuselage, wing and tail. The analyses of axisymmetric bodies and two-dimensional airfoils are considered as the first step for fuselage and wing designs respectively. The two-dimensional airfoil results are modified usually to account for the

effect of three-dimensional wing flow.

The incompressible potential flow over axisymmetric bodies and wings is essentially governed by the Laplace equation. Although the Laplace equation is one of the simplest and well known of all partial differential equations, the number of known closed-form solutions is quite small. This is due to the non-homogeneous boundary conditions for the partial differential equation and the requirement for the body surface to be a coordinate surface of the one of the orthogonal coordinate system for which the Laplace equation can be solved by separation of variables. As a consequence, approximate solutions become more useful in practical applications. One typical example is the slender-body theory where the body boundary condition is simplified for small slenderness ratio and angle of attack. In many important fields successful approximations are found and some of these are discussed in [1]*. The present study is an application of the slender body theory.

Many previous investigators have attempted to solve the potential flow problem around a slender body. The idea of using a distribution of singularities inside the body was first treated by von Karman [2]. For the axisymmetric motion, he used a continuous distribution of sources along the axis of the given body and gave a method for computing the distribution strength. For the lateral flow past a given body he used a continuous distribution of doublets along the axis with the doublet axes normal to the body axis. It is difficult to obtain a closed-form solution for the exact problem; however, an approximate closed-form solution may be obtained, if the shape of the body satisfies certain

*The numbers in brackets indicate references.

conditions. The body should be slender and should not have any discontinuities in its surface slope. Zedan and Dalton [3,4] and Kuhlman and Shu [5,6] extended the method by dividing the singularity distribution into elements and employing piecewise linear or polynomial functions to represent the variations of the intensity of the source distribution over each line element. The effects of the order of the distribution, the number of elements, the normalization of the body coordinates, the slenderness ratio and the geometry of the profile on the performance of the method were studied in detail. It was concluded that each of these factors should be chosen appropriately in order to have accurate results.

Another approach to obtain approximate solutions to the slender-body problem is to use the perturbation method. In 1967 Handelsman and Keller [7] introduced a method to give a uniformly-valid approximate solution of axially symmetric potential flow containing a small parameter, known as slenderness ratio ϵ . The source strength distribution satisfied a linear integral equation. A uniform asymptotic solution to the integral equation was obtained. The left-hand side of the integral equation was expanded in the power series of ϵ^2 and the right-hand side in the power series of ϵ^2 and a power series in ϵ^2 multiplied by $\epsilon^2(\log \epsilon^2)$ without taking account of the dependence of the source strength on ϵ . It was assumed also that the source strength vanishes in an interval near each end of the body and that the profile curve of the body is analytic. It was possible to give a complete uniformly-valid solution to any order of approximation in this way. The method used to determine the axially symmetric potential flow about a slender body of revolution is presented in [7].

The axial singularity method can be applied to a two-dimensional airfoil in a similar manner to solve the potential flow problem. Similarly, one can have an alternative approach that will simplify the mathematical conditions of the problem and enable the construction of an approximate closed-form solution. Such an approach is called the classical thin airfoil theory. The thin airfoil theory breaks down near stagnation points and near the edges of the airfoil. This is because the assumption of small perturbation is not valid in the neighborhood of such points; the perturbation velocity is of the same order of magnitude as the undisturbed velocity. For a survey of these difficulties and the methods that are developed to relieve them one should make reference to Van Dyke [1]. The first approach is the method of matched asymptotic expansions and the second is the method of strained coordinates [8]. The method of strained coordinates has been modified by Hoogstraten [9]. However, these methods are so complicated that only the first two terms of a uniform expansion are generally obtained. Geer and Keller [10] presented the method to obtain a uniform asymptotic solution for potential flow around a thin symmetric airfoil by adopting the method of Handelsman and Keller [7]. This idea was extended and modified by Geer [11] to obtain the complete uniform asymptotic expansion for the non-symmetric airfoil. This perturbation method is presented in Chap. 2. Since the method to obtain the complete uniform asymptotic expansion for potential flow past axisymmetric and two-dimensional bodies is known, the only interest here is the assessment of the perturbation method. Such questions as: how large can the slenderness ratio be or what are the advantages and disadvantages of this method over other existing methods are addressed. In the light of these considerations, some

programs have been developed to obtain the pressure distributions for slender axisymmetric bodies and thin airfoils. In order to make comparisons, some exact solutions and solutions obtained by using an existing surface-singularity-panel method have been formulated and presented in the latter part of Chap. 2. Much effort has been devoted to obtain the expressions of the asymptotic expansions for the potential function, with the emphasis on some axisymmetric slender bodies and thin airfoils, and these are presented in Chap. 3. The pressure distributions on axisymmetric bodies and airfoils obtained by the perturbation analysis method are compared with the results generated by the panel method as well as exact solutions whenever available. These results are presented in Chap. 4. The perturbation analysis method can be applied to solve the electrostatic and magnetostatic potentials around a slender conducting body [10-13]. Recently, Homentcovschi even modified this method to solve two-dimensional elasticity problems [14].

Chapter 2

THEORETICAL FORMULATION

Basic potential flow theory is reviewed in this chapter. The problem under consideration in this study is that of the steady irrotational flow of incompressible, inviscid fluid, for which the Navier-Stokes equations can be reduced to the classical Laplace equation. Consider a body immersed in an ideal fluid and a space-fixed reference frame. Then the surface of the body is described by

$$F(x_1, x_2, x_3) = 0 \quad (2.1)$$

The variables x_1 , x_2 and x_3 are the Cartesian coordinate system used in the analysis. Because the fluid is incompressible, the continuity equation implies that the divergence of velocity must be zero

$$\nabla \cdot \bar{V} = 0 \quad (2.2)$$

Helmholtz's theorem states that the vorticity of an initially irrotational, inviscid fluid is zero. Mathematically, one has

$$\nabla \times \bar{V} = 0 \quad (2.3)$$

and it follows that

$$\bar{V} = \nabla\phi \quad (2.4)$$

Here ϕ is the velocity potential. The substitution of Eq. (2.4) into Eq. (2.2), gives the governing Laplace differential equation for incompressible potential flow, i.e.,

$$\nabla^2\phi = 0 \quad (2.5)$$

In order to solve for the potential ϕ , Eq. (2.5) should satisfy the boundary conditions

$$\nabla\phi \cdot \nabla F = 0 \quad \text{on} \quad F(x_1, x_2, x_3) = 0 \quad (2.6)$$

Also, the components of the velocity should vanish in a certain way with distance from the body as that distance tends to infinity [15]. The Bernoulli equation relating pressure and velocity is given by

$$C_p = \frac{P - P_\infty}{\frac{1}{2} \rho U_\infty^2} = 1 - \left(\frac{U_s}{U_\infty}\right)^2 \quad (2.7)$$

Once the velocity on the surface of the body, U_s , is determined, the pressure distribution can be computed through Eq. (2.7).

2.1 Perturbation Analysis Technique

A large number of perturbation techniques to obtain approximate solutions to physical potential flow problems is available in the literature [1,7-12]. In this chapter, the special perturbation

technique developed by Handelsman and Keller [7,10-12] is reviewed in detail.

2.1.1 Axially Distributed Singularity Method for Axisymmetric Body

Consider the steady state of incompressible, inviscid and irrotational fluid past an axially symmetric rigid body which is at zero angle of attack to the uniform stream, see Fig. 2.1. It is convenient to analyze the problem by introducing cylindrical coordinates (r, θ, x) with origin at the body's nose and the x -axis along its line of symmetry. The surface of the body is described by an equation $r = \epsilon R(x)$, where ϵ is the slenderness ratio, i.e., the ratio of the maximum radius of the body to its length. If one uses the length of the body as a unit of length, then the body intercepts the x -axis at $x=0$ and $x=1$. Then, the maximum value of $R(x)$ in absolute value is one. In this chapter, the slender body of revolution is considered, and ϵ is considered to be a small value.

Since it is assumed that the flow is irrotational, the velocity potential surrounding an axially symmetric body is given as

$$\phi = \phi^0 + \phi^b \quad (2.8)$$

where ϕ^0 is the potential of the incident flow while ϕ^b is the perturbation potential. The perturbation potential ϕ^b is due to the presence of the body, and this is to be determined. This is represented by a superposition of point sources distributed along the x -axis inside the body. The boundary conditions for this problem are the non-penetration (or tangent-flow) condition:

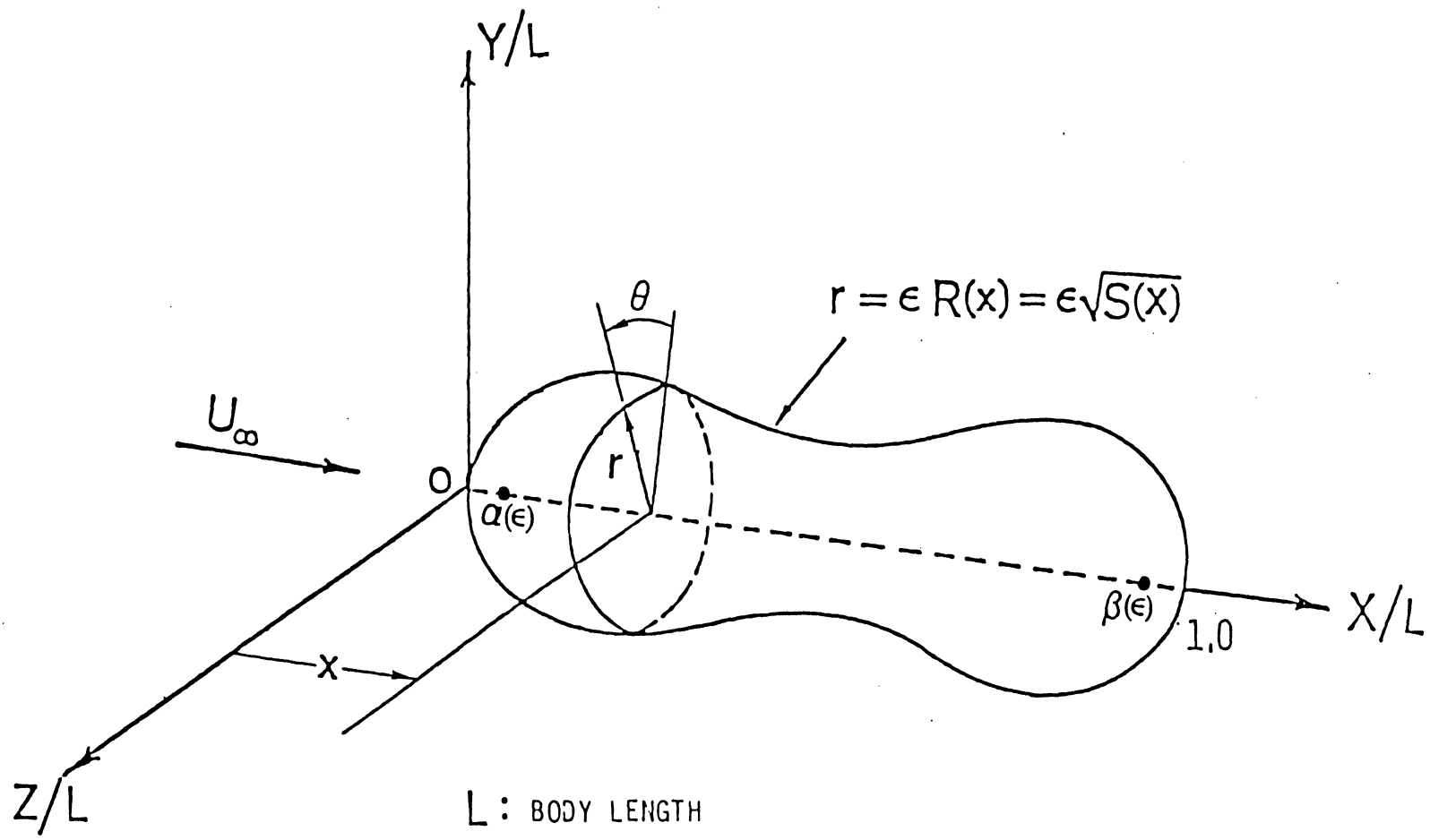


Fig. 2.1 Axially symmetric body immersed in a uniform stream.

$$\nabla\phi \cdot \bar{n} = 0 \quad \text{on} \quad r = \epsilon R(x) \quad (2.9)$$

and the infinity condition:

$$\phi^b \rightarrow 0 \quad \text{as} \quad r \rightarrow \text{infinity} \quad (2.10)$$

where \bar{n} is the unit outward normal vector to the surface of the body. Due to the axial symmetry of the flow, both ϕ^b and ϕ^0 are independent of θ and the equation of the profile curve depends on ϵ , so that ϕ^b is a function of x , r^2 and ϵ . In this study, our aim is to obtain an asymptotic expansion of ϕ^b with respect to ϵ^2 around $\epsilon = 0$. We define $S(x) = R^2(x)$ and then the cross-sectional area of the body at x is $\pi\epsilon^2 S(x)$. Assume that $S(x)$ is analytic on $0 < x < 1$, with $S(0) = 0 = S(1)$ and it can be expanded in power series about endpoints as follows:

$$S(x) = \sum_{n=1}^{\infty} c_n x^n \quad (2.11)$$

$$S(x) = \sum_{n=1}^{\infty} d_n (1-x)^n \quad (2.12)$$

where $c_n = S^{(n)}(0) / n!$ and $d_n = (-1)^n S^{(n)}(1) / n!$. It is assumed that c_1 and d_1 are non-zero, i.e., the radius of curvature at each end of the body is not zero. The perturbation potential ϕ^b is used to represent the superposition of point sources distributed along a segment of the x -axis inside the body with unknown source strength density $f(x, \epsilon)$ per

unit length [7]. Thus,

$$\phi(x, r^2; \epsilon) = \phi^0(x, r^2) - \frac{1}{4\pi} \int_{\alpha(\epsilon)}^{\beta(\epsilon)} \frac{f(\xi, \epsilon) d\xi}{[(x-\xi)^2 + r^2]^{1/2}} \quad (2.13)$$

where $\alpha(\epsilon)$ and $\beta(\epsilon)$ are constants which determine the extent of the source distribution and must be found in addition to $f(x, \epsilon)$, and they satisfy the inequalities $0 < \alpha < \beta < 1$.

The potential function ϕ can be related to stream function ψ by $\psi_x = -r\phi_r$ and $\psi_r = r\phi_x$. Thus, one can rewrite Eq. (2.13) as

$$\psi(x, r^2; \epsilon) = \psi^0(x, r^2) - \frac{1}{4\pi} \int_{\alpha(\epsilon)}^{\beta(\epsilon)} \frac{(x-\xi) f(\xi, \epsilon) d\xi}{[(x-\xi)^2 + r^2]^{1/2}} \quad (2.14)$$

The boundary condition, Eq. (2.9), implies that there is no flow of fluid through the surface of the body, i.e.,

$$\int_{\alpha(\epsilon)}^{\beta(\epsilon)} f(\xi, \epsilon) d\xi = 0 \quad (2.15)$$

Since the body is a continuation of the axial streamline for the total flow, one can obtain

$$\psi[x, \epsilon^2 S(x); \epsilon] = 0 \quad (2.16)$$

Using Eqs. (2.15) and (2.16) in Eq. (2.14), it follows that

$$\psi^0[x, \epsilon^2 S(x)] = \frac{1}{4\pi} \int_{\alpha(\epsilon)}^{\beta(\epsilon)} \frac{(x-\xi) f(\xi, \epsilon) d\xi}{[(x-\xi)^2 + \epsilon^2 S(x)]^{1/2}} \quad (2.17)$$

Equation (2.17) is a linear integral equation from which $f(\xi, \epsilon)$, $\alpha(\epsilon)$

and $\beta(\epsilon)$ need to be determined. The uniform asymptotic expansion of the solution of this equation is obtained by adopting the method of Handelsman and Keller [7]. Since the left side of Eq. (2.17) is analytic in x for $0 < x < 1$, $f(x, \epsilon)$ must be analytic in its domain of definition $\alpha < x < \beta$, and the coefficients in the expansion of $f(x, \epsilon)$ with respect to ϵ^2 are assumed to be continuous in the interval $0 < x < 1$. Both α and β are found to be power series in ϵ^2 of the form

$$\alpha(\epsilon) = \sum_{n=1}^{\infty} \alpha_n \epsilon^{2n} \quad (2.18a)$$

$$\beta(\epsilon) = 1 - \sum_{n=1}^{\infty} \beta_n \epsilon^{2n} \quad (2.18b)$$

In order to obtain an asymptotic expansion of the source strength density $f(x, \epsilon)$ of Eq. (2.17) with respect to ϵ^2 , one first expands each side of Eq. (2.17) with respect to ϵ^2 without taking account of the dependency of f on ϵ^2 . The left side can be expanded in a power series in ϵ^2 because ψ^0 is analytic in r^2 . The right side can be expanded asymptotically in powers of ϵ^2 and powers of ϵ^2 multiplied by $\log(\epsilon^2)$ with coefficients which are linear expressions in f . When both sides are expanded, Eq. (2.17) becomes

$$4\pi \sum_{j=1}^{\infty} \psi_j(x) S^j(x) \epsilon^{2j} = \int_{\alpha(\epsilon)}^x f d\xi - \int_x^{\beta(\epsilon)} f d\xi + \sum_{j=1}^{\infty} \epsilon^{2j} (L_j + \log \epsilon^2 G_j) f \quad (2.19a)$$

$$\text{where } \psi_j(x) = \frac{1}{j!} \left(\frac{\partial}{\partial r^2} \right)^j \psi^0(x, r^2) \Big|_{r^2=0} \quad (2.19b)$$

In Eq. (2.19a) L_j and G_j are linear operators defined by Eqs. (4.13)-(4.15) in [7], with ϵ replaced by ϵ^2 . Upon differentiating Eq. (2.19a) with respect to x , and by noting that

$$\frac{d}{dx} \left[\int_{\alpha}^x f d\xi - \int_x^{\beta} f d\xi \right] = 2 f(x, \epsilon) \quad (2.20)$$

there is obtained

$$4\pi \sum_{j=1}^{\infty} \frac{d}{dx} [\psi_j(x) S^j(x)] \epsilon^{2j} = 2f(x, \epsilon) + \sum_{j=1}^{\infty} \epsilon^{2j} \frac{d}{dx} (L_j + \log \epsilon^2 G_j) f \quad (2.21)$$

To solve Eq. (2.21), the asymptotic solution for f is supposed to be of the form

$$f(x, \epsilon) = \sum_{n=1}^{\infty} \sum_{m=0}^{n-1} \epsilon^{2n} (\log \epsilon^2)^m f_{nm}(x) \quad (2.22)$$

where $f_{nm}(x)$ are functions of x and must be determined by substituting Eq. (2.22) into Eq. (2.21), one obtains

$$4\pi \sum_{n=1}^{\infty} \frac{d}{dx} [\psi_n S^n(x)] \epsilon^{2n} = 2 \sum_{n=1}^{\infty} \sum_{m=0}^{n-1} \epsilon^{2n} (\log \epsilon^2)^m f_{nm}(x) + \sum_{n=1}^{\infty} \sum_{m=0}^{n-1} \sum_{j=1}^{\infty} \epsilon^{2(j+m)} (\log \epsilon^2)^m \frac{d}{dx} (L_j + \log \epsilon^2 G_j) f_{nm}(x) \quad (2.23)$$

For each n and m , the coefficients of $\epsilon^{2n}(\log \epsilon^2)^m$ on both sides of Eq. (2.23) can be obtained as follows:

$$f_{10} = 2\pi \frac{d}{dx}(\psi_1 S) \quad (2.24a)$$

$$f_{n0} = 2\pi \frac{d}{dx}(\psi_n S^n) - \frac{1}{2} \sum_{j=1}^{n-1} \frac{d}{dx}(L_j f_{n-j,0}) \quad n > 2 \quad (2.24b)$$

$$f_{1m} = 0 \quad m > 1 \quad (2.24c)$$

$$f_{nm} = -\frac{1}{2} \left[\sum_{j=1}^{n-1} \frac{d}{dx}(L_j f_{n-j,m}) + \sum_{j=1}^{n-1} \frac{d}{dx}(G_j f_{n-j,m-1}) \right] \quad n > 2, m > 1 \quad (2.24d)$$

The $f_{nm}(x)$ can be determined recursively by starting with $n=0, m=0$. Thus, once the L_j and G_j are evaluated, Eqs. (2.22)-(2.24d) will yield the desired asymptotic solution for $f(x, \epsilon)$ in terms of coefficients ψ_n . Inserting Eq. (2.22) into Eq. (2.13), the asymptotic expansion of ϕ is obtained as

$$\phi(x, r^2; \epsilon) = \phi^0(x, r^2) - \frac{1}{4\pi} \sum_{n=1}^{\infty} \sum_{m=0}^{n-1} \epsilon^{2n} (\log \epsilon^2)^m \int_{\alpha(\epsilon)}^{\beta(\epsilon)} \frac{f_{nm}(\xi) d\xi}{[(x-\xi)^2 + r^2]^{1/2}} \quad (2.25)$$

The method to obtain the asymptotic expansion with respect to ϵ about $\epsilon = 0$ of the integral operator in Eq. (2.17) is available in [7].

Let the integral operator applied to a function $F(x)$ which is independent of ϵ be

$$I(x, \epsilon) = \int_{\alpha(\epsilon)}^{\beta(\epsilon)} \frac{F(\xi)(x-\xi) d\xi}{[(x-\xi)^2 + \epsilon^2 S(x)]^{1/2}} \quad (2.26)$$

where $\alpha(\epsilon)$ and $\beta(\epsilon)$ are given in Eqs. (2.18a) and (2.18b). By adding and subtracting integrals to Eq. (2.26), one finds

$$I(x, \epsilon) = \int_{\alpha}^x F(\xi) d\xi - \int_x^{\beta} F(\xi) d\xi + \int_{\alpha}^x F(\xi) \left[\frac{(x-\xi)}{[(x-\xi)^2 + \epsilon^2 S(x)]^{1/2}} - 1 \right] d\xi \\ + \int_x^{\beta} F(\xi) \left[\frac{(x-\xi)}{[(x-\xi)^2 + \epsilon^2 S(x)]^{1/2}} + 1 \right] d\xi \quad (2.27)$$

On the right-hand side of Eq. (2.27), one sets $x-\xi=v$ and $\xi-x=v$ to the third and fourth integral respectively. Then, Eq. (2.27) becomes

$$I(x, \epsilon) = \int_{\alpha(\epsilon)}^x F(\xi) d\xi - \int_x^{\beta(\epsilon)} F(\xi) d\xi + W(x, \epsilon) + V(x, \epsilon) \quad (2.28)$$

$$\text{Here, } W(x, \epsilon) = \int_0^{x-\alpha} F(x-v) [v(v^2 + \epsilon^2 S)^{-1/2} - 1] dv \quad (2.28a)$$

$$V(x, \epsilon) = - \int_0^{\beta-x} F(x+v) [v(v^2 + \epsilon^2 S)^{-1/2} - 1] dv \quad (2.28b)$$

To find the asymptotic expansion of W and V , the binomial expansion is considered

$$v(v^2 + \epsilon^2 S)^{-1/2} - 1 = \sum_{j=1}^{\infty} \left(\frac{\epsilon^2 S}{v^2} \right)^j a_j \quad (2.28c)$$

where $a_j = (-1)^j \left(\frac{1}{2}\right) \left(\frac{3}{2}\right) \dots \left(\frac{1}{2} + j - 1\right) / j!$. This expansion is not valid throughout the domains of integration because these domains extend to $v=0$. Therefore, special treatment should be applied. To $F(x+v)$ in the integrand of Eq. (2.28b), one adds and subtracts the two leading

terms in its Taylor series at $v=0$. To $[v(v^2 + \epsilon^2 S)^{-1/2} - 1]$, one again adds and subtracts the leading terms of its binomial expansion. Thus, Eq. (2.28b) can be written as

$$\begin{aligned}
 -V(x, \epsilon) = & F(x) \int_0^{\beta-x} [v(v^2 + \epsilon^2 S)^{-1/2} - 1] dv + F'(x) \int_0^{\beta-x} v [v(v^2 + \epsilon^2 S)^{-1/2} - 1] dv \\
 & + \int_0^{\beta-x} [v(v^2 + \epsilon^2 S)^{-1/2} - \sum_{j=0}^1 a_j \left(\frac{\epsilon^2 S}{v^2}\right)^j] [F(x+v) - \sum_{j=0}^1 \frac{F^{(j)}(x) v^j}{j!}] dv \\
 & + a_1 \epsilon^2 S \int_0^{\beta-x} [F(x+v) - \sum_{j=0}^1 \frac{F^{(j)}(x) v^j}{j!}] v^{-2} dv \quad (2.29)
 \end{aligned}$$

An analysis of the order of accuracy is described in Appendix A of [7]. It shows that the first two integrals are $O(\epsilon)$ and $O(\epsilon^2 \log \epsilon^2)$, respectively. The third term is $O(\epsilon^2)$, but the fourth integral is $O(\epsilon^3)$, so that it is asymptotically negligible compared to the three terms. To obtain the asymptotic expansion of the fourth integral in Eq. (2.29), one can apply the same procedure. To the first factor of the integrand, one adds and subtracts the second term in the binomial expansion given by Eq. (2.28c). To the second factor one can add and subtract the next two terms of the Taylor expansion of $F(x+v)$ about $v=0$. In this manner, a sum of integrals is obtained; some of which can be evaluated explicitly, others can be expanded as power series in ϵ^2 , and the remaining term is asymptotically small compared to the other terms. The same procedure can be applied to the remainder, and this can be done repeatedly. Thus, $V(x, \epsilon)$ can be expressed as a series of integrals which are successively smaller in ϵ^2 as ϵ tends to zero. Furthermore, $W(x, \epsilon)$ can be treated in an exactly analogous way, so one obtains

$$\begin{aligned}
W(x, \epsilon) + V(x, \epsilon) &= \sum_{n=1}^{\infty} a_n S^n(x) \epsilon^{2n} [H_n(x, \epsilon) - \tilde{H}_n(x, \epsilon)] \\
&+ \sum_{n=1}^{\infty} \frac{F^{(2n)}(x)}{(2n)!} [P_n(x, \epsilon) - \tilde{P}_n(x, \epsilon)] \\
&- \sum_{n=0}^{\infty} \frac{F^{(2n+1)}(x)}{(2n+1)!} [K_n(x, \epsilon) + \tilde{K}_n(x, \epsilon)] \quad (2.30)
\end{aligned}$$

where, H_n , P_n , K_n are defined by

$$H_n(x, \epsilon) = \int_0^{x-\alpha} v^{-2n} \left[F(x-v) - \sum_{j=1}^{2n-1} \frac{F^{(j)}(x) v^j}{j!} \right] dv \quad (2.30a)$$

$$P_n(x, \epsilon) = \int_0^{x-\alpha} v^{2n} \left[v(v^2 + \epsilon^2 S)^{-1/2} - \sum_{j=0}^n a_j \left(\frac{\epsilon^2 S}{v^2} \right)^j \right] dv \quad (2.30b)$$

$$K_n(x, \epsilon) = \int_0^x v^{2n+1} \left[v(v^2 + \epsilon^2 S)^{-1/2} - \sum_{j=0}^n a_j \left(\frac{\epsilon^2 S}{v^2} \right)^j \right] dv \quad (a_0=1) \quad (2.30c)$$

The functions \tilde{H}_n , \tilde{P}_n , and \tilde{K}_n are defined by Eqs. (2.30a), (2.30b) and (2.30c) respectively, with $(x-\alpha)$ replaced by $(\beta-x)$. To determine the asymptotic expansion of $I(x, \epsilon)$, one must expand asymptotically the integrals Eqs. (2.30a) and (2.30b). $\tilde{H}_n(x, \epsilon)$ and $\tilde{H}_n(x, \epsilon)$ can be expanded directly as Taylor series in ϵ^2 about $\epsilon = 0$. The integrals Eqs. (2.30b) and (2.30c) have been analyzed in detail in Appendix B of [7]. Appendix A in [7] shows that $P_n = O(\epsilon^{2n+1})$, $K_n = O(\epsilon^{2n+2} \log \epsilon^2)$ and the same holds true for \tilde{P}_n and \tilde{K}_n . However, in the difference $P_n - \tilde{P}_n$, which occurs in Eq. (2.30), the odd powers of ϵ will be cancelled. By using the results of Appendix B in [7] to Eq. (2.30), one finds that $I(x, \epsilon)$ has the asymptotic expansion

$$I(x, \epsilon) = W(x, \epsilon) + V(x, \epsilon) = \sum_{j=1}^{\infty} \epsilon^{2j} [L_j + (\log \epsilon^2) G_j] F(x) \quad (2.31)$$

Here, L_j and G_j are linear operators defined by Eqs. (4.13)-(4.15) in [7], with ϵ replaced by ϵ^2 . The functions g_k , \tilde{g}_k , t_{ij} , \tilde{t}_{ij} , h_k , \tilde{h}_k in Eq. (4.14) are defined by Eqs. (B10)-(B17) in Appendix B of [7] when ϵ is replaced by ϵ^2 .

We now return to determine the coefficients α_n and β_n in the expansions of $\alpha(\epsilon)$ and $\beta(\epsilon)$, respectively. From Eq. (2.24a) it follows that $f_{10}(x)$ is analytic on $0 < x < 1$, because ψ_1 is analytic and $S(x)$ is analytic with $S(0) = 0 = S(1)$ and $S'(0) \neq 0 \neq S'(1)$. It then follows that from the recursive nature of Eqs. (2.24a)-(2.24d), the function $f_{nm}(x)$ will be analytic for $0 < x < 1$ if both $G_j F(x)$ and $L_j F(x)$ are analytic, provided that $F(x)$ is analytic. This will be true if all of these functions g_k , \tilde{g}_k , h_k , \tilde{h}_k are analytic. The functions $g_k(x)$ and $\tilde{g}_k(x)$ are defined in Appendix B of [7] as

$$g(x, \epsilon) = \sum_{k=0}^{\infty} g_k(x) \epsilon^{2k} = \{[x - \alpha(\epsilon)] + \epsilon^2 S(x)\}^{1/2} \quad (2.32a)$$

$$\tilde{g}(x, \epsilon) = \sum_{k=0}^{\infty} \tilde{g}_k(x) \epsilon^{2k} = \{[x - \beta(\epsilon)] + \epsilon^2 S(x)\}^{1/2} \quad (2.32b)$$

where $\alpha(\epsilon)$ and $\beta(\epsilon)$ are defined in Eq. (2.18a) and (2.18b) respectively. The functions $g_k(x)$ depends on the coefficients α_k in the expansion of $\alpha(\epsilon)$. They are singular at $x=0$ except for certain values of α_k , so the appropriate α_k should be chosen such that $g_k(x)$ can be regular at $x=0$. To relate $g_k(x)$ with α_k , one can square both sides of Eq. (2.32a) and equate the coefficients of the same power of ϵ . Similarly, $\tilde{g}_k(x)$ can be related to β_k at $x=1$. Detailed derivation of α_k and β_k is

available in Appendix A. Using the results Eqs. (A9) and (A17), the expressions for $\alpha(\epsilon)$ and $\beta(\epsilon)$ are given by

$$\alpha(\epsilon) = \frac{c_1}{4} \epsilon^2 - \frac{c_1 c_2}{16} \epsilon^4 + \frac{(c_1^2 c_3 + 2c_1 c_2)}{64} \epsilon^6 + O(\epsilon^8) \quad (2.33)$$

$$\beta(\epsilon) = 1 - \frac{d_1}{4} \epsilon^2 + \frac{d_1 d_2}{16} \epsilon^4 - \frac{(d_1^2 d_3 + 2d_1 d_2)}{64} \epsilon^6 + O(\epsilon^8) \quad (2.34)$$

The functions $h_k(x)$ are defined in terms of the square root of $g_k(x)$. Once the α_k are chosen appropriately to make $g_k(x)$ analytic, then it implies that $h_k(x)$ are also regular. Similarly, the $\tilde{h}_k(x)$ are also regular at $x=1$, since $\tilde{g}_k(x)$ are made analytic. Therefore, $L_j F(x)$, $G_j(x)$ and $f_{nm}(x)$ are analytic provided that $F(x)$ is analytic on $0 < x < 1$.

The asymptotic expansion of $\phi(x, r^2; \epsilon)$ can be obtained by using the appropriate $f_{nm}(x)$, $\alpha(\epsilon)$ and $\beta(\epsilon)$ which are determined by Eqs. (2.24a)-(2.24d), (2.33) and (2.34) respectively in Eq. (2.25). Once the potential of the flowfield is found, the aerodynamic properties of any given axisymmetric slender body can be evaluated.

2.1.2 Line Distribution of Singularities Inside a Two-dimensional Airfoil

In Sec. 2.1.1, the potential flow past an axially symmetric slender body has been described and the same technique can be applied to the two-dimensional airfoil. This idea was presented earlier in [10,11]. In this section, the problem will be analyzed in terms of the functions of a complex variable. Similar assumptions are made here as in Sec. 2.1.1. Consider the two-dimensional potential motion of an ideal fluid past an arbitrary airfoil which is shown in Fig. 2.2. The problem is

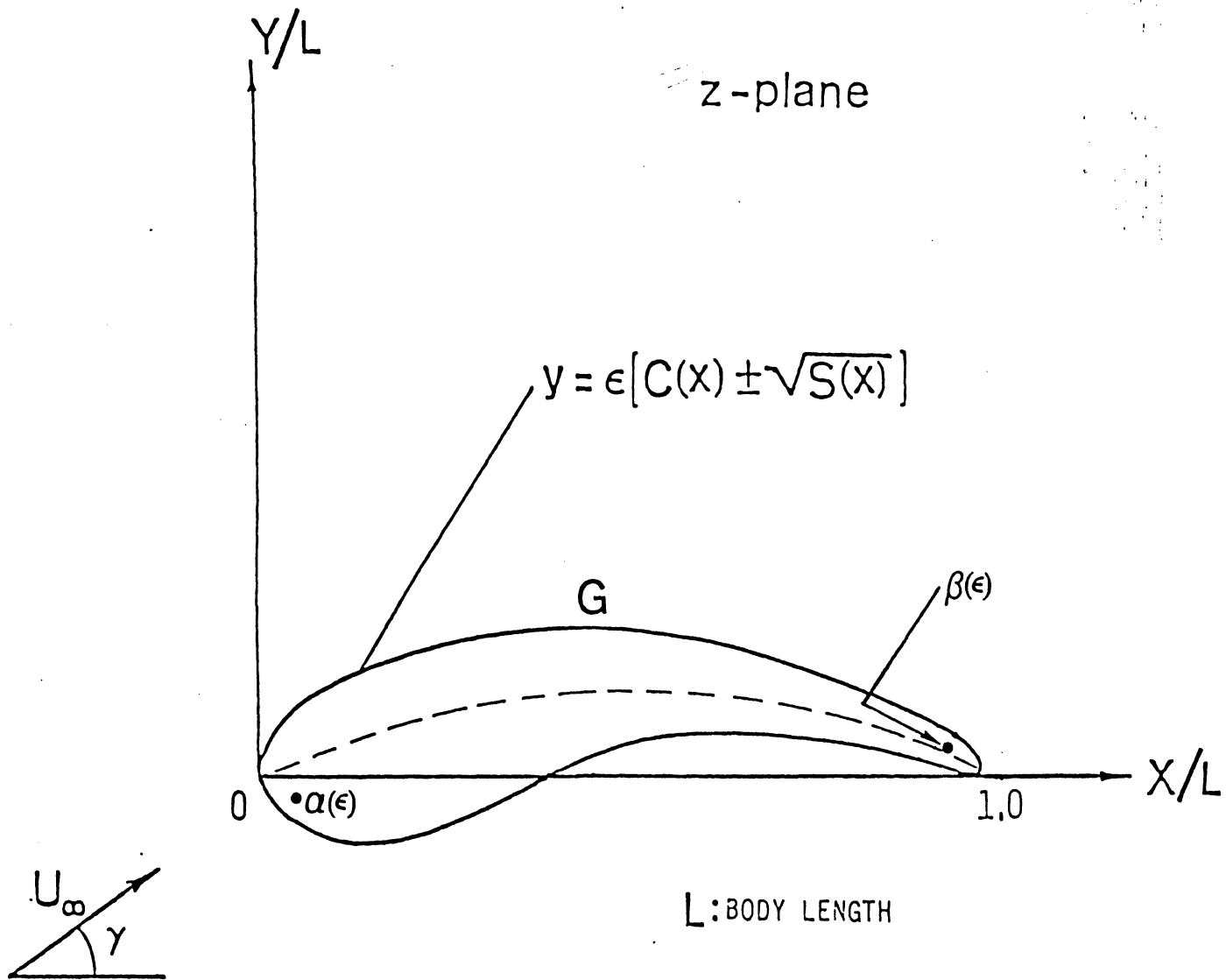


Fig. 2.2 Uniform stream past a two-dimensional airfoil with an arbitrary angle of attack.

analyzed in Cartesian coordinate (x,y) with the origin at the leading edge of the airfoil and the trailing edge is some distance intercepts on the x -axis. Now, one should recall the relationship between the potential, the stream function and the velocity components in two-dimensional motion. As before, the potential is ϕ and the stream function is ψ . The combination of ϕ and ψ into an analytic function as a complex potential $\phi(z)$, is given by

$$\phi(z) = \phi(x,y) + i\psi(x,y) \quad (2.35)$$

and the x - y plane refers to the z -plane ($z = x + iy$).

For this study, it is convenient to think of ϕ as either the real or imaginary part of a function

$$\phi(z) = \phi^0(z) + \phi^b(z) \quad (2.36)$$

which is analytic in the $z = x + iy$ plane outside the profile curve G of the airfoil. The potential ϕ^0 is the potential of the incident flow on the airfoil, while ϕ^b is due to the presence of the body. The potential ϕ^b is represented by the superposition of complex potentials of point sources and vortices distributed along an appropriate arc inside the airfoil. The boundary conditions of this problem are

no penetration condition: $\nabla\phi \cdot \bar{n} = 0$ on G

infinity condition: $\phi^b = \frac{\Gamma}{2\pi} \tan^{-1}(y/x) + O(1/r)$ as $r \rightarrow \text{infinity}$

where \bar{n} is the unit outward normal vector to the surface and Γ is the total circulation about the airfoil.

The equation of the profile G of the thin airfoil is given by $y = \epsilon[C(x) \pm \sqrt{S(x)}]$ on $0 < x < 1$, and ϵ is defined as slenderness ratio. This is assumed to be small for a thin airfoil. The leading and trailing edges intercept x -axis at $x=0$ and $x=1$ respectively, and the $\max. |C(x) \pm \sqrt{S(x)}| = 1$. It is assumed that both $C(x)$ and $S(x)$ are analytic on $0 < x < 1$, with $C(x)$ and $S(x)$ vanishing at $x=0$ and $x=1$. These functions can be expanded in a Taylor series at the endpoints as

$$C(x) = \sum_{n=1}^{\infty} c_n x^n, \quad C(x) = \sum_{n=1}^{\infty} \tilde{c}_n (1-x)^n$$

$$S(x) = \sum_{n=1}^{\infty} d_n x^n, \quad S(x) = \sum_{n=1}^{\infty} \tilde{d}_n (1-x)^n \quad (2.37)$$

where $c_n = \frac{C^{(n)}(0)}{n!}$, $\tilde{c}_n = \frac{(-1)^n C^{(n)}(1)}{n!}$

$$d_n = \frac{S^{(n)}(0)}{n!}, \quad \tilde{d}_n = \frac{(-1)^n S^{(n)}(1)}{n!} \quad (2.38)$$

with $d_1 \neq 0 \neq \tilde{d}_1$.

In order to solve for ϕ , it is convenient to find a function, Eq. (2.35), which is analytic in $z = x + iy$ outside G and satisfies the condition

$$\operatorname{Re} \left\{ [i - \epsilon(C' \pm S')] / 2 \sqrt{S} \right\} \frac{d\phi}{dz} = 0 \quad \text{on } G \quad (2.39)$$

Equation (2.39) is verified and explained in Appendix B. Here, ϕ^b represents the superposition of the potential due to point sources and vortices distributed along an arc inside the slender airfoil. Thus,

$$\phi^b(z) = -\frac{1}{2\pi} \int_{\alpha(\epsilon)}^{\beta(\epsilon)} \ln(z-\xi) \tilde{f}(\xi, \epsilon) d\xi \quad (2.40)$$

where $\tilde{f}(\xi, \epsilon)$ is the unknown source strength density, which is a complex expression. The constants $\alpha(\epsilon)$ and $\beta(\epsilon)$ determine the extent of the source distribution and they can be determined after $\tilde{f}(\xi, \epsilon)$ is found and they must be inside G.

Using Eqs. (2.39) and (2.40) in Eq. (2.36), one obtains

$$\begin{aligned} & \text{Re} \{ [i - \epsilon(C' \pm S'/2\sqrt{S})] \frac{d\phi^0}{dz} [x + i\epsilon(C \pm \sqrt{S})] \} \\ &= \text{Re} \left\{ \frac{1}{2\pi} [i - \epsilon(C' \pm S'/2\sqrt{S})] \int_{\alpha}^{\beta} \frac{\tilde{f}(\xi, \epsilon) d\xi}{x + i\epsilon(C \pm \sqrt{S}) - \xi} \right\} \end{aligned} \quad (2.41)$$

Equation (2.41) is a pair of equations, corresponding to where the upper (plus sign) and lower (minus sign) surfaces of G, is obtained. By adding and subtracting these two equations, a pair of coupled linear integral equations can be obtained. Upon denoting $x + i\epsilon(C + \sqrt{S})$ and $x + i\epsilon(C - \sqrt{S})$ by x_{pu} and x_{pl} respectively, one has

$$\begin{aligned} & 2\pi \text{Re} \{ i(1 + i\epsilon C') \left[\frac{d\phi^0(x_{pu})}{dz} + \frac{d\phi^0(x_{pl})}{dz} \right] - \frac{\epsilon S'}{2\sqrt{S}} \left[\frac{d\phi^0(x_{pu})}{dz} - \frac{d\phi^0(x_{pl})}{dz} \right] \} \\ &= \text{Re} \left\{ i \int_{\alpha}^{\beta} \frac{2(x + i\epsilon C - \xi)(1 + i\epsilon C') + \epsilon^2 S'}{(x + i\epsilon C - \xi)^2 + \epsilon^2 S} \tilde{f}(\xi, \epsilon) d\xi \right\} \end{aligned} \quad (2.42)$$

and

$$2\pi \operatorname{Re} \{ i(1+i\epsilon C') \sqrt{S} \left[\frac{d\phi^0(xp_u)}{dz} - \frac{d\phi^0(xp_l)}{dz} \right] - \frac{\epsilon}{2} S' \left[\frac{d\phi^0(xp_u)}{dz} + \frac{d\phi^0(xp_l)}{dz} \right] \}$$

$$= \operatorname{Re} \left\{ \epsilon \int_{\alpha}^{\beta} \frac{2S(1+i\epsilon C') - S'(x+i\epsilon C-\xi)}{(x+i\epsilon C-\xi)^2 + \epsilon^2 S} \tilde{f}(\xi, \epsilon) d\xi \right\} \quad (2.43)$$

In Eq. (2.42) and (2.43), $\tilde{f}(\xi, \epsilon)$, $\alpha(\epsilon)$ and $\beta(\epsilon)$ need to be determined.

Both $\alpha(\epsilon)$ and $\beta(\epsilon)$ are found to be power series in ϵ of the form [11]

$$\alpha(\epsilon) = \sum_{n=1}^{\infty} \alpha_n \epsilon^n, \quad \beta(\epsilon) = 1 - \sum_{n=1}^{\infty} \beta_n \epsilon^n \quad (2.44)$$

Using the results of [10] as an instructive example, the function

$\tilde{f}(x, \epsilon)$ shall be of the form

$$\tilde{f}(x, \epsilon) = \frac{f(x, \epsilon)}{\sqrt{[\beta(\epsilon) - x][x - \alpha(\epsilon)]}} \quad (2.45)$$

where $\tilde{f}(x, \epsilon)$ is singular in x at $x = \alpha(\epsilon)$ and $x = \beta(\epsilon)$. The function $\tilde{f}(x, \epsilon)$ is assumed to be analytic before finding its asymptotic expansion about $\epsilon = 0$. Following the procedures given in [10,11], both sides of Eqs. (2.42) and (2.43) can be expanded with respect to ϵ , without taking account of the dependency of f on ϵ . Since ϕ^0 is an analytic function of $x + i\epsilon[C(x) \pm \sqrt{S(x)}]$, the left-hand sides of Eqs. (2.42) and (2.43) can be expanded in a power series in ϵ . Then, Eqs. (2.42) and (2.43) become

$$\sum_{j=0}^{\infty} \epsilon^j J_j(x) = \operatorname{Re} \left\{ i \sum_{j=0}^{\infty} \epsilon^j L_j^0 [f(x, \epsilon)] \right\} \quad (2.46)$$

$$\sum_{j=0}^{\infty} \epsilon^j K_j(x) = \text{Re} \left\{ \sum_{j=0}^{\infty} \epsilon^j L_j^1 [f(x, \epsilon)] \right\} \quad (2.47)$$

Here, $J_j(x)$ and $K_j(x)$ are defined as

$$\begin{aligned} J_j(x) = 2\pi \text{Re} \left\{ 2i \phi_j(x) \sum_{k=0}^{[j/2]} \binom{j}{2k} c^{j-2k}(x) s^k(x) \right. \\ \left. - \phi_{j-1}(x) \left[2c'(x) \sum_{k=0}^{[(j-1)/2]} \binom{j-1}{2k} c^{j-1-2k}(x) s^k(x) \right. \right. \\ \left. \left. + s'(x) \sum_{k=0}^{[(j-2)/2]} \binom{j-1}{2k+1} c^{j-2k-1}(x) s^k(x) \right] \right\} \quad (2.48a) \end{aligned}$$

$$\begin{aligned} K_j(x) = 2\pi \text{Re} \left\{ 2i \phi_j(x) \sum_{k=0}^{[(j-1)/2]} \binom{j}{2k+1} c^{j-2k-1}(x) s^{k+1}(x) \right. \\ \left. - \phi_{j-1}(x) \left[2c'(x) \sum_{k=0}^{[(j-2)/2]} \binom{j-1}{2k} c^{j-2k-2}(x) s^{k+1}(x) \right. \right. \\ \left. \left. + s'(x) \sum_{k=0}^{[(j-1)/2]} \binom{j-1}{2k} c^{j-1-2k}(x) s^k(x) \right] \right\} \quad (2.48b) \end{aligned}$$

$$\text{where } \phi_j(x) = \binom{j}{j!} \left\{ \left(\frac{d}{dz} \right)^{j+1} \phi^0(z) \right\}_{z=x} \quad (2.48c)$$

In Eqs. (2.48a) and (2.48b), the notation $\binom{n}{j} = n!/(j!(n-j)!)$ has been used and $[n]$ is the greatest integer not exceeding n . Applying the same idea of expanding integral operators asymptotically as in Sec. 2.1.1, one can expand the right sides of (2.42) and (2.43). To do this, consider the integral operators $I^p(x, \epsilon)$, $p=0,1$ applied to a function $F(z)/[(\beta-z)(z-\alpha)]^{1/2}$ and $F(z)$ is independent of ϵ . The integral operators I^p are defined as

$$I^0(x, \epsilon) = \int_{\alpha}^{\beta} \frac{2[x+i\epsilon C(x)-z][1+i\epsilon C'(x)] + \epsilon^2 S'(x) F(z)}{\{[x+i\epsilon C(x)-z]^2 + \epsilon^2 S(x)\} \sqrt{(\beta-z)(z-\alpha)}} dz \quad (2.49a)$$

$$I^1(x, \epsilon) = \epsilon \int_{\alpha}^{\beta} \frac{2S(x)[1+i\epsilon C'(x)] - S'(x)[x+i\epsilon C(x)-\zeta] F(\zeta)}{\{[x+i\epsilon C(x)-\zeta]^2 + \epsilon^2 S(x)\} \sqrt{(\beta - \zeta)(\zeta - \alpha)}} d\zeta \quad (2.49b)$$

The constants $\alpha(\epsilon)$ and $\beta(\epsilon)$ are defined in Eq. (2.44), where the coefficients α_n and β_n need to be determined. The operator $I^P(x, \epsilon)$ can be expanded by following the similar method as given in [7] and by using the results derived in [11], one obtains

$$I^P(x, \epsilon) = \sum_{q=0}^{\infty} \epsilon^q L_q^P[F(x)] \quad (2.50)$$

The linear operators L_q^P , $p = 0, 1$ are defined in Appendix C. From the definitions given in Appendix C, one has two simple operators

$$L_0^0 [F(x)] = -4 \int_0^{\frac{\pi}{2}} (\sin^2 \theta - x)^{-1} [F(\sin^2 \theta) - F(x)] d\theta \quad (2.51)$$

$$L_0^1 [F(x)] = 2\pi \sqrt{\frac{S(x)}{x(1-x)}} F(x) \quad (2.52)$$

To solve Eqs. (2.46) and (2.47), an asymptotic solution for $f(x, \epsilon)$ is assumed as

$$f(x, \epsilon) = \sum_{n=0}^{\infty} f_n(x) \epsilon^n \quad (2.53)$$

Here, the functions $f_n(x)$ are to be determined. By substituting Eq. (2.53) into Eqs. (2.46) and (2.47), one obtains

$$\sum_{j=0}^{\infty} \epsilon^j J_j(x) = \text{Re} \left[i \sum_{j=0}^{\infty} \sum_{n=0}^{\infty} \epsilon^{j+n} L_j^0 [f_n(x)] \right] \quad (2.54)$$

$$\sum_{j=0}^{\infty} \epsilon^j K_j(x) = \operatorname{Re} \left[\sum_{j=0}^{\infty} \sum_{n=0}^{\infty} \epsilon^{j+n} L_j^1 [f_n(x)] \right] \quad (2.55)$$

By equating coefficients of the like powers of ϵ in the corresponding equations, Eqs. (2.54) and (2.55), finds

$$\operatorname{Im} \{L_0^1 [f_n(x)]\} = -J_n(x) - \operatorname{Im} \left[\sum_{j=1}^n L_j^0 [f_{n-j}(x)] \right] \quad (2.56)$$

$$\operatorname{Re} \{L_0^1 [f_n(x)]\} = K_n(x) - \operatorname{Re} \left[\sum_{j=1}^n L_j^1 [f_{n-j}(x)] \right] \quad (2.57)$$

Using the results of Eqs.(2.51) and (2.52), one finds that

$$\begin{aligned} \operatorname{Im} \{L_0^0 [f_n(x)]\} &= \operatorname{Im} \{L_0^0 [f_n(x)]\} = L_0^0 [\operatorname{Im} f_n(x)] \\ &= -4 \int_0^{\frac{\pi}{2}} \frac{\operatorname{Im} [f_n(\sin^2 \theta)] - \operatorname{Im} [f_n(x)]}{(\sin^2 \theta - x)} d\theta \end{aligned} \quad (2.58)$$

$$\operatorname{Re} \{L_0^1 [f_n(x)]\} = 2\pi \sqrt{\frac{S(x)}{x(1-x)}} \operatorname{Re} [f_n(x)] \quad (2.59)$$

Applying the results of inversion of operators in [10] with Eqs. (2.58) and (2.59) in Eqs. (2.56) and (2.57) respectively, one has

$$\operatorname{Im} f_n(x) = \tilde{f}_n(x) + \operatorname{Im} f_n(0) \quad (2.60)$$

where

$$\tilde{f}_n(x) = \frac{x}{2\pi} \left\{ J_n(x) + \operatorname{Im} \sum_{j=1}^n L_j^0 [f_{n-j}(x)] \right\}$$

$$-\frac{x}{\pi^2} \int_0^{\frac{\pi}{2}} \frac{\cos^2 \theta}{(\sin^2 \theta - x)} \left[J_n(\xi) + \text{Im} \sum_{j=1}^n L_j^0 [f_{n-j}(\xi)] \right]_{\xi=x}^{\xi=\sin^2 \theta} d\theta \quad (2.61)$$

and

$$\text{Re } f_n(x) = \frac{1}{2\pi} \sqrt{\frac{x(1-x)}{S(x)}} \left\{ K_n(x) - \text{Re} \sum_{j=1}^n L_j^1 [f_{n-j}(x)] \right\} \quad n > 0 \quad (2.62)$$

In Eq. (2.61), the notation $[G(\xi)]_{\xi=b}^{\xi=a} = G(a) - G(b)$. From Eqs. (2.61) and (2.62), the function $f_n(x)$ can be determined recursively, once the constants $\text{Im } f_n(0)$ are found. In order to determine $\text{Im } f_n(0)$, one has to use the condition that

$$\text{Im} \int_{\alpha}^{\beta} f(\xi, \epsilon) d\xi = \Gamma$$

where

$$\Gamma = \sum_{j=0}^{\infty} \Gamma_j \epsilon^j \quad (2.63)$$

Here, each Γ_j is a prescribed constant independent of ϵ . By using Eqs. (2.45), (2.53) and Eq. (2.61) in Eq. (2.63) can be expressed as

$$\Gamma = \sum_{j=0}^{\infty} \epsilon^j \int_{\alpha}^{\beta} \frac{\tilde{f}_j(\zeta) d\zeta}{\sqrt{(\beta - \zeta)(\zeta - \alpha)}} + \pi \sum_{j=0}^{\infty} \epsilon^j \text{Im } f_j(0) \quad (2.64)$$

By setting $\zeta = (\beta - \alpha) \sin^2 \theta + \alpha$ and expanding each integrand in Eq. (2.64) in Taylor series about $\epsilon = 0$, one obtains

$$\begin{aligned} \Gamma &= 2 \sum_{j=0}^{\infty} \epsilon^j \text{Im} \sum_{n=0}^j \frac{1}{n!} \int_0^{\frac{\pi}{2}} \left\{ \left(\frac{\partial}{\partial \epsilon} \right)^n i f_{j-n} [(\beta - \alpha) \sin^2 \theta + \alpha] \right\}_{\epsilon=0} d\theta \\ &+ \pi \sum_{j=0}^{\infty} \text{Im } f_j(0) \end{aligned} \quad (2.65)$$

Equating coefficients of like powers of ϵ on each side of Eq. (2.63) and (2.65), yields

$$\text{Im } f_n(0) = \frac{\Gamma_n}{\pi} - \frac{2}{\pi} \sum_{k=0}^n \frac{1}{k!} \int_0^{\frac{\pi}{2}} \left\{ \left(\frac{\partial}{\partial \epsilon} \right)^k \tilde{f}_{n-k} [(\beta - \alpha) \sin^2 \theta + \alpha] \right\}_{\epsilon=0} d\theta \quad (2.66)$$

Since $\tilde{f}_0(x)$ depends only on $J_0(x)$, the $\text{Im } f_n(0)$ can be determined recursively from Eq. (2.66). Thus, functions $f_n(x)$ can be found through Eqs. (2.61), (2.62) and (2.66) in a recursive manner.

Determination of the constants $\alpha(\epsilon)$ and $\beta(\epsilon)$ is discussed now. From Eqs. (2.61) and (2.62), one knows that $\text{Re } f_0(x)$ and $\text{Im } f_0(x)$ depend on $\phi^0(z)$ which is analytic. Thus, it follows from the recursive nature of Eqs. (2.61), (2.62) and (2.66) that all the $\text{Re } f_0(x)$ and $\text{Im } f_0(x)$ must be analytic for $0 < x < 1$ if the $L_q^p[F(x)]$ is analytic. This will be true if and only if each $g_j(x)$ and $h_j(x)$ in Eqs. (C2) and (C3) is analytic on the interval $0 < x < 1$. In the manner of Appendix A, one can determine α_k uniquely by demanding that $g(x, \epsilon)$ is regular at $x=0$. Similarly, all of the β_k can be determined by requiring that the function $h(x, \epsilon)$ is regular at $x=1$. By squaring both sides of Eqs. (C2) and (C3) and equating the coefficients of the same power in ϵ , one can find out all the appropriate α_k and β_k , such that singularities at $x=0$ and $x=1$ of functions $g_j(x)$ and $h_j(x)$ are eliminated. The similar technique for the determination of $\alpha(\epsilon)$ and $\beta(\epsilon)$ is given in Appendix A, and the general expressions for α_k and β_k are available in Appendix C. Using the results in Appendix C and the definitions of Eqs. (2.37) and (2.38), the leading terms for $\alpha(\epsilon)$ and $\beta(\epsilon)$ are given by

$$\alpha(\epsilon) = \frac{d_1}{4} \epsilon^2 - i \frac{c_1 d_1}{4} \epsilon^3 - \frac{d_1(d_2 + 4c_1^2)}{16} \epsilon^4 + O(\epsilon^5) \quad (2.67)$$

$$\beta(\epsilon) = 1 - \frac{\tilde{d}_1}{4} \epsilon^2 - i \frac{\tilde{c}_1 \tilde{d}_1}{4} \epsilon^3 + \frac{\tilde{d}_1 (\tilde{d}_2 + 4\tilde{c}_1^2)}{16} \epsilon^4 + O(\epsilon^5) \quad (2.68)$$

Once $f(x, \epsilon)$ has been obtained, the expression for $\phi(z)$ is obtained by using Eqs. (2.45), (2.53) in (2.40) and (2.36) is given by

$$\phi(z, \epsilon) = \phi^0(z) - \frac{1}{2\pi} \sum_{k=0}^{\infty} \epsilon^k \int_{\alpha(\epsilon)}^{\beta(\epsilon)} \frac{\ln(z-\zeta) f_k(\zeta) d\zeta}{\sqrt{[\beta(\epsilon) - \zeta][\zeta - \alpha(\epsilon)]}} \quad (2.69)$$

Equation (2.69) is the desired uniform asymptotic expansion for ϕ .

Suppose now that the thin airfoil has a sharp trailing edge such that near $x=1$, $S(x)$ has the expansion

$$S(x) = \sum_{j=2n+1}^{\infty} \tilde{d}_j (1-x)^j, \quad \tilde{d}_{2n+1} \neq 0 \quad n > 1 \quad (2.70)$$

where $\tilde{d}_j = (-1)^j S^{(j)}(1)/j$. From Eq. (2.70), it follows that one can take $\beta(\epsilon)=1$, the asymptotic expansion obtained above remains valid when Eq. (2.70) holds. The mathematical proof is available in Sec. 7 of [10,11]. Physically, the velocity of the fluid near the sharp trailing edge should be finite. As the velocity of the fluid with the potential given by Eq. (2.69) near the trailing edge is examined, the first term in Eq. (2.69), $\phi^0(z)$ obviously gives a finite velocity at the trailing edge, because $\phi^0(z)$ is analytic at $z=1$. The remaining terms in Eq. (2.69) contribute velocity components of the form

$$\int_{\alpha(\epsilon)}^1 \frac{1}{z - \zeta} \frac{F(\zeta)}{\sqrt{[\zeta - \alpha(\epsilon)](1-\zeta)}} d\zeta \quad (2.70a)$$

Equation (2.70a) remains bounded as $z \rightarrow 1$, if and only if $F(1)=0$.

Therefore, one shall make each $f_k(x)$, $k > 0$ vanishes at $x=1$ by properly choosing the arbitrary constants of $\text{Im } f_k(0)$. The mathematical proof of choosing $\text{Im } f_k(0)$, so that each $f_k(x)$, $k > 0$ vanishes at $x=1$, is shown in Sec. 7 of [10], i.e.,

$$\text{Im } f_{k+1}(0) = -f_{k+1}(1) \quad (2.71)$$

If the flow described by ϕ^0 is a uniform stream, the circulation can be determined by Eq. (2.65), such that the lift $L(\epsilon)$ of the airfoil is given by

$$L(\epsilon) = \rho U_\infty \Gamma(\epsilon) \quad (2.72)$$

where ρ is the density of the fluid and U_∞ is the speed of the uniform stream at infinity. By using Eqs. (2.65) and (2.71), one finds that Eq. (2.72) becomes

$$L(\epsilon) = \rho U_\infty \sum_{j=0}^{\infty} \epsilon^j 2 \text{Im} \sum_{k=0}^j \frac{1}{k!} \int_0^{\frac{\pi}{2}} \left\{ \left(\frac{\partial}{\partial \epsilon} \right)^k i \tilde{f}_{j-k} [(\beta - \alpha) \sin^2 \theta + \alpha] \right\}_{\epsilon=0} d\theta - \pi \tilde{f}_j(1) \quad (2.73)$$

The uniform asymptotic expansion for $\phi(z; \epsilon)$ can be determined by finding $f_n(x)$, $\alpha(\epsilon)$, and $\beta(\epsilon)$. Then, the velocity, pressure distributions on the surface, and also the lift coefficient of an arbitrary airfoil can be determined.

2.1.3 Second Order Joukowski Airfoil

Certain assumptions have been made in analyzing the problem in Sec. 2.1.2. The upper and lower surface of the thin airfoil have the equations $y = \epsilon[C(x)+\sqrt{S(x)}]$ and $y = \epsilon[C(x)-\sqrt{S(x)}]$ for $0 < x < 1$; with $C(0)=S(0)=C(1)=S(1)=0$. The equations of the thickness and the camber line of the airfoil are $y = \epsilon\sqrt{S(x)}$ and $y = \epsilon C(x)$, respectively. Here ϵ is the slenderness ratio, while $S(x)$ and $C(x)$ give the thickness and camber distributions. Varying ϵ produces a family of affinely related profiles. More examples are given by Van Dyke in [1]. Now one expects to seek an expression for a thin Joukowski airfoil by using the perturbation method. The parametric form of the Joukowski airfoil is easily obtained by means of conformal mapping [15]. One employs a transformation $x(\xi,\eta)$, $y(\xi,\eta)$, where the ξ - η plane refers to as the ζ -plane which will map the region and its boundaries in the ζ -plane into another desired configuration in the x - y plane, which is referred to as the z -plane. Fig. 2.3 shows the notation of the Joukowski transformation of a circle into an airfoil. The center of the circle with radius a at any arbitrary point is given by $\mu = m e^{i\delta}$. The symbol μ_0 denotes the intersection of the vector $a e^{-i\beta}$ with the y -axis. A circle with center at μ_0 and radius of magnitude $|\mu_0 - \zeta_T|$ transforms into a circular arc, which is considered as the skeleton of the airfoil. The arbitrary circle, the points of which are described by

$$\zeta = a e^{i\theta} + \mu \quad (2.74)$$

transforms into an airfoil. The angle β determines the mean curvature

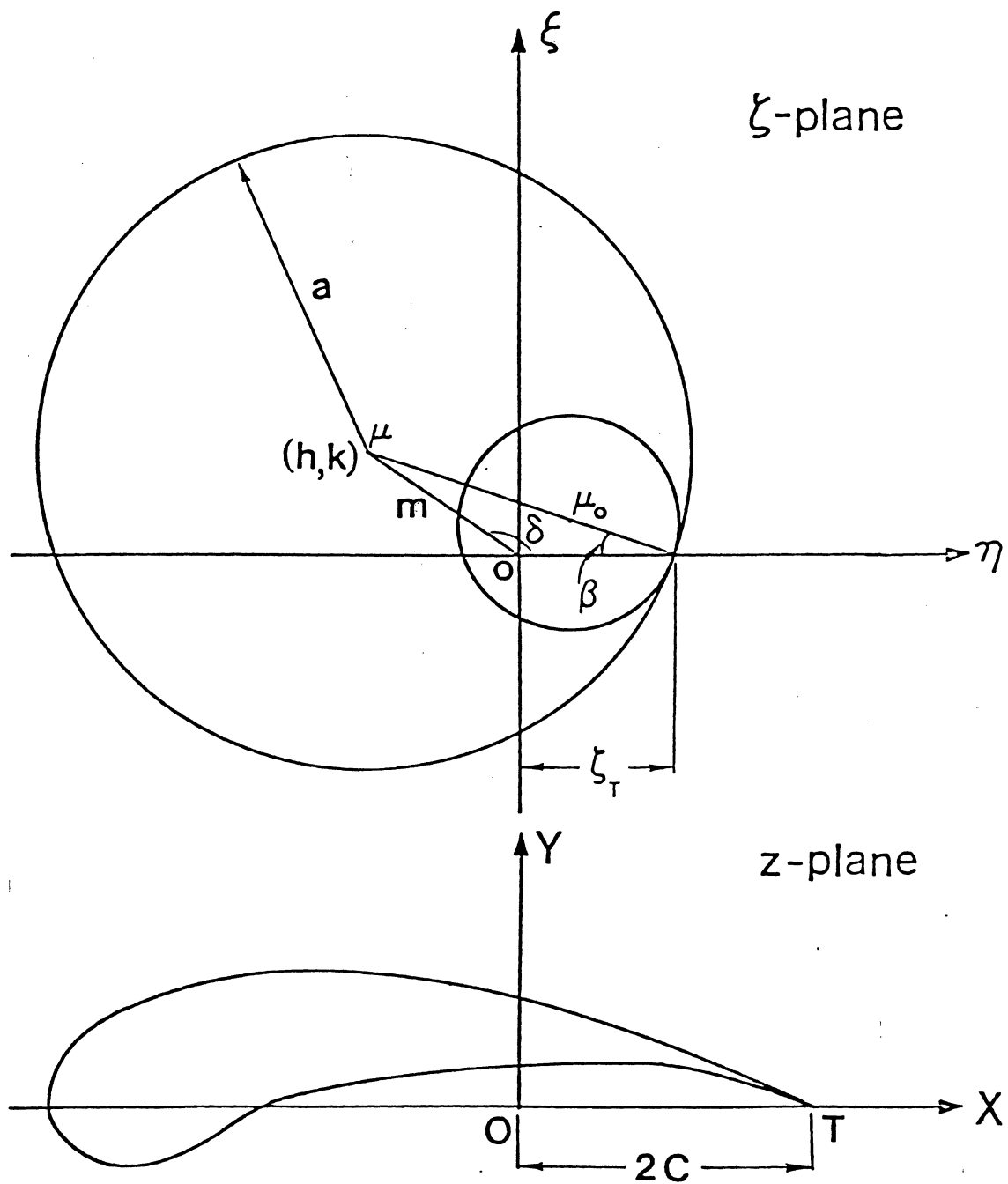


Fig. 2.3 Illustrating the derivation of an arbitrary Joukowski airfoil.

of the profile and the magnitude $|\mu - \mu_0|$ determines the thickness of the profile.

The circle is chosen such that it passes through $z = z_T = C$, where C is real positive number. The corresponding point on the airfoil is given by

$$Z(\zeta) = \zeta + \frac{C^2}{\zeta} \quad (2.75)$$

It should recall that the center μ of the circle, its radius a , and the angle β are connected by

$$C = a e^{-i\beta} + m e^{i\delta} \quad (2.76)$$

Since C is a real positive number, one can separate the real and imaginary parts of Eq. (2.76) as follows:

$$C = a \cos\beta + m \cos\delta \quad (2.77a)$$

$$a \sin\beta = m \sin\delta \quad (2.77b)$$

Using Eq. (2.74) in Eq. (2.75), with the expressions given by Eqs. (2.77a) and (2.77b), $Z(\zeta)$ can be separated into real and imaginary parts as x and y respectively. After further simplification, the parametric form of the airfoil is obtained as follows:

$$x = a(\cos\theta + h) \left[1 + \frac{C^2}{a^2(1 + h^2 + k^2 + 2h \cos\theta + 2k \sin\theta)} \right] \quad (2.78a)$$

$$y = a(\sin\theta + k) \left[1 - \frac{c^2}{a^2(1 + h^2 + k^2 + 2h \cos\theta + 2k \sin\theta)} \right] \quad (2.78b)$$

$$\text{where } h = (m/a) \cos\delta \quad , \quad k = (m/a) \sin\delta \quad (2.79)$$

The trailing-edge point of the airfoil is denoted by Z_T with $\theta = -\beta$ in Eq. (2.75), one finds $x = \text{Re}(Z_T) = 2C$ and $y = \text{Im}(Z_T) = 0$. Thus, the trailing edge of the airfoil intercepts the x-axis at the point T with $OT=2C$. In order to have an asymptotic expression for a thin Joukowski airfoil a small parametric, ϵ_1 should be introduced to expand the available equations in power series. Generally the quantities h , k , β , and m should be small. If we choose $m=\epsilon_1 C$, then Eqs. (2.77a), (2.77b) and (2.79) can be expanded to the second order of accuracy as follows:

$$a = \frac{C}{\cos\beta} (1 - \epsilon_1 \cos\delta) \quad (2.80a)$$

$$h = (\cos\beta \cos\delta) \epsilon_1 + O(\epsilon_1^2) \quad (2.80b)$$

$$k = (\cos\beta \sin\delta) \epsilon_1 + O(\epsilon_1^2) \quad (2.80c)$$

Using Eqs. (2.80a)-(2.80c) in Eqs. (2.78a) and (2.78b), and retaining the terms with order of ϵ_1 , one obtains

$$x = \frac{C}{\cos\beta} \{ \cos\theta(1 + \cos^2\beta) + \epsilon_1 [-\cos\delta(\cos\theta + \cos\beta)(1 + \cos^2\beta) \\ + 2 \cos^2\beta \cos\theta(\cos\delta - \cos\beta \cos\delta \cos\theta - \cos\beta \sin\delta \sin\theta)] \}$$

$$+ 0(\epsilon_1^2) \quad (2.81a)$$

$$y = C \sin \theta \cos \delta \epsilon_1 \left[2 \cos^2 \beta \cos \theta - \left(\cos \beta + \frac{1}{\cos \beta} \right) \right] \\ + C \sin \theta \frac{\sin^2 \beta}{\cos \beta} + C \epsilon_1 \sin \delta [\sin^2 \beta + 2 \sin^2 \theta \cos^2 \beta] + 0(\epsilon_1^2) \quad (2.81b)$$

By examining carefully the order of magnitude of $\sin \beta$, $\cos \beta$, $\sin^2 \beta$ and $\cos^2 \beta$, one finds that both $\cos \beta$ and $\cos^2 \beta$ are $O(1)$ and $\sin \beta$ and $\sin^2 \beta$ are $O(\epsilon_1)$ and $O(\epsilon_1^2)$ respectively. Neglecting the terms of $O(\epsilon_1)$, Eq. (2.81a) can be further simplified as

$$x = 2C \cos \theta + 0(\epsilon_1) \quad (2.82)$$

Furthermore, Eq. (2.81b) can be simplified by comparing the order of magnitude of $\sin \beta$, $\sin^2 \beta$, $\cos \beta$ and $\cos^2 \beta$ as mentioned. To retain terms of $O(\epsilon_1)$, Eq. (2.81b) becomes

$$y = 2C \epsilon_1 \cos \delta \sin \theta (\cos \theta - 1) + 2C \epsilon_1 \sin \delta \sin^2 \theta + 0(\epsilon_1^2) \quad (2.83)$$

Introducing the nondimensional quantities $\tilde{x} = x/2C$, and $\tilde{y} = y/2C$, Eqs. (2.82) and (2.83) become

$$\tilde{x} = \cos \theta + 0(\epsilon_1) \quad (2.84a)$$

$$\tilde{y} = \epsilon_1 \cos \delta \sin \theta (\cos \theta - 1) + \epsilon_1 \sin \delta \sin^2 \theta + 0(\epsilon_1^2) \quad (2.84b)$$

Upon eliminating $\sin \theta$ and $\cos \theta$ in terms of \tilde{x} , Eq. (2.84b) becomes

$$\begin{aligned} \tilde{y} = & \epsilon_1(-\cos\delta)(1 - \tilde{x}) \sqrt{1 - \tilde{x}^2} + \epsilon_1 \sin\delta(1 - \tilde{x}^2) \\ & + O(\epsilon_1^2) \end{aligned} \quad -1 < x < 1 \quad (2.85)$$

Obviously, if $\delta = \pi$, Eq. (2.85) will yield a symmetrical second order Joukowski airfoil, while the second term vanishes. It is consistent to the second order Joukowski airfoil shown in Sec. 4.6 of [1]. It also implies that the second term represents the equation of the camber line. Therefore, Eq. (2.85) can be rewritten as

$$y = \tilde{y}_s + \tilde{y}_c \quad (2.86)$$

where $\tilde{y}_s = \epsilon_1(-\cos\delta)(1 - \tilde{x}) \sqrt{1 - \tilde{x}^2}$ and $\tilde{y}_c = \epsilon_1 \sin\delta(1 - \tilde{x}^2)$.

To make Eq. (2.86) consistent with the required form of equation, simple translation and scaling of the coordinates are done, such that Eq.

(2.86) becomes

$$y_s = 2(-\cos\delta) \epsilon_1 \sqrt{x(1-x)^3} \quad (2.87b)$$

$$y_c = 2 \sin\delta \epsilon_1 x(1-x) \quad 0 < x < 1 \quad (2.87b)$$

By defining $\epsilon = 2(-\cos\delta)\epsilon_1$, with ϵ is the slenderness ratio, Eq. (2.87b)

yields $y_s = \epsilon \sqrt{S(x)}$ and $y_c = \epsilon C(x)$

where

$$S(x) = x(1-x)^3 \quad (2.88a)$$

$$C(x) = Ax(1 - x) \quad , \quad A = -\tan\delta \quad (2.88b)$$

$S(x)$ and $C(x)$ give the thickness and camber distributions of an airfoil respectively, and A is related to the airfoil camber.

2.2 Other Solution Techniques

2.2.1 Some Exact Solutions

The analytical solutions of potential flow problems associated with the motion of a solid body through an ideal fluid are considered here. The final aim is to determine the pressure distribution over the surface of the body and the lift force acting on the body whenever available. The analytical solution for ellipsoidal body of revolution and two-dimensional elliptic airfoil are obtained in this section.

1. Analytical Solution for Ellipsoidal Body in Uniform Stream

Consider a rigid ellipsoidal body moving through a uniform ideal fluid. The flow is assumed to be steady, incompressible and irrotational. To simplify the problem, a body-fixed reference frame and elliptical coordinate system (ξ, η, β) are introduced. The derivation is described in Appendix D. Using the results of Eq. (D5a), one is able to obtain $\bar{U} = U_\xi \bar{e}_\xi + U_\eta \bar{e}_\eta$ where $U_\xi = \frac{1}{h_\eta h_\beta} \frac{\partial \psi}{\partial \eta}$ and $U_\eta = -\frac{1}{h_\xi h_\beta} \frac{\partial \psi}{\partial \xi}$. Here, U_ξ and U_η are velocity components in ξ and η directions respectively, and

$$\frac{\partial^2 \psi}{\partial \xi^2} + \frac{\partial^2 \psi}{\partial \eta^2} - \coth \xi \frac{\partial \psi}{\partial \xi} - \cot \eta \frac{\partial \psi}{\partial \eta} = 0 \quad (2.89)$$

Consider the Neumann boundary condition on $\xi = \xi_0$ and the infinity

condition as ξ tend to infinity. Making reference to Appendix D, the boundary conditions can be simplified as follows:

$$\psi(\xi, \eta) = C' \quad \text{on } \xi = \xi_0 \quad (2.90a)$$

$$\psi(\xi, \eta) \rightarrow \frac{U_\infty A^2}{2} \sinh^2 \xi \sin^2 \eta + C'' \quad \text{as } \xi \rightarrow \text{infinity} \quad (2.90b)$$

Equation (2.89) along with Eqs. (2.90a)-(2.90b) can be solved by separation of variables. One finds out that the velocity component in \bar{e}_ξ direction on the body surface is zero (due to the no penetration on the surface of the body), and the velocity in \bar{e}_η direction is given by

$$U_s = \frac{U_\infty \sin \eta}{\left[\cosh \xi_0 + \sinh^2 \xi_0 \ln \left(\frac{\cosh \xi_0 - 1}{\sinh \xi_0} \right) \right] \sqrt{\cosh^2 \xi_0 - \cos^2 \eta}} \quad (2.91)$$

With application of Bernoulli equation, the pressure distribution on the surface of the ellipsoidal body is given by

$$C_p = 1 - \left(\frac{U_s}{U_\infty} \right)^2 \quad (2.92)$$

2. Analytical Solution for Elliptic Airfoil in Uniform Stream

In Sec. 2.1.3 the idea of conformal mapping has been introduced to get the shape of an airfoil. Here, the pressure distribution over the airfoil, by means of Joukowski transformation is discussed. This method can be used directly to the actual problem of by means of mapping the flow past an arbitrary circle, for which the solution is already known. To define the arbitrary circle, we describe the points by

$$\zeta = r_0 e^{i\theta} \quad (2.93)$$

where $r_0 = (a+b)/2$ with a and b are the major and minor semi-axis lengths of the ellipse respectively. Making reference to [15], the complex velocity on the airfoil surface is given by

$$W(z) = \frac{i 2U_\infty \sin\theta e^{-i\theta}}{\frac{dz}{d\zeta}} \quad (2.94)$$

where $dz/d\zeta = 1 - C^2/\zeta^2$ and $C = (\sqrt{a^2 - b^2})/2$. After simplification, the velocity distribution along the contour of the ellipse is given by

$$\frac{U_s(x)}{U_\infty} = \frac{(1+k)(a^2 - x^2)^{1/2}}{[a^2 + x^2(k^2 - 1)]^{1/2}} \quad (2.95)$$

where $k = b/a$. The pressure distribution on the elliptic airfoil can be computed through the Bernoulli equation.

2.2.2 Panel Method

A considerable number of panel methods has been developed in the past two decades to analyze the steady, inviscid and irrotational flow fields past a body of arbitrary geometry. The incompressible flowfield is governed by the Laplace equation which can be transformed to an integral equation relating the perturbation potential to the source and doublet singularities distributed over the surface. There are different discretization techniques among panel methods for solving the integral equation. Basically, all the methods approximate the surface by elemental panels of prescribed geometric shape and singularity variation

and the integral equation is solved by enforcing a boundary condition at a control point or points on the panel. There is a summarized table in [16], showing several useful panel methods with panel geometry, singularity variation and boundary condition specification. In this section the governing equation and the basic idea of discretization are reviewed.

Consider steady, inviscid, irrotational and incompressible fluid flow in a bounded domain D , Fig. 2.4, governed by the Laplace equation

$$\nabla^2 \phi = 0 \quad (2.96)$$

where $\bar{V} = \bar{U}_\infty + \nabla\phi$. The perturbation potential $\phi(P)$ at any point P can be expressed as the potential induced by a combination of source (σ), and doublet (μ) singularities distribution over a bounded surface S

$$\phi(P) = \iint_S \sigma \left(-\frac{1}{4\pi r}\right) dS + \iint_S \mu \frac{\partial}{\partial n} \left(\frac{1}{4\pi r}\right) dS \quad (2.97)$$

where r is the distance from the point P to the bounded surface and \bar{n} represents the normal to the surface S directed into the fluid domain. The boundary condition in this study is the flow tangency condition or

$$\bar{V} \cdot \bar{n} = 0 \quad (2.98)$$

Since there are two unknowns σ and μ , while there is one boundary condition, there exists an infinite number of source and doublet combinations which satisfy Eq. (2.97) and one can specify the doublet

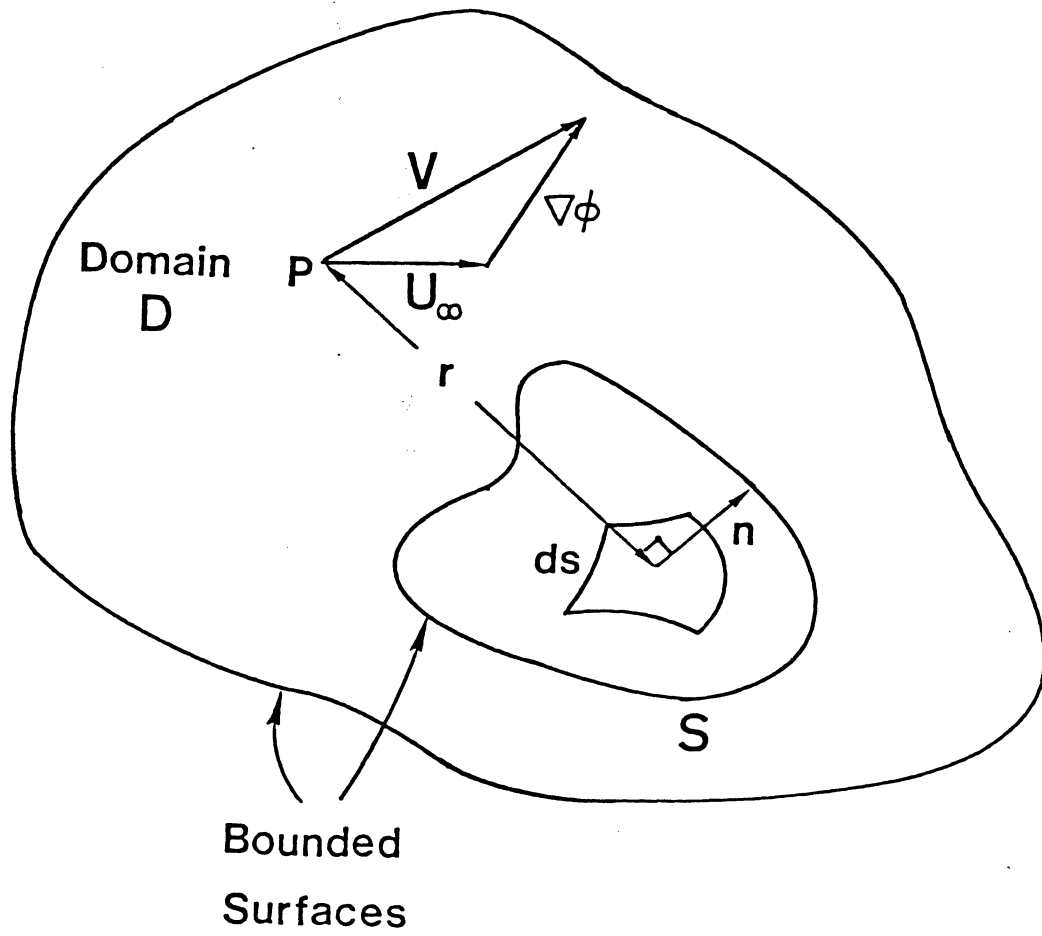


Fig. 2.4 Body immersed in a bounded flowfield.

strength and solve for the source strength or vice-versa. Using the idea of real external and imaginary internal fields introduced in [17], the condition for the perturbation potential interior to the region is constant and set equal to zero, i.e.,

$$\phi_I = 0 \quad \text{or} \quad \phi = \mu \quad (2.99)$$

Thus, it follows that

$$\sigma = \nabla\phi \cdot \bar{n} \quad (2.100)$$

For Neumann problems, the source density distribution is given by Eq. (2.100), the doublet distribution is to be determined. For Dirichlet problems, the doublet distribution is known from the prescribed potential on the boundaries, and the source distribution is to be determined.

In order to introduce lift, wake networks extending from the trailing edge to downstream infinity are considered. As the free stream Reynolds number increases, the thickness of the wake region diminishes and is often assumed to be zero. Since fluid properties are continuous across the wake, the wake region is usually modelled as a stream surface having zero pressure loading imposed by the surrounding flow. The wakes can be represented by a doublet sheet with zero thickness and streamwise doublet gradient, emanating from the trailing edge and parallel to the free stream. Determination of the strength of the wake constitutes the Kutta condition which is available in [16]. Some typical numerical schemes were already presented in the literature [16-21].

Chapter 3

APPLICATION OF PERTURBATION METHOD

3.1 Perturbation Technique for Slender Bodies of Revolution

The formulations of Sec. 2.1.1 are applied to the case of a uniform ideal fluid flow past an axisymmetric slender body. The coordinate system is fixed to the body and the velocity of the stream at infinity is U_∞ . The incident stream function is given by

$$\psi^0(x, r^2) = U_\infty r^2 / 2 \quad (3.1)$$

The stream function ψ^0 can be expanded in powers of ϵ^2 and the coefficients $\psi_j(x)$ can be obtained by using Eq. (3.1) in Eq. (2.19b); this yields

$$\psi_1(x) = U_\infty / 2, \quad \psi_j(x) = 0 \quad \text{for } j > 2 \quad (3.2)$$

By inserting these coefficients into Eqs. (2.24a) - (2.24d) together with the definition of operators L_j and G_j , the first six leading terms of $f_{nm}(x)$ are given as follows:

$$f_{10}(x) = \pi U_\infty S' \quad (3.3a)$$

$$f_{20}(x) = -\frac{1}{2} \frac{d}{dx} (L_1 f_{10})$$

$$\begin{aligned}
&= -\frac{\pi}{4} U_{\infty} \frac{d}{dx} \left\{ \frac{SS'}{x} - \frac{SS'}{1-x} - SS'' + S''S \log \left[\frac{4x(1-x)}{S(x)} \right] \right. \\
&+ S \int_0^{1-x} [S'(x+v) - S'(x) - vS''(x)] v^{-2} dv \\
&\left. - S \int_0^x [S'(x-v) - S'(x) + vS''(x)] v^{-2} dv \right\} \quad (3.3b)
\end{aligned}$$

$$f_{21}(x) = -\frac{1}{2} \frac{d}{dx} (G_1 f_{10}) = \frac{\pi}{4} U_{\infty} \frac{d}{dx} (SS'') \quad (3.3c)$$

$$f_{30}(x) = 0 \quad (3.3d)$$

$$\begin{aligned}
f_{31}(x) &= -\frac{1}{2} \frac{d}{dx} (L_1 F_{21} + G_2 f_{10} + G_2 f_{20}) \\
&= \frac{1}{4} \left(\frac{d}{dx} (S f'_{20}) - \frac{1}{8} \frac{d}{dx} (S^2 f''_{10}) \right) \\
&- \frac{d}{dx} [f'_{21} \{ S \log \left[\frac{4x(1-x)}{S} \right] - S \} + \left(\frac{S}{x} - \frac{S}{1-x} \right) f_{21}] \\
&+ S \int_0^x [f_{21}(x-v) - f_{21}(x) + v f'_{21}(x)] v^{-2} dv \\
&- S \int_0^{1-x} [f_{21}(x+v) - f_{21}(x) - v f'_{21}(x)] v^{-2} dv \quad (3.3e)
\end{aligned}$$

$$f_{32}(x) = -\frac{1}{2} \frac{d}{dx} (G_1 f_{21}) = \frac{\pi}{16} U_{\infty} \frac{d}{dx} \left[S \frac{d^2}{dx^2} (SS''') \right] \quad (3.3f)$$

Equations (3.3a) - (3.3f), together with (2.18a) and (2.18b) depend upon the profile curve. The expressions for $f_{nm}(x)$, $\alpha(\varepsilon)$ and $\beta(\varepsilon)$ can be evaluated if $S(x)$ is specified. The complete asymptotic expansion for $\phi(x, r^2; \varepsilon)$ can be obtained from Eq. (2.25) with $\phi^0 = U_{\infty} x$. The flow

velocity components over the body surface can be determined by taking appropriate derivatives of ϕ . Next the Bernoulli equation is used and the pressure coefficient on the body surface is evaluated as

$$C_p = 1 - \left(\frac{U_s}{U_\infty}\right)^2 \quad (3.4)$$

where U_s is the velocity distribution on the surface of the body. The profile curve is defined by $r = \epsilon \sqrt{S(x)}$ on $0 < x < 1$.

In this study, two different axisymmetric bodies are analyzed, and their profiles are given as follows:

1. Ellipsoidal Body

$$S(x) = 4x(1 - x)$$

2. Dumbbell Shaped Body

$$S(x) = 4bx(1 - x)[1 - bx(1 - x)] \quad , \quad b > 2$$

With the profile shape $r = \epsilon \sqrt{S(x)}$ on $0 < x < 1$ mentioned, one can obtain explicit expressions for $f_{nm}(x)$, $\alpha(\epsilon)$ and $\beta(\epsilon)$ from Eqs. (3.3a)-(3.3f), (2.18a) and (2.18b) respectively for each of the above two cases (Figs. 3.1 and 3.2). Lists of the required expressions are presented in Appendix E.

3.2 Perturbation Technique for Thin Airfoils

The formulation given in Sec. 2.1.2 is applied to the flow problem when the airfoil is at rest in an ideal fluid which has unit velocity at infinity. The airfoil is at an arbitrary angle of attack γ to the x -axis. Thus, the complex potential for the incident stream is given by

$$\phi^0(z) = e^{-i\gamma} z \quad (3.5)$$

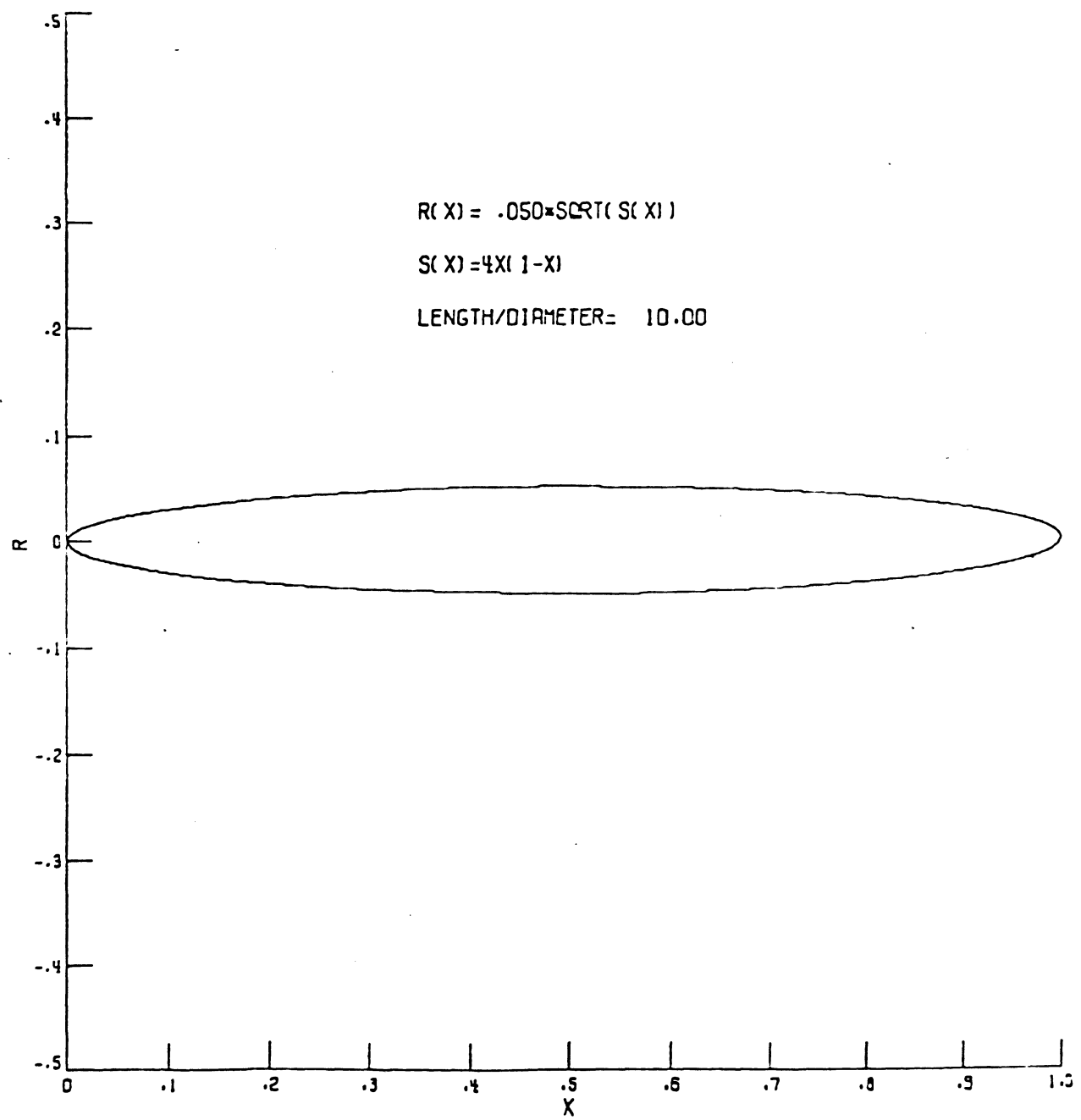


Fig. 3.1 Ellipsoidal body geometry with $\epsilon = 0.05$

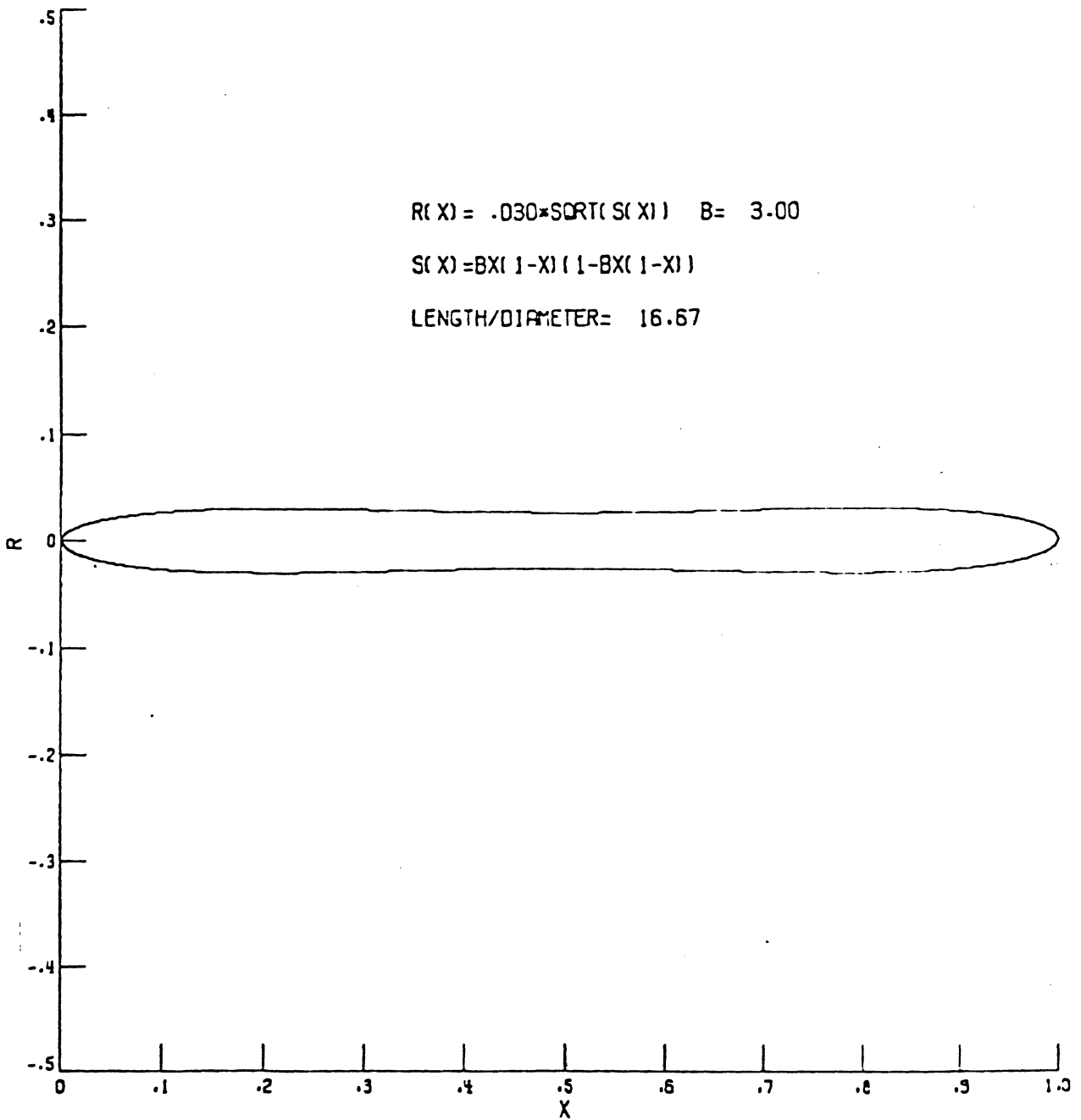


Fig. 3.2 Dumbbell shaped body geometry with $\epsilon = 0.03$, $b = 3$

Introducing Eq. (3.5) in Eq. (2.48c), one obtains

$$\phi_j(x) = \begin{cases} e^{-i\gamma} & \text{if } j = 0 \\ 0 & \text{if } j > 1 \end{cases} \quad (3.6)$$

Using Eq. (3.6) in Eqs. (2.48a) and (2.48b) yields

$$\begin{aligned} J_0(x) &= 4\pi \sin\gamma \\ J_1(x) &= -4\pi C'(x) \cos\gamma \\ J_j(x) &= 0 & \text{if } j > 2 \\ K_1(x) &= -2\pi S'(x) \cos\gamma \\ K_j(x) &= 0 & \text{if } j = 0, 2, \dots \end{aligned} \quad (3.7)$$

The functions $f_n(x)$ are obtained by inserting these coefficients together with the expressions in Appendix C defining the operator L_j^P , into Eqs. (2.61) and (2.62). The three leading terms $f_n(x)$ are computed as follows:

$$\text{Re } f_0(x) = 0 \quad (3.8a)$$

$$\tilde{f}_0(x) = 2x \sin\gamma \quad (3.8b)$$

$$\text{Im } f_0(x) = \frac{\Gamma_0}{\pi} - \sin\gamma \quad (3.8c)$$

$$\text{Re } f_1(x) = -\frac{1}{2\pi} \left[\sqrt{\frac{x(1-x)}{S(x)}} 2\pi S' \cos\gamma + \text{Re } L_1^1 [f_0(x)] \right] \quad (3.9a)$$

$$\tilde{f}_1(x) = \frac{x}{2\pi} \left\{ \text{Im } L_1^0 [f_0(x)] - 4\pi C'(x) \cos\gamma \right\} \quad (3.9b)$$

$$\begin{aligned}
& -\frac{x}{\pi^2} \int_0^{\frac{\pi}{2}} \frac{\cos^2 \theta}{\sin^2 \theta - x} \left[\text{Im } L_1^0 [f_0(\xi)] - 4\pi C'(\xi) \cos \gamma \right]_{\xi=x}^{\xi=\sin^2 \theta} d\theta \\
\text{Im } f_1(0) &= \frac{\Gamma_1}{\pi} - \frac{2}{\pi} \int_0^{\frac{\pi}{2}} \tilde{f}_1(\sin^2 \theta) d\theta \quad (3.9c)
\end{aligned}$$

$$\text{Re } f_2(x) = -\frac{1}{2\pi} \sqrt{\frac{x(1-x)}{S(x)}} \left[\text{Re } L_1^1 [f_1(x)] + \text{Re } L_2^1 [f_0(x)] \right] \quad (3.10a)$$

$$\tilde{f}_2(x) = \frac{x}{2\pi} \left\{ \text{Im } L_1^0 [f_1(x)] + \text{Im } L_2^0 [f_0(x)] \right\} \quad (3.10b)$$

$$\begin{aligned}
& -\frac{x}{\pi^2} \int_0^{\frac{\pi}{2}} \frac{\cos^2 \theta}{\sin^2 \theta - x} \left[\text{Im } L_1^0 [f_1(\xi)] + \text{Im } L_2^0 [f_0(\xi)] \right]_{\xi=x}^{\xi=\sin^2 \theta} d\theta \\
\text{Im } f_2(0) &= \frac{\Gamma_2}{\pi} - \frac{2}{\pi} \int_0^{\frac{\pi}{2}} [f_2(\sin^2 \theta) + 2 \sin \gamma (\alpha_2 \cos^2 \theta - \beta_2 \sin^2 \theta)] d\theta \quad (3.10c)
\end{aligned}$$

The operators L_1^0 , L_1^1 , L_2^0 , and L_2^1 are given in Appendix C. When Eqs. (3.8a)-(3.10c) are used in Eqs. (2.53) and (2.45) they give the asymptotic expansion for $f(x, \epsilon)$ up to $O(\epsilon^3)$. Once $f(x, \epsilon)$ has been found, one can obtain an expression of $\phi(z; \epsilon)$ by using Eq. (2.69) and the pressure coefficient can be evaluated from Eq. (3.4). Since Eqs. (3.8a)-(3.10c), (2.67) and (2.68) are functions of $S(x)$ and $C(x)$, once they are specified, the complete expansion for $\phi(z; \epsilon)$ up to $O(\epsilon^3)$ can be determined.

In this study, elliptic airfoils and second order Joukowski airfoils have been analyzed using the above method. For a symmetric airfoil the function $C(x)$ is set to zero; only the thickness solution has to be solved. If the airfoil is symmetric and is set at zero angle of attack, then there is no circulation about the airfoil and all Γ_n are set equal to zero in determining the constants $\text{Im } f_n(0)$. Moreover, if

the airfoil has a sharp trailing edge, special treatment is applied to obtain each Γ_n , which is given in Eq. (2.71). The profile curve of the thin airfoil is defined by $y = \epsilon[C(x) \pm S(x)]$ on $0 < x < 1$, with small slenderness ratio ϵ . Three different airfoils are used as test cases, Figs. 3.3, 3.4 and 3.5, and their geometries are as follows:

1. Elliptic Airfoil

$$S(x) = 4x(1 - x)$$

2. Symmetrical Second Order Joukowski Airfoil

$$S(x) = x(1 - x)^3$$

3. Cambered Second Order Joukowski Airfoil

$$C(x) = Ax(1 - x)$$

$$S(x) = x(1 - x)^3$$

Here, A is related to the airfoil camber and is defined in Eq.

(2.88b). Using the above information, expressions for

$f_n(x)$, Γ_n , $\alpha(\epsilon)$ and $\beta(\epsilon)$ can be derived in each case. A brief derivation and the lists of the resulting expressions are included in Appendix E.

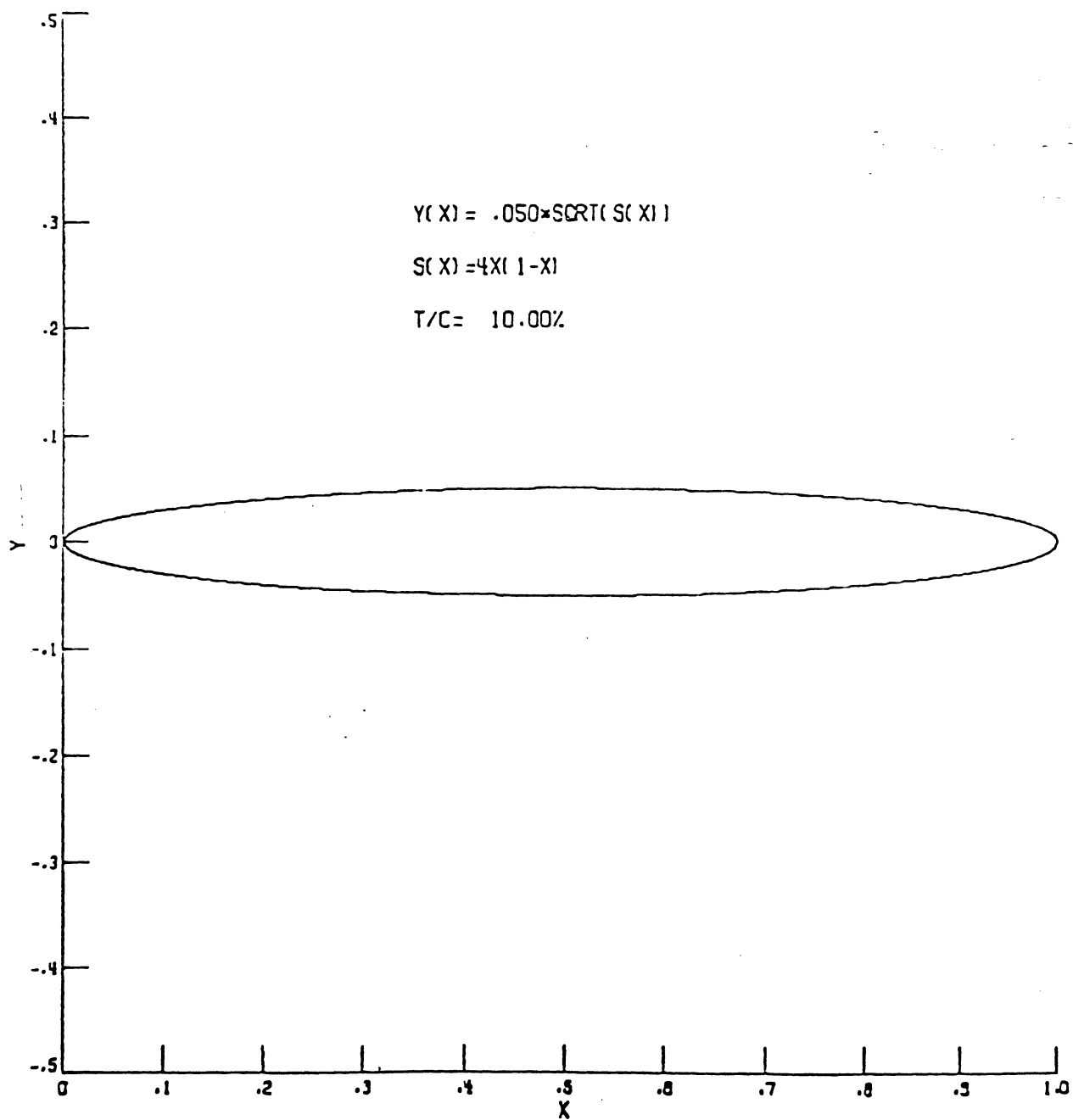


Fig. 3.3 Elliptic airfoil of 10% thickness.

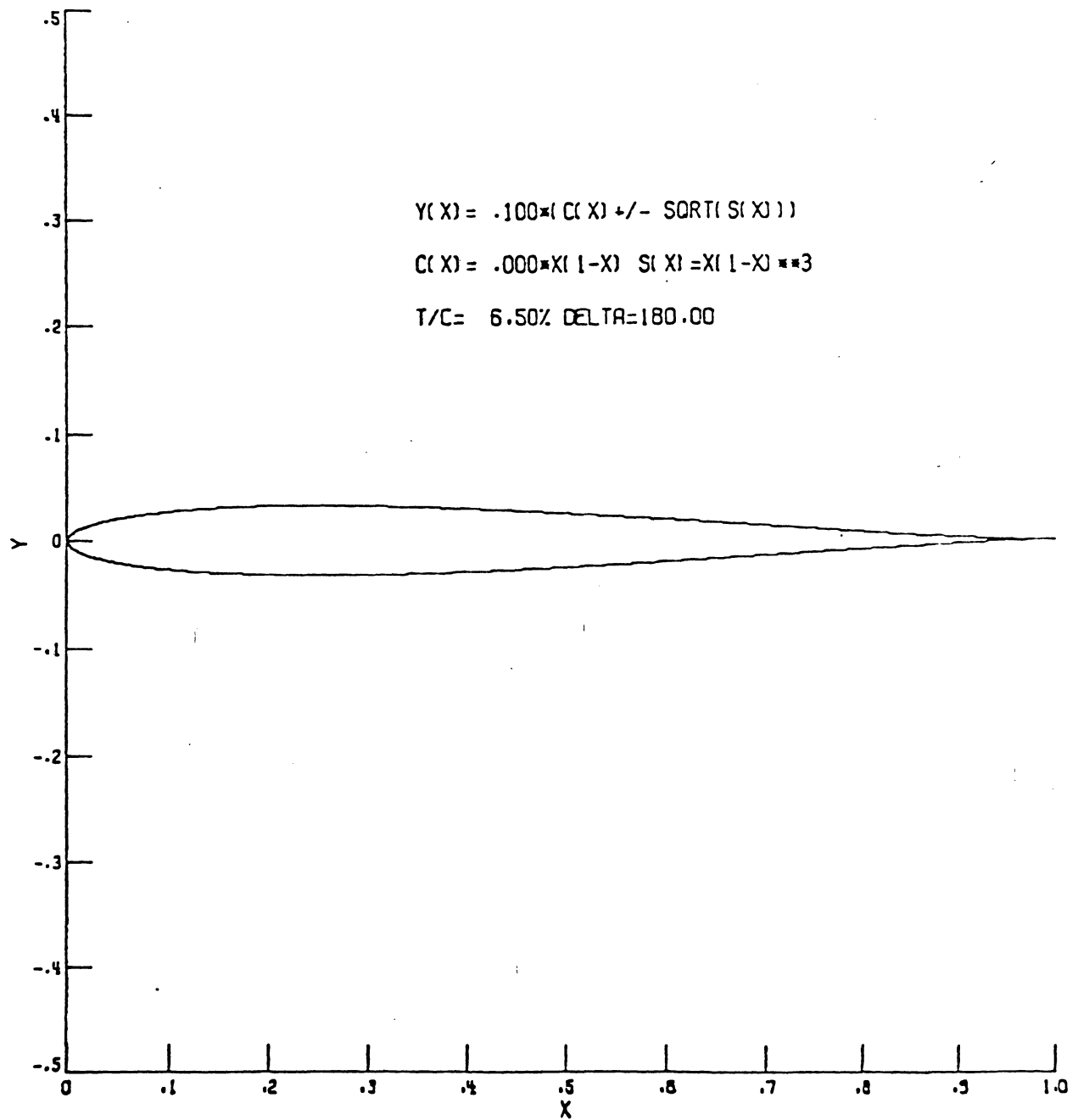


Fig. 3.4 Symmetrical Joukowski airfoil of 6.5% thickness.

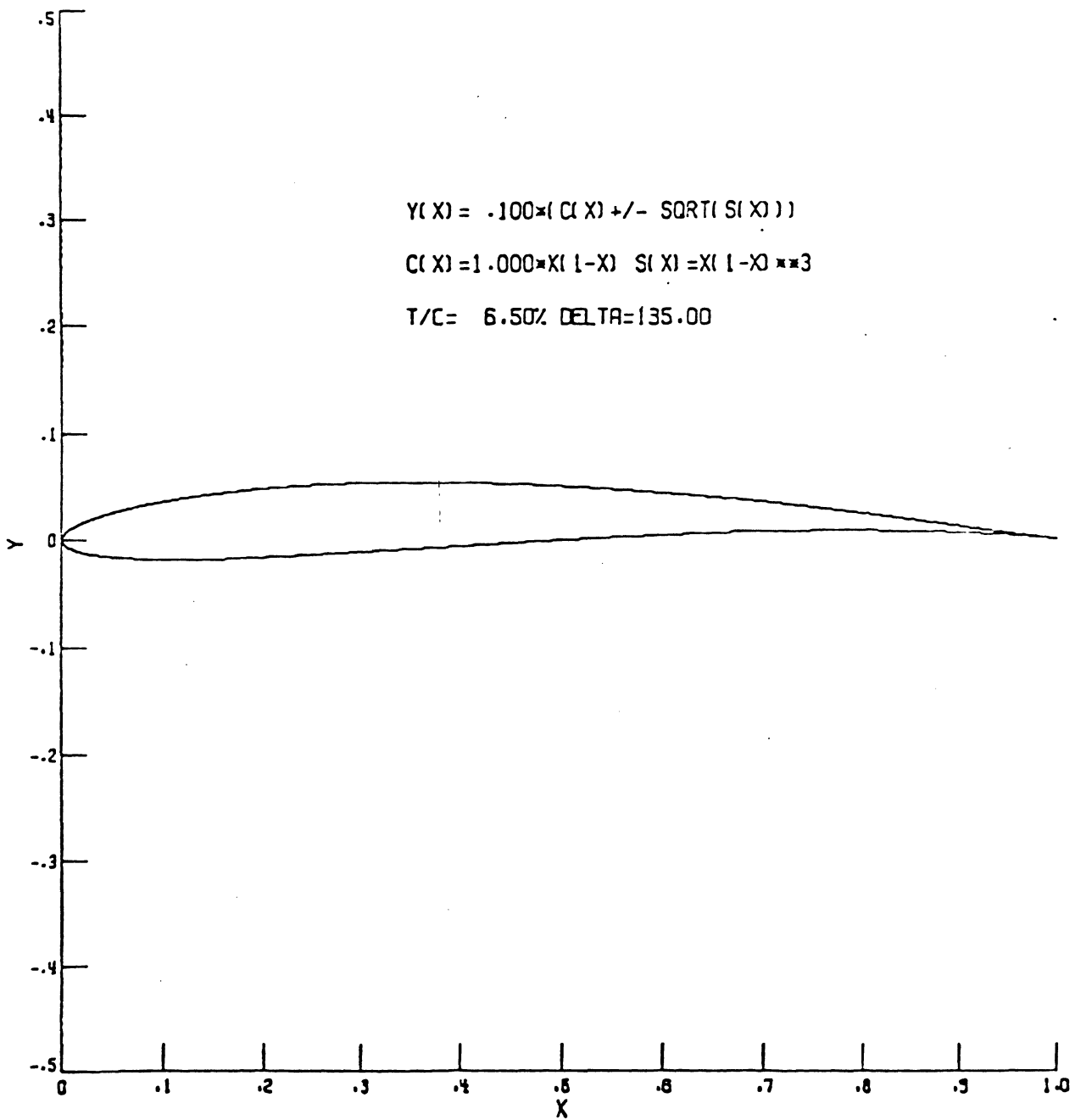


Fig. 3.5 Cambered Joukowski airfoil of 6.5% thickness.

Chapter 4

RESULTS AND DISCUSSION

In this chapter an assessment of the merits of the perturbation analysis method is made. The pressure distribution on axisymmetric bodies and two-dimensional airfoils obtained by the above method are compared with those of panel method as well as exact solutions whenever available. The results of the panel method are obtained by using the low-order panel method code (program VSAERO, developed by Maskew [18]). The analytical expressions for the ellipsoidal body and elliptic airfoil are available in the literature presented in Sec. 2.2.1.

4.1 Axisymmetric Bodies

Since the analytical expression for an ellipsoidal body is available, this body is selected to demonstrate the accuracy of the perturbation analysis method with the variations of the slenderness ratio and also the number of terms in the expansion of ϕ . Figs. 4.1a-4.2c illustrate a comparison of the pressure distributions, as calculated by the perturbation analysis method with different order of accuracy in the expansion of ϕ , with analytical solutions for the two values $\epsilon = 0.1$ and $\epsilon = 0.2$, corresponding to $L/d = 5$ and 2.5 , respectively. The results show that the perturbation solutions agree well with the exact solutions to a high order of accuracy, i.e., up to $O(\epsilon^8)$. With the same order of accuracy in ϕ up to $O(\epsilon^8)$, the pressure

distributions obtained from the perturbation analysis method and the panel method are compared with the exact solutions, with different numbers of panels in the chordwise direction for $\epsilon = 0.10$. The calculations are presented in Figs. 4.3a-4.3c. It is seen that the results using 30x6 panels and 50x6 panels yield better agreement with the exact solutions than using 10x6 panels. Again for the same order of accuracy in ϕ up to $O(\epsilon^8)$, and using 50x6 panels, three sets of pressure distributions are compared with four different values of ϵ . The results are presented in Figs. 4.4a-4.4c. The perturbation solutions agree well with the exact solution with small slenderness ratio up to 0.1, and the panel solutions compare well with exact solutions for all values of ϵ . The dumbbell shaped body is also analyzed by the perturbation analysis method with the expansion of ϕ up to $O(\epsilon^4)$, as well as by the panel method. A comparison of pressure distributions obtained by the above method and the panel method, using 50x6 panels, with different values of ϵ and profile parameter b are presented in Figs. 4.5a-4.6b. For small ϵ and b , the perturbation solutions agree well with that generated by the panel method. In the present examples, each perturbation case required only 2 seconds computing time versus 5 seconds (30x6 panels) or 14 seconds (50x6 panels) for the panel method. This computation time comparison is based on the CDC Cyber 173.

4.2 Two-Dimensional Airfoils

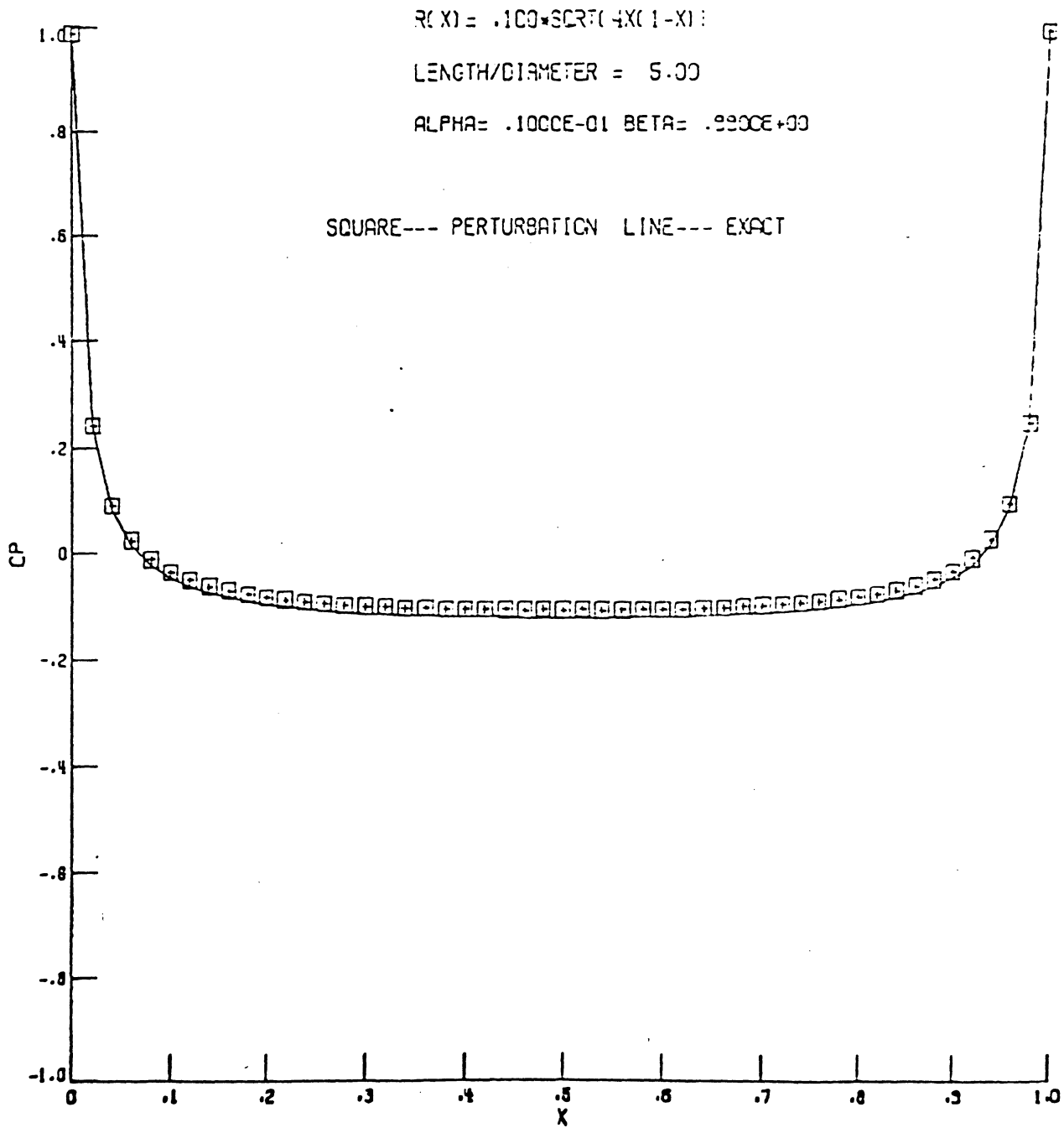
The analytical pressure distribution on the surface of the elliptic airfoil is available in the literature discussed in Sec. 2.2.1. It is convenient to do numerical experiments for the perturbation analysis method using this airfoil. Perturbation analysis solutions for an

elliptic airfoil, set at zero angle of attack, are compared with exact solutions, with different order of accuracy in ϕ expansion for $\epsilon = 0.10$ and $\epsilon = 0.15$, corresponding to the t/C ratio = 20% and 40% respectively, as presented in Figs. 4.7a-4.8b. It is apparent that the perturbation analysis solution gives quite good agreement with the analytical solution for high order of accuracy in ϕ up to $O(\epsilon^4)$. The pressure distributions calculated from the perturbation analysis method are compared with the exact solutions, with different values of slenderness ratio and these are shown in Figs. 4.9a-4.9c. The results show that the perturbation solutions agree closely with exact solutions up to 20 percent thick elliptic airfoil.

Results of the symmetrical second order Joukowski airfoil obtained by the perturbation analysis method with the order of accuracy of ϕ expansion up to $O(\epsilon^3)$ are compared with the panel method in the following section. Here, 3.25%, 6.5%, 10% and 13% thick airfoils are chosen as the test cases. For the calculation presented, the thickness of the airfoil, angle of attack, and the number of panels are given for each of the calculation. The calculations presented in Figs. 4.10a-4.10c and 4.11a-4.11c are obtained using different numbers of panels in the chordwise direction for symmetrical Joukowski airfoil of 6.5% thickness at 0° and 6° angles of attack, respectively. The results do not give a smooth curve near some regions of the leading edge until 50 panels are used. A comparison of the perturbation analysis solutions for the symmetrical second order Joukowski airfoil at 0° , 6° and 12° angles of attack with panel method are presented in Figs. 4.12a-4.15c. The perturbation solutions agree with the panel solutions except in some region on the leading edge of the airfoil surface. Table 4.1 illus-

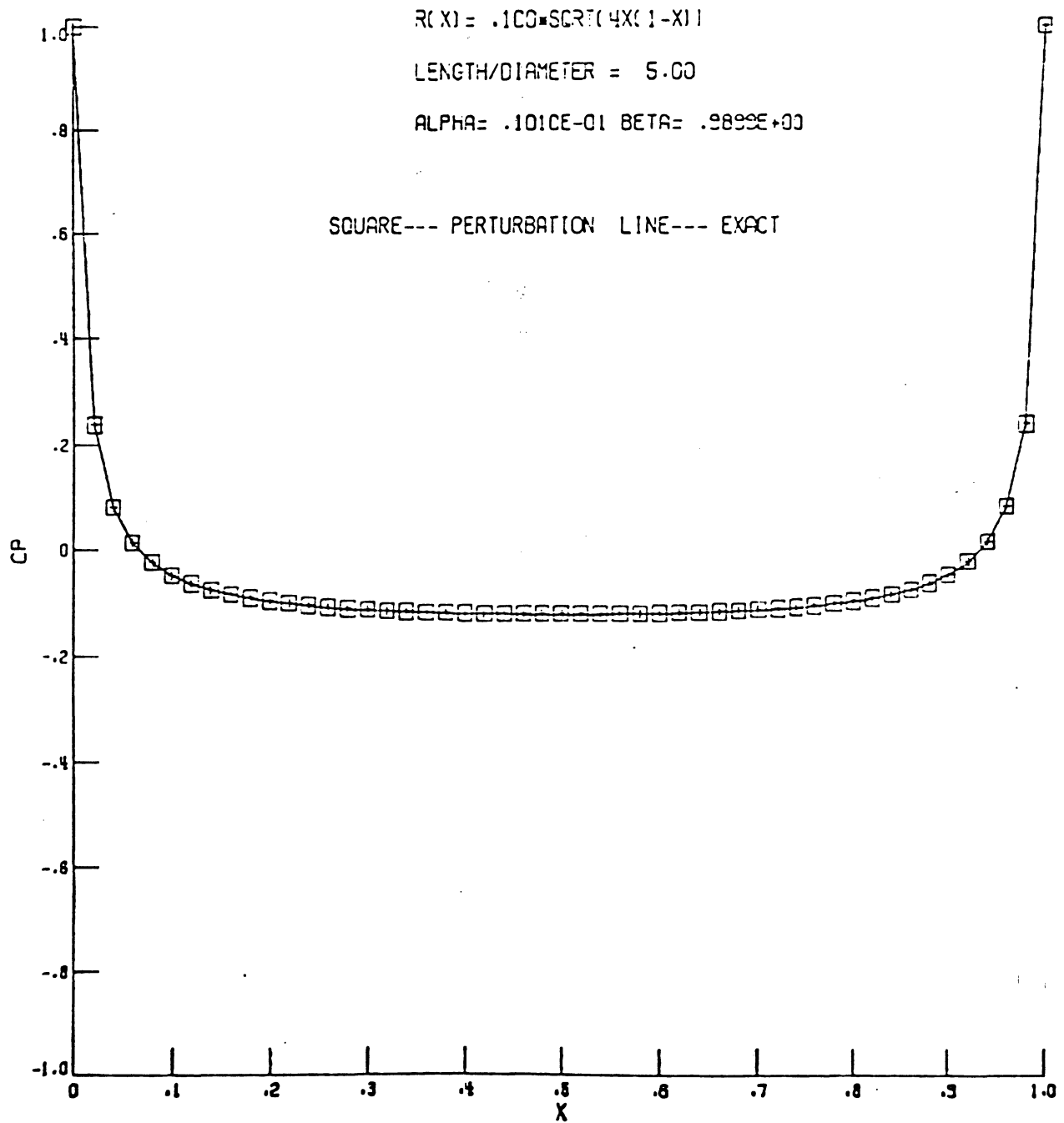
trates the appreciable difference between the lift coefficients of the two methods from the exact solutions.

The perturbation analysis method has been applied to the cambered second order Joukowski airfoil with the order of accuracy in the expansion for ϕ up to $O(\epsilon^3)$. Calculations are presented in Figs. 4.16a-4.19c. The results generated by the panel method with 0° , 6° and 12° angles of attack are used for comparison. Both pressure distributions agree closely for small slenderness ratio and angle of attack up to $\epsilon = 0.03248$ and $\gamma = 6^\circ$ respectively, except at some regions near the leading edge. The lift coefficients obtained from the perturbation analysis and the panel method compared with the exact solutions are shown in Table 4.2 . In the present example, the computation time for each perturbation case required 8 seconds, while 0.5 seconds (10 panels), 2 seconds (30 panels) and 5 seconds (50 panels) were required for each panel-method solution.



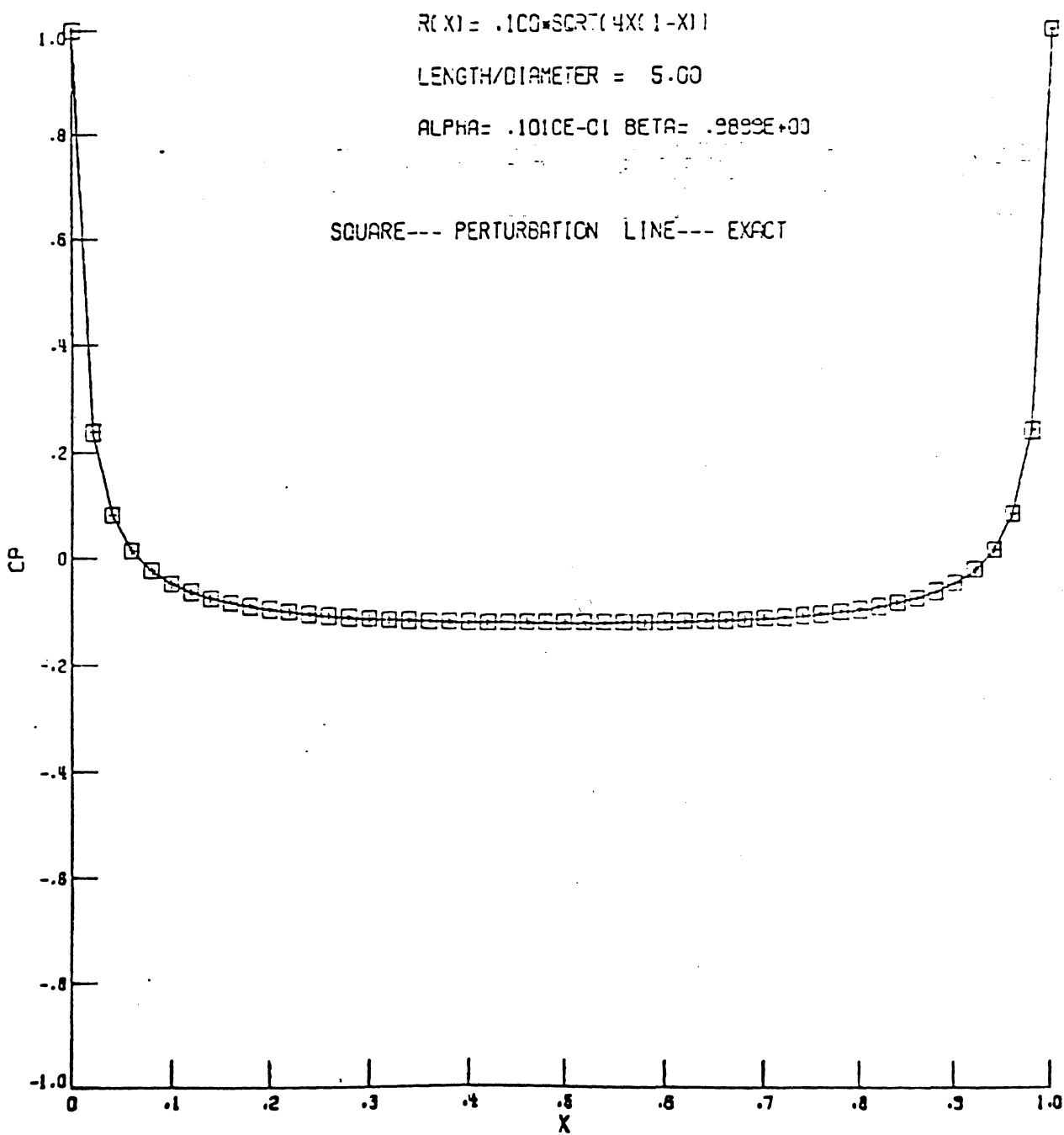
(a) $\epsilon = 0.1$; ϕ expanded up to ϵ^2 .

Fig. 4.1 Comparison of pressure distributions from the perturbation analysis method with the analytical solution for ellipsoidal body.



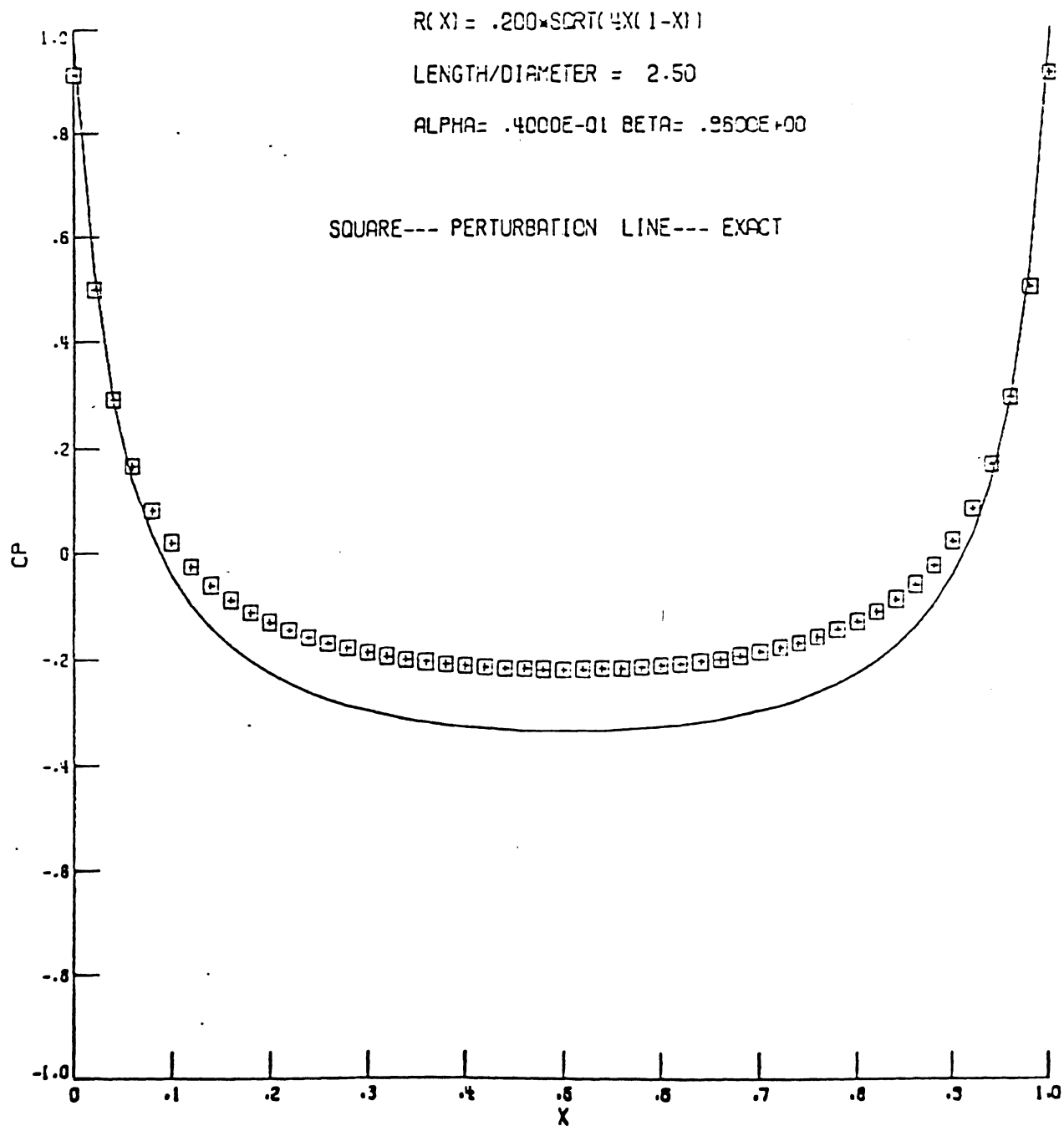
(b) $\epsilon = 0.1$; ϕ expanded up to ϵ^4 .

Fig. 4.1 Continued



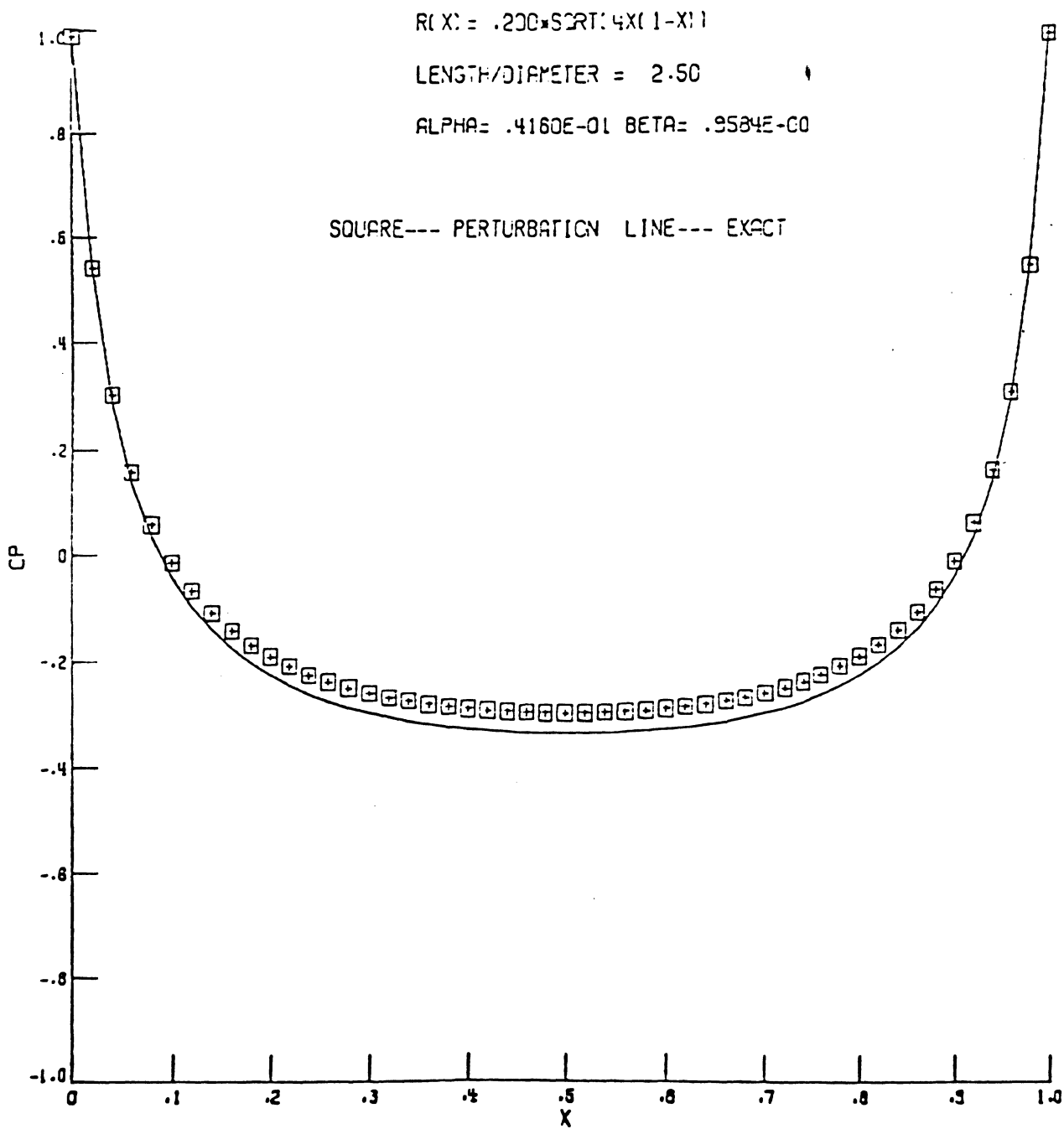
(c) $\epsilon = 0.1$; ϕ expanded up to ϵ^6 .

Fig. 4.1 Concluded.



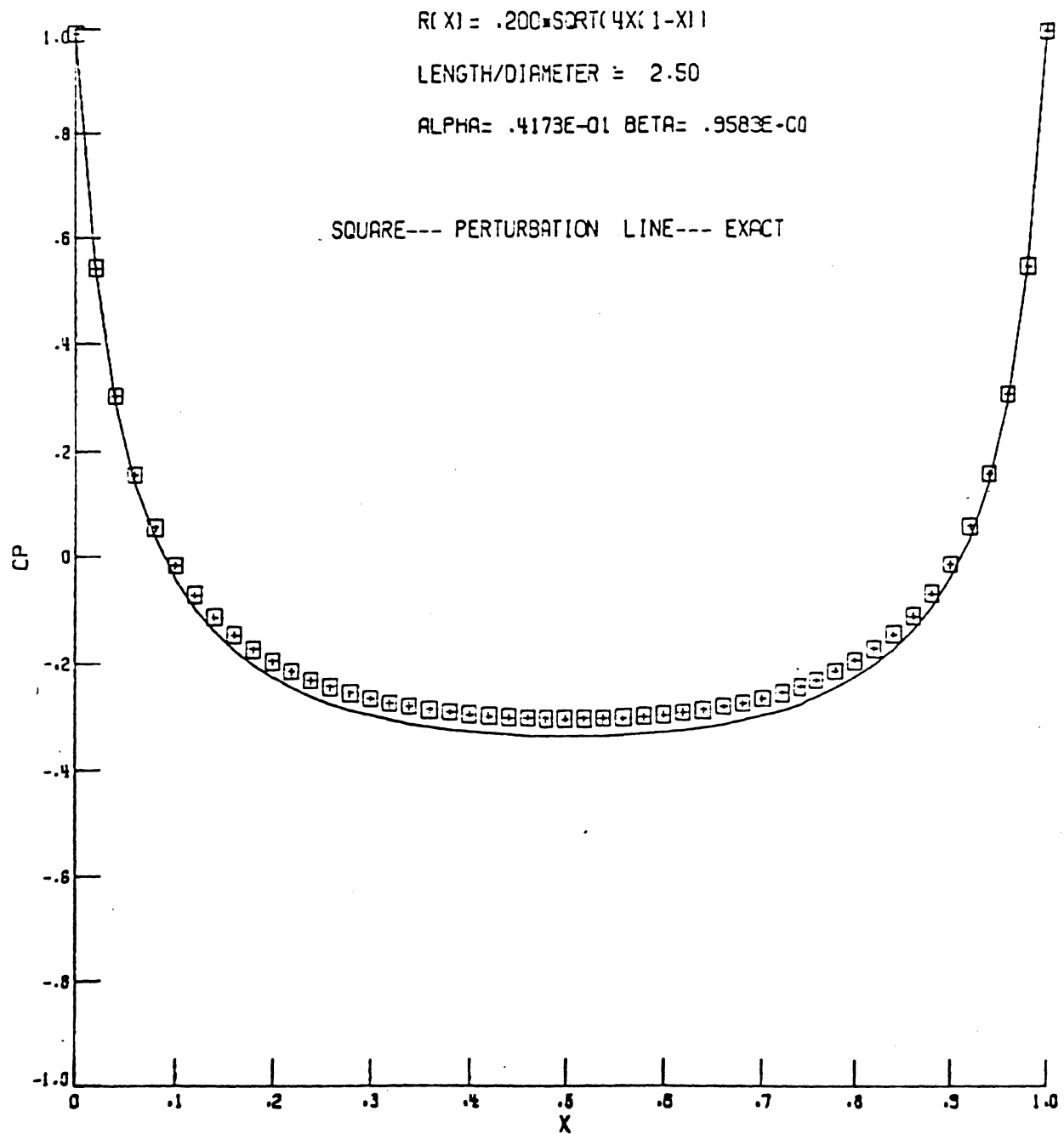
(a) $\epsilon = 0.2$; ϕ expanded up to ϵ^2 .

Fig. 4.2 Comparison of pressure distributions from the perturbation analysis method with the analytical solution for ellipsoidal body.



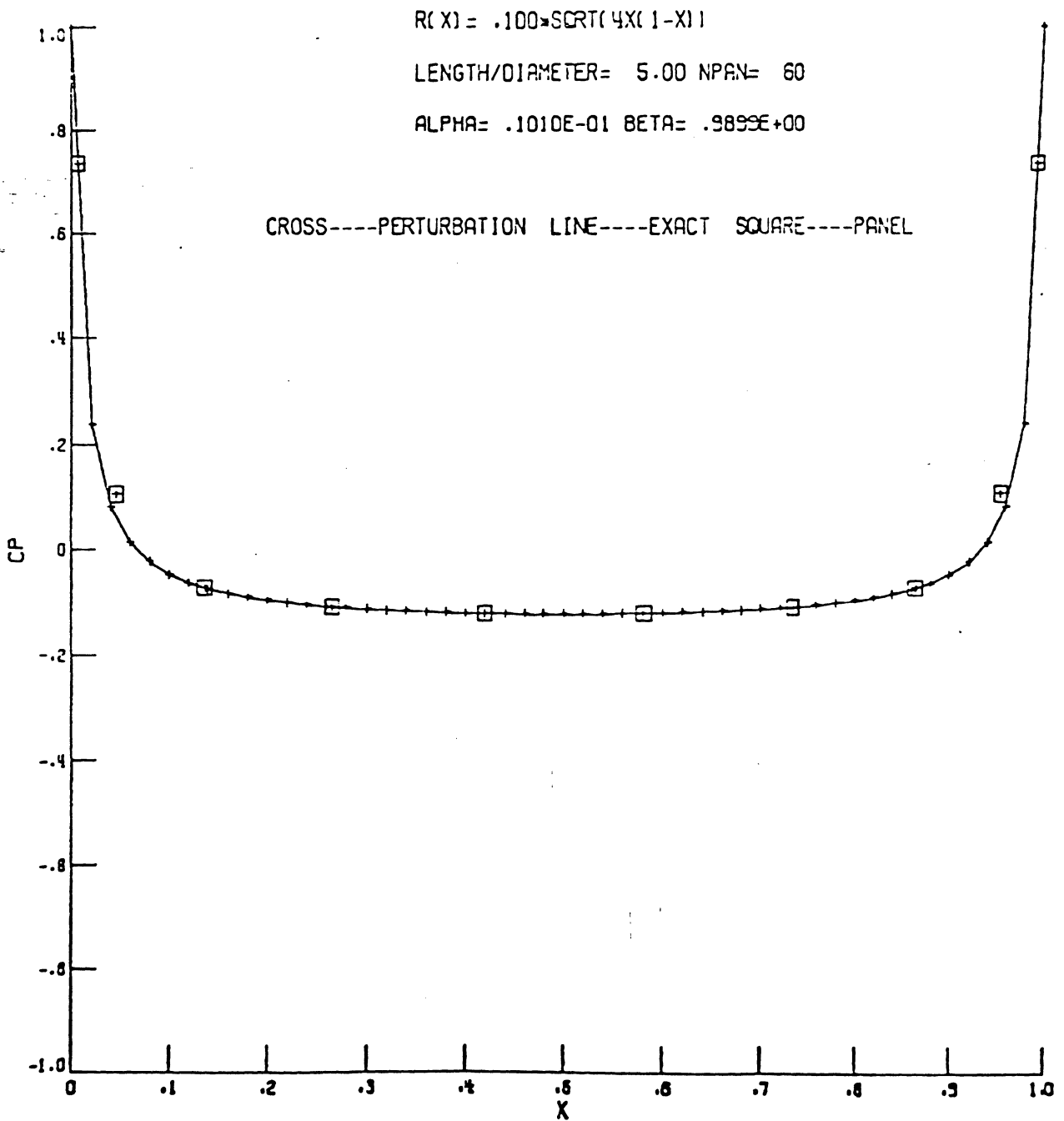
(b) $\epsilon = 0.2$; ϕ expanded up to ϵ^4 .

Fig. 4.2 Continued.



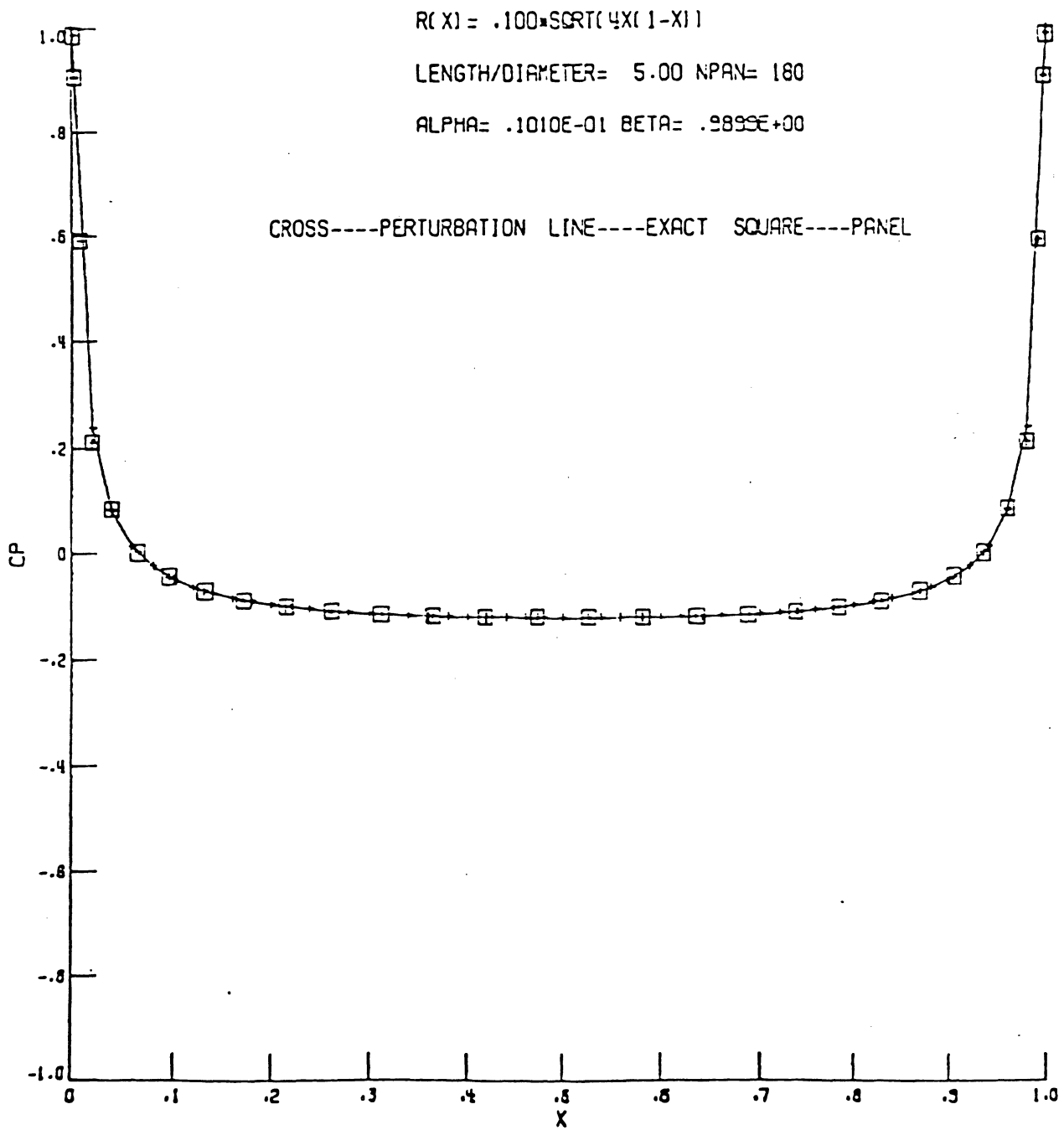
(c) $\epsilon = 0.2$; ϕ expanded up to ϵ^6 .

Fig. 4.2 Concluded.



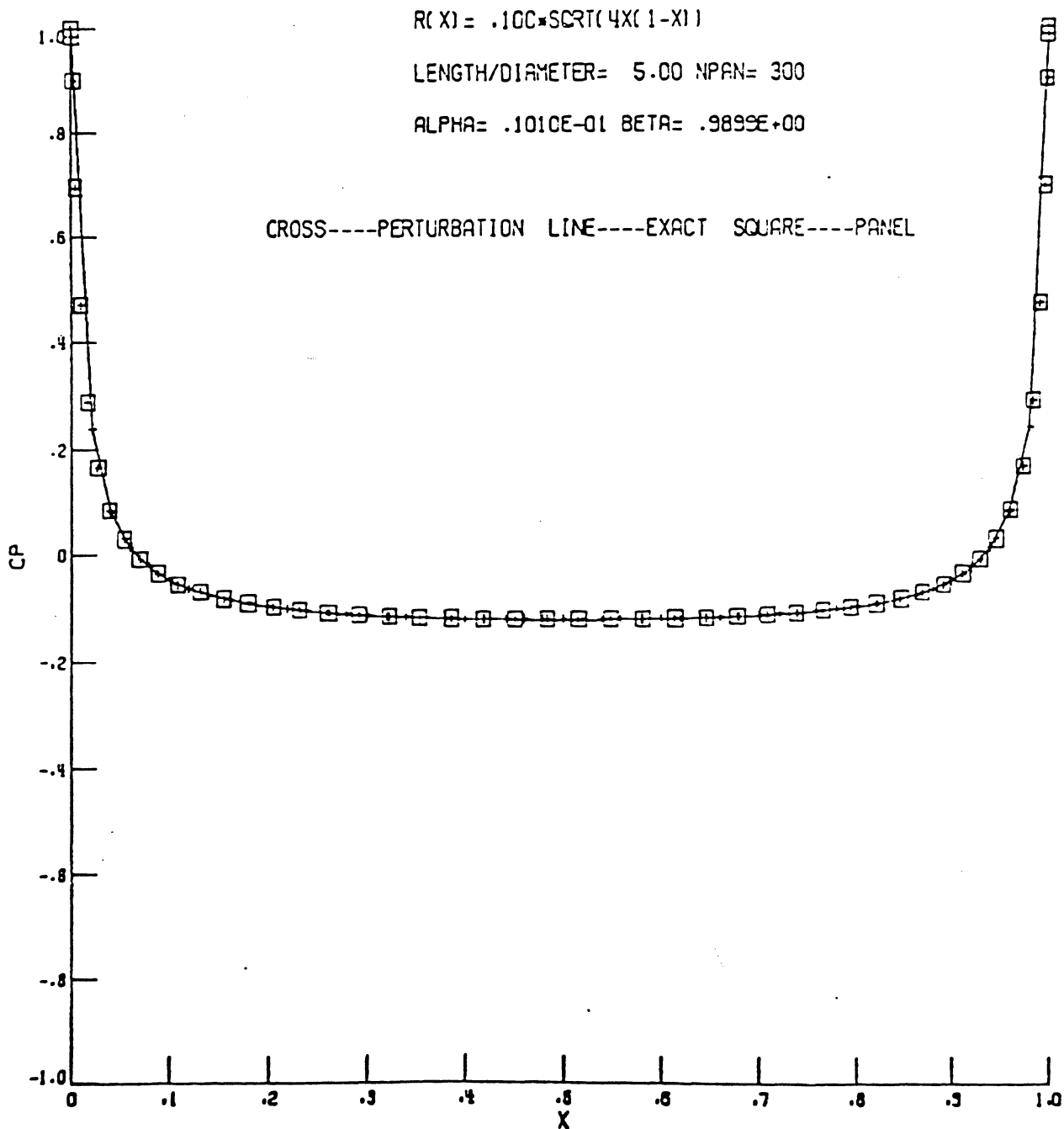
(a) $\epsilon = 0.1$; ϕ expanded up to ϵ^6 ; 60 panels with cosine spacing.

Fig. 4.3 Comparison of the perturbation and exact solutions with the panel method for ellipsoidal body.



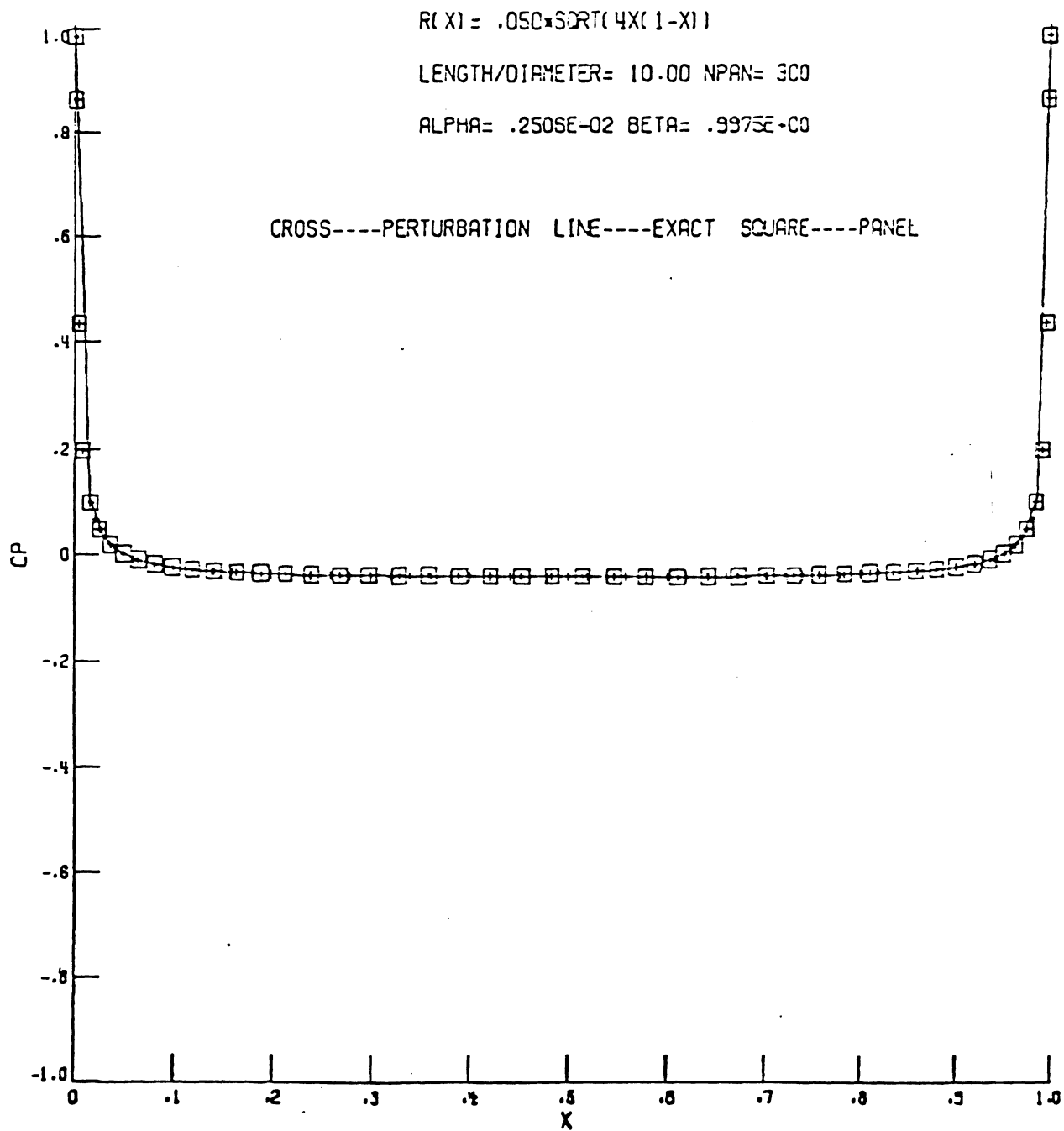
(b) $\epsilon = 0.1$; ϕ expanded up to ϵ^6 ; 180 panels with cosine spacing.

Fig. 4.3 Continued.



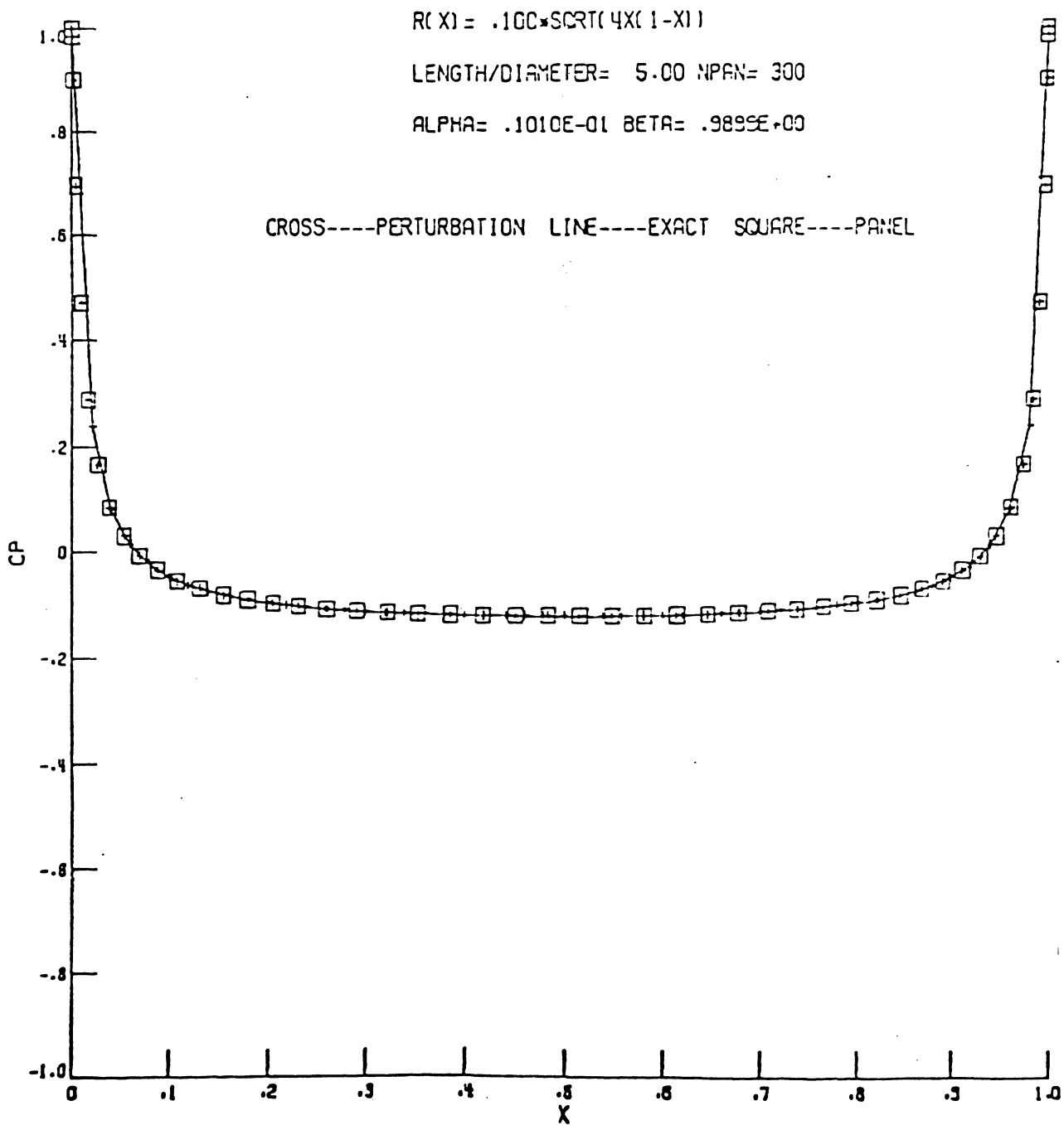
(c) $\epsilon = 0.1$; ϕ expanded up to ϵ^6 ; 300 panels with cosine spacing.

Fig. 4.3 Concluded.



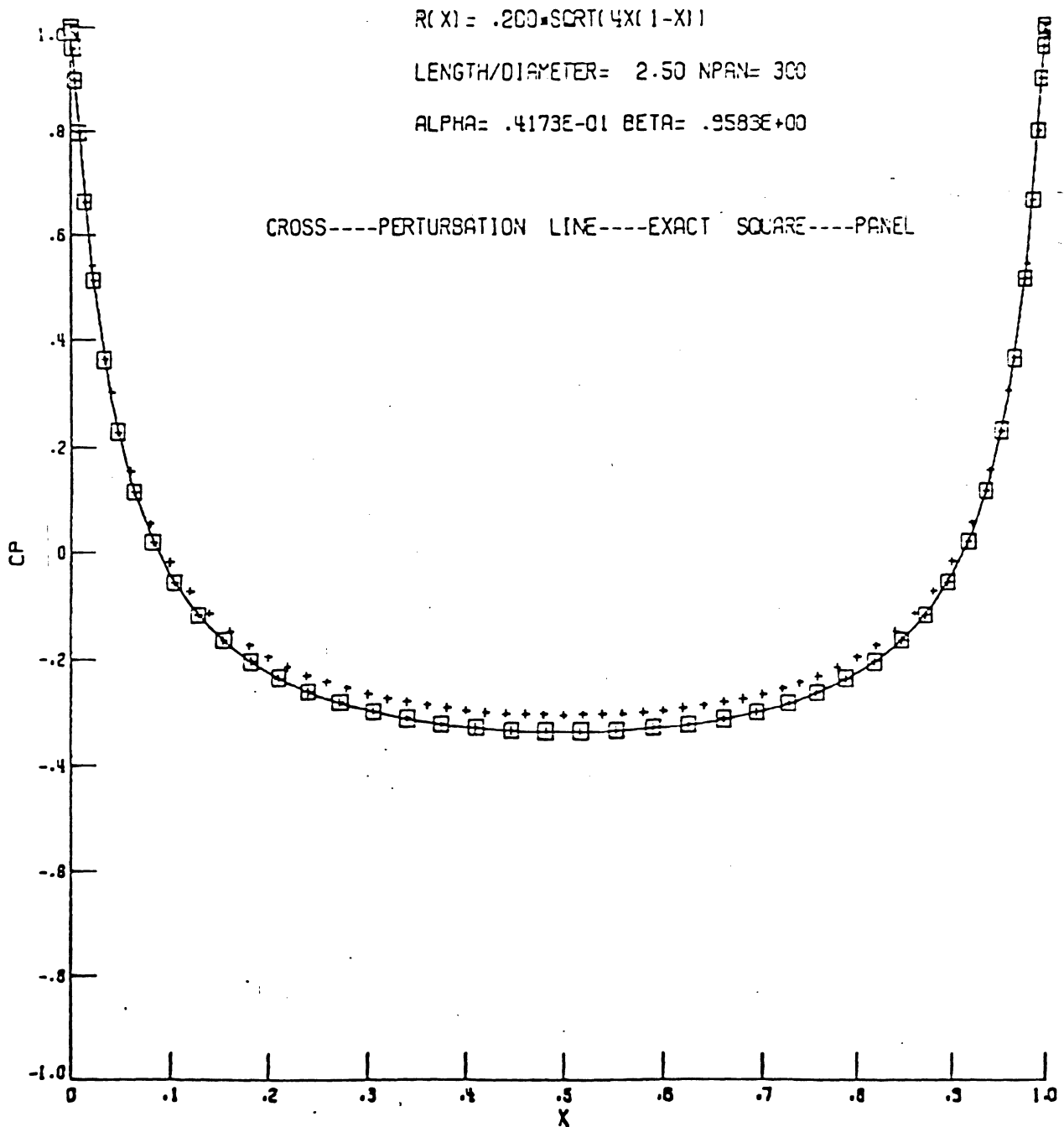
(a) $\epsilon = 0.05$; ϕ expanded up to ϵ^6 ; 300 panels with cosine spacing.

Fig. 4.4 Pressure distributions from the perturbation analysis and the panel methods are compared with the exact solution for ellipsoidal body.



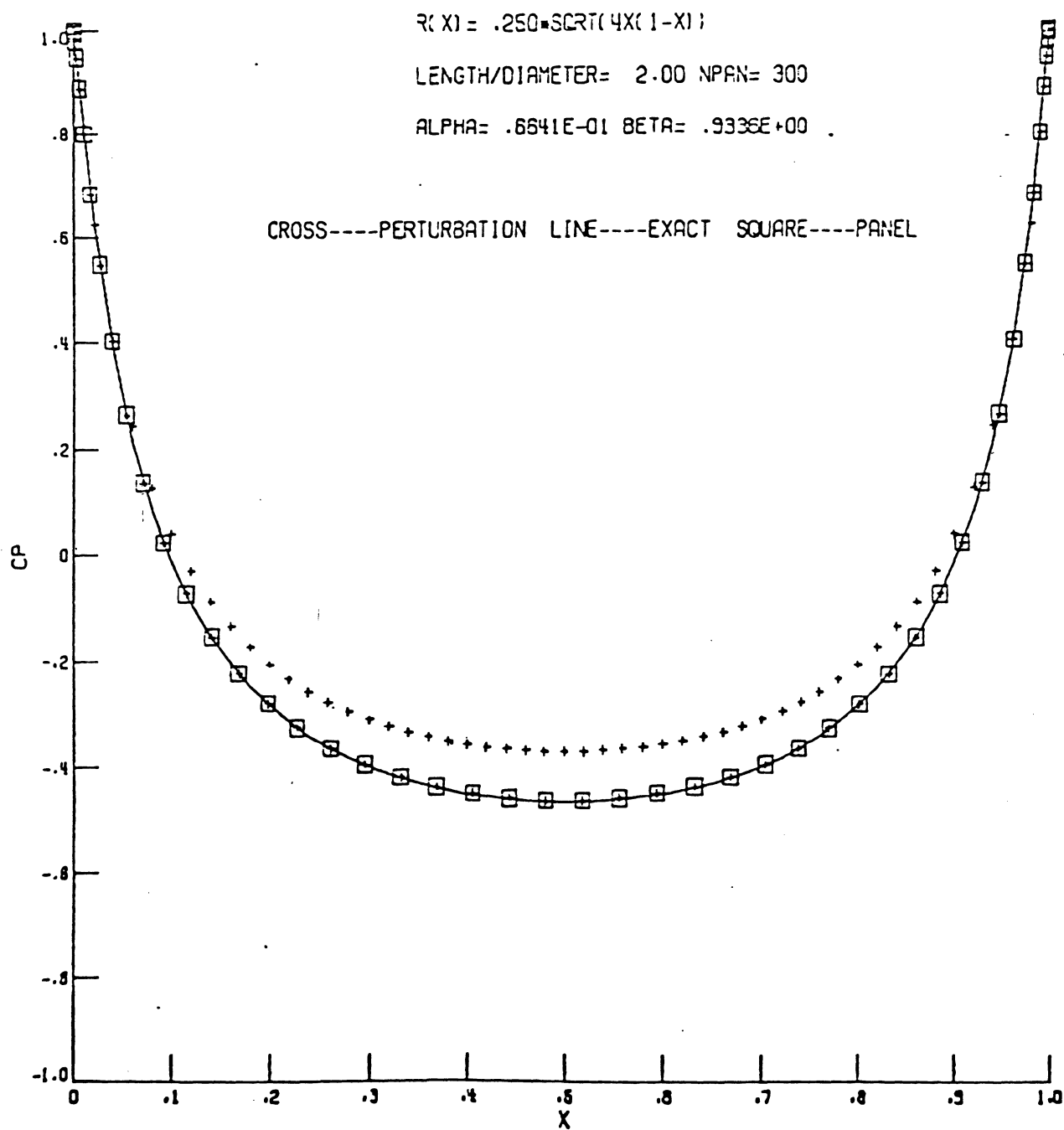
(b) $\epsilon = 0.10$; ϕ expanded up to ϵ^6 ; 300 panels with cosine spacing.

Fig. 4.4 Continued.



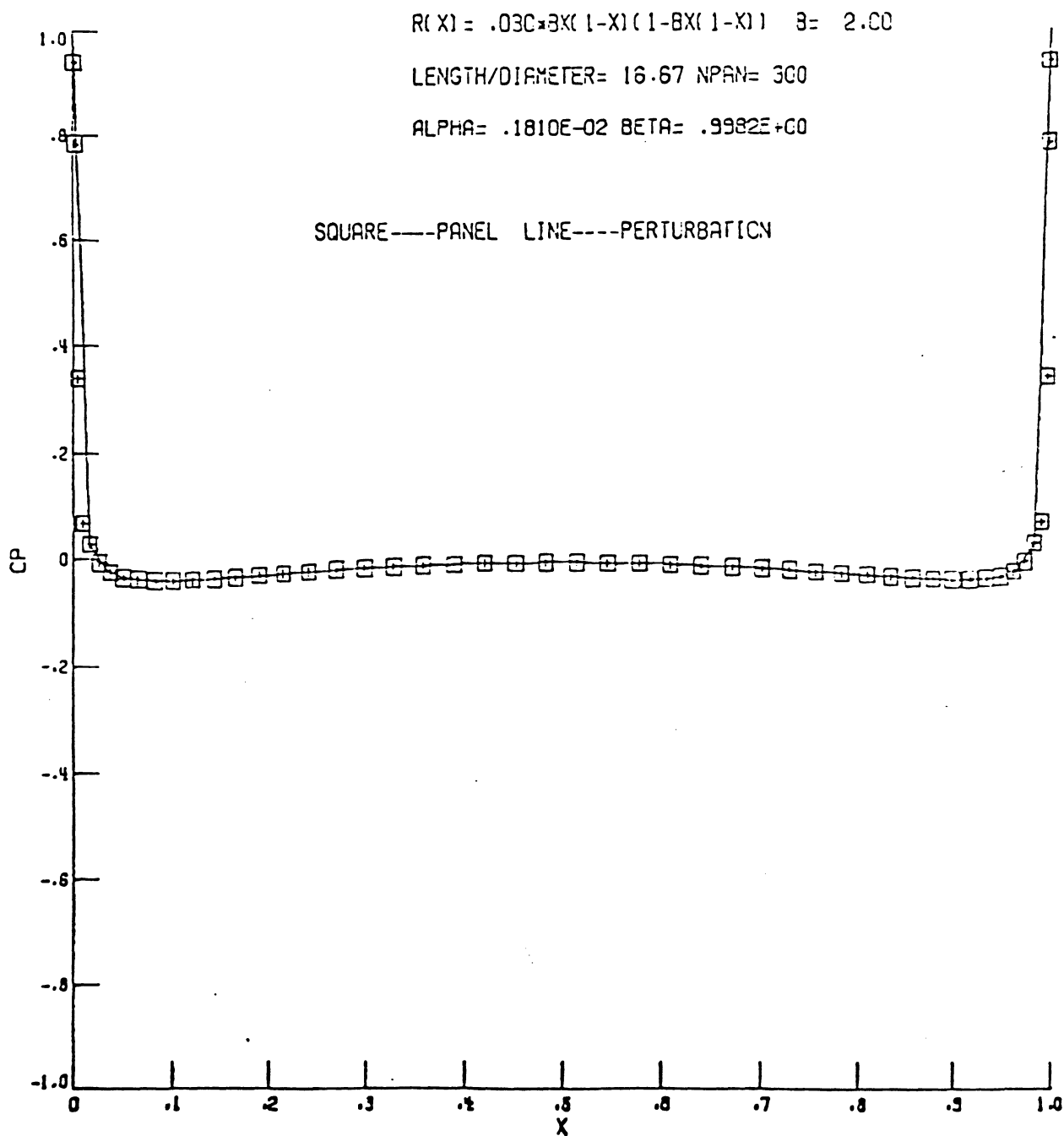
(c) $\epsilon = 0.20$; ϕ expanded up to ϵ^6 ; 300 panels with cosine spacing.

Fig. 4.4 Continued.



(d) $\epsilon = 0.25$; ϕ expanded up to ϵ^6 ; 300 panels with cosine spacing.

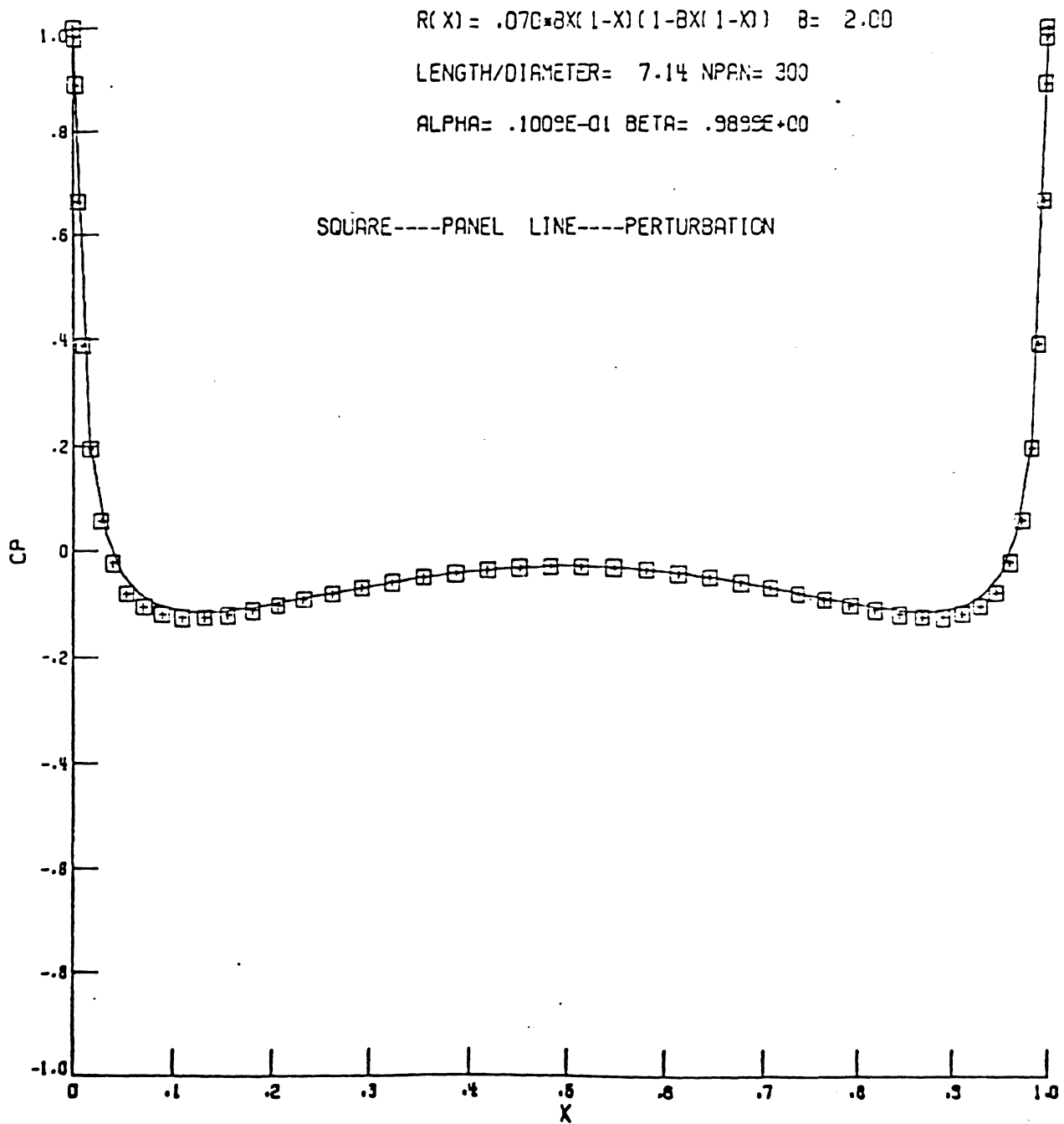
Fig. 4.4 Concluded.



(a) $\epsilon = 0.03$; $b = 2$; ϕ expanded up to ϵ^4 ;

300 panels with cosine spacing.

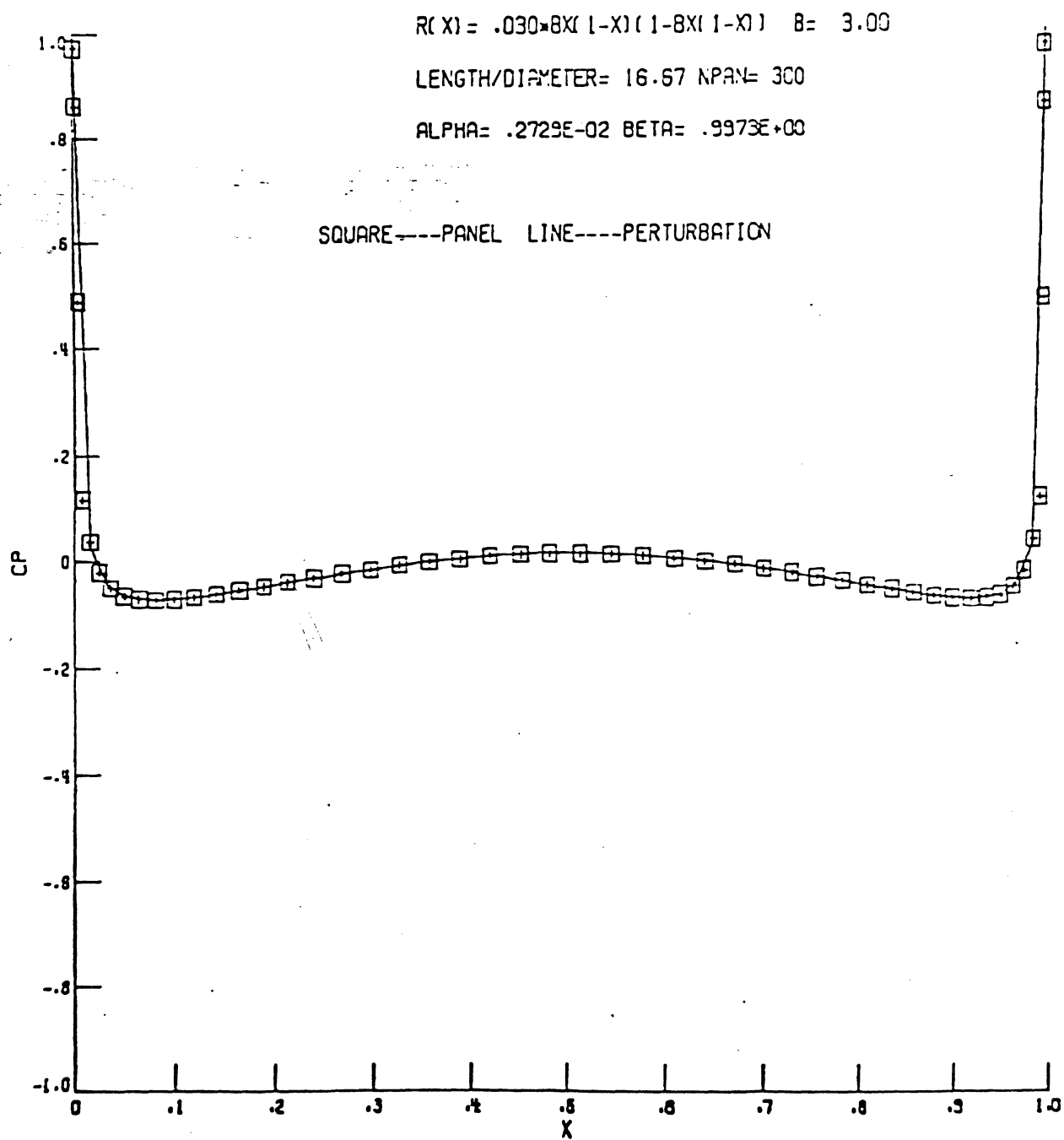
Fig. 4.5 Comparison of pressure distributions from the perturbation analysis method with the panel method for dumbbell shaped body.



(b) $\epsilon = 0.07$; $b = 2$; ϕ expanded up to ϵ^4 ;

300 panels with cosine spacing.

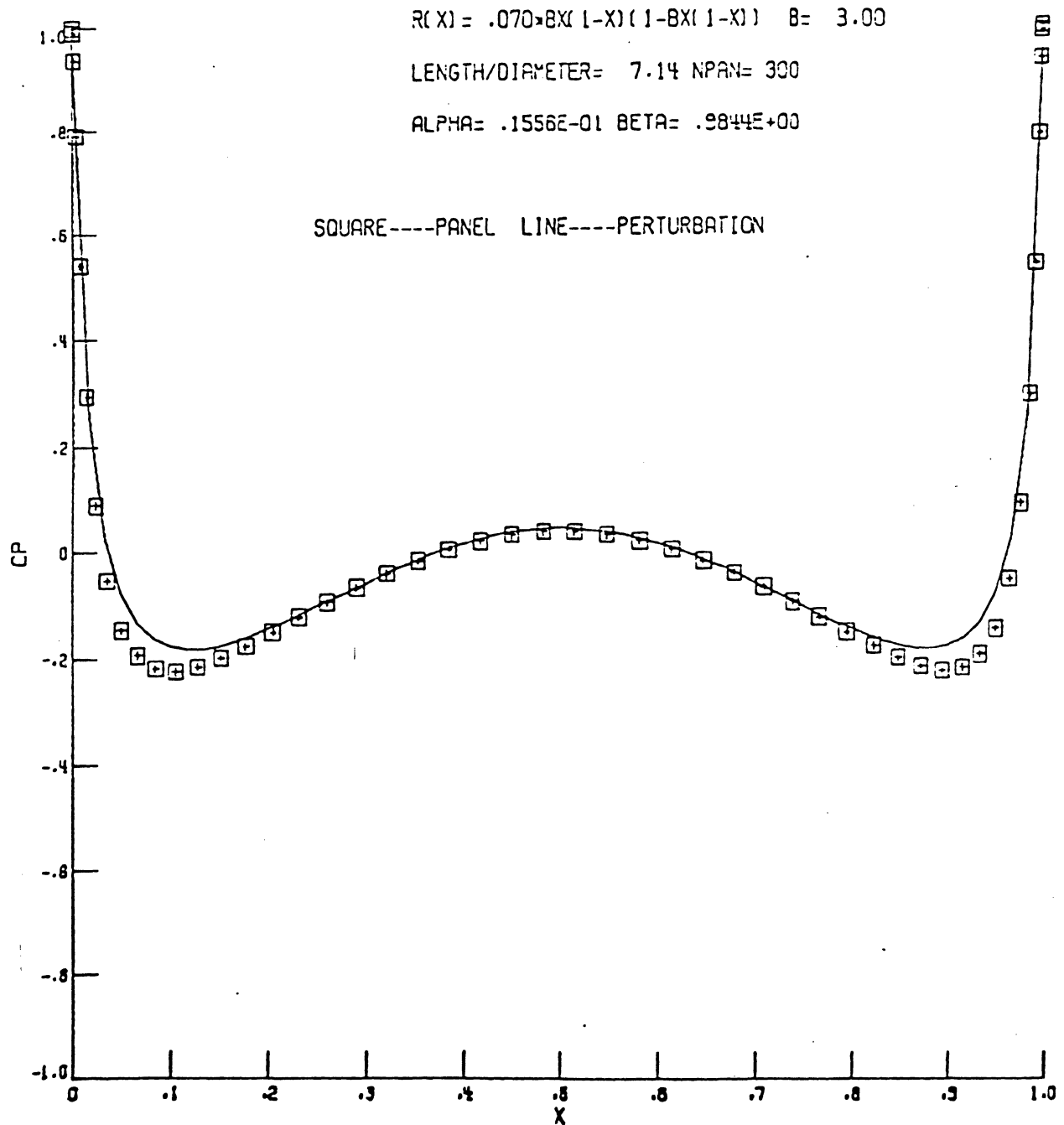
Fig. 4.5 Concluded.



(a) $\epsilon = 0.03$; $b = 3$; ϕ expanded up to ϵ^4 ;

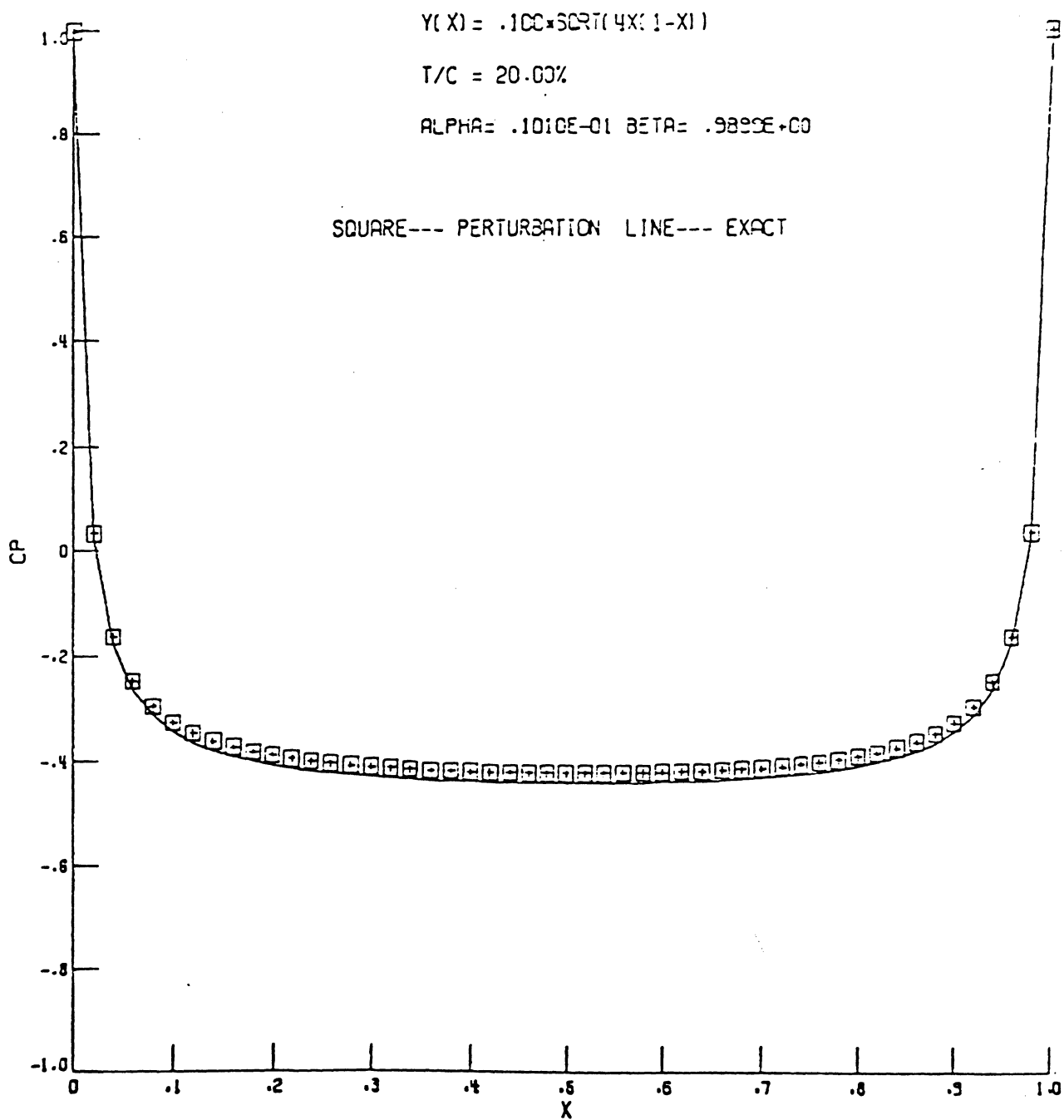
300 panels with cosine spacing.

Fig. 4.6 Comparison of pressure distributions from the perturbation analysis method with the panel method for dumbbell shaped body.



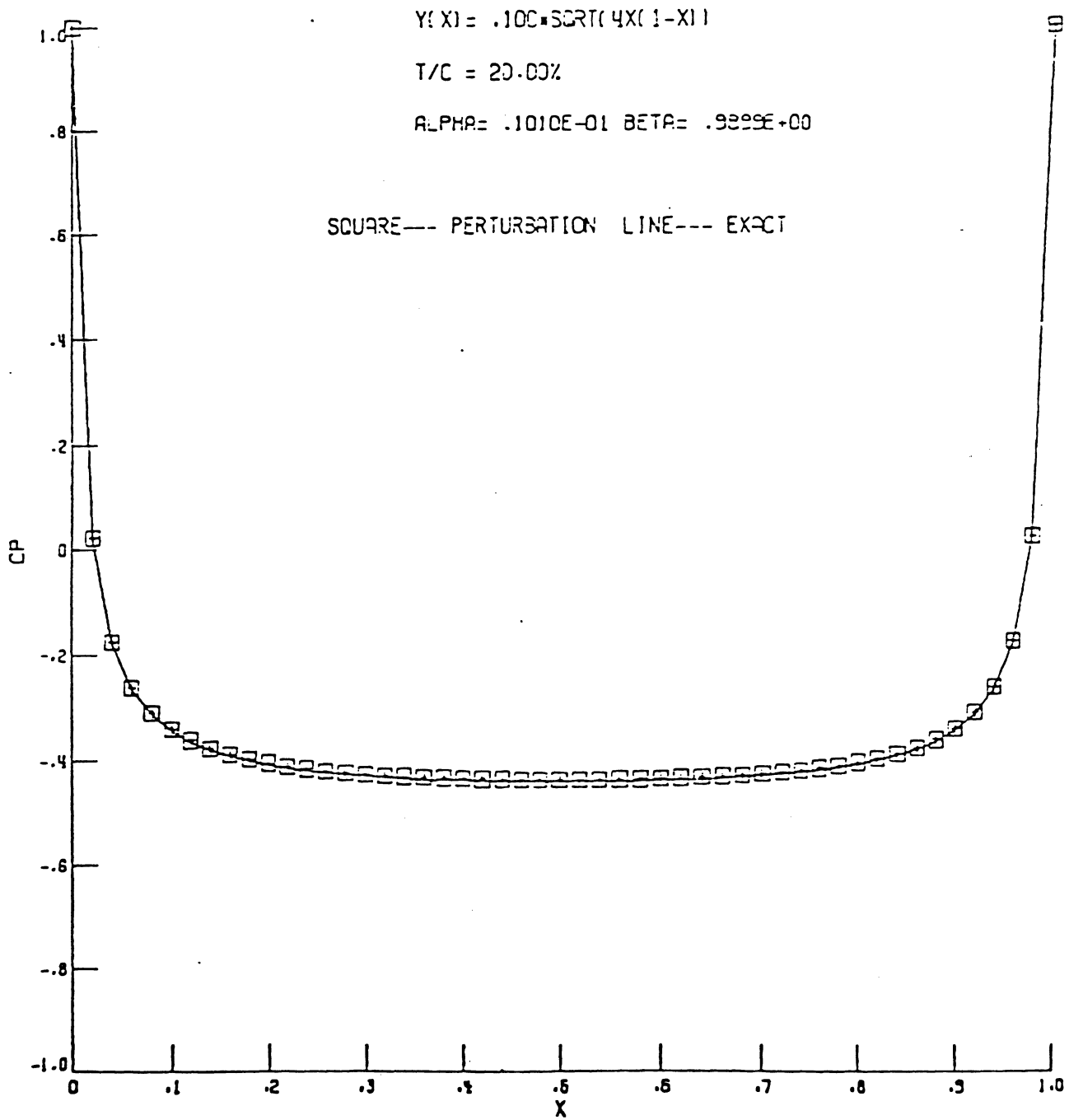
(b) $\epsilon = 0.07$; $b = 3$; ϕ expanded up to ϵ^4 ;
 300 panels with cosine spacing.

Fig. 4.6 Concluded.



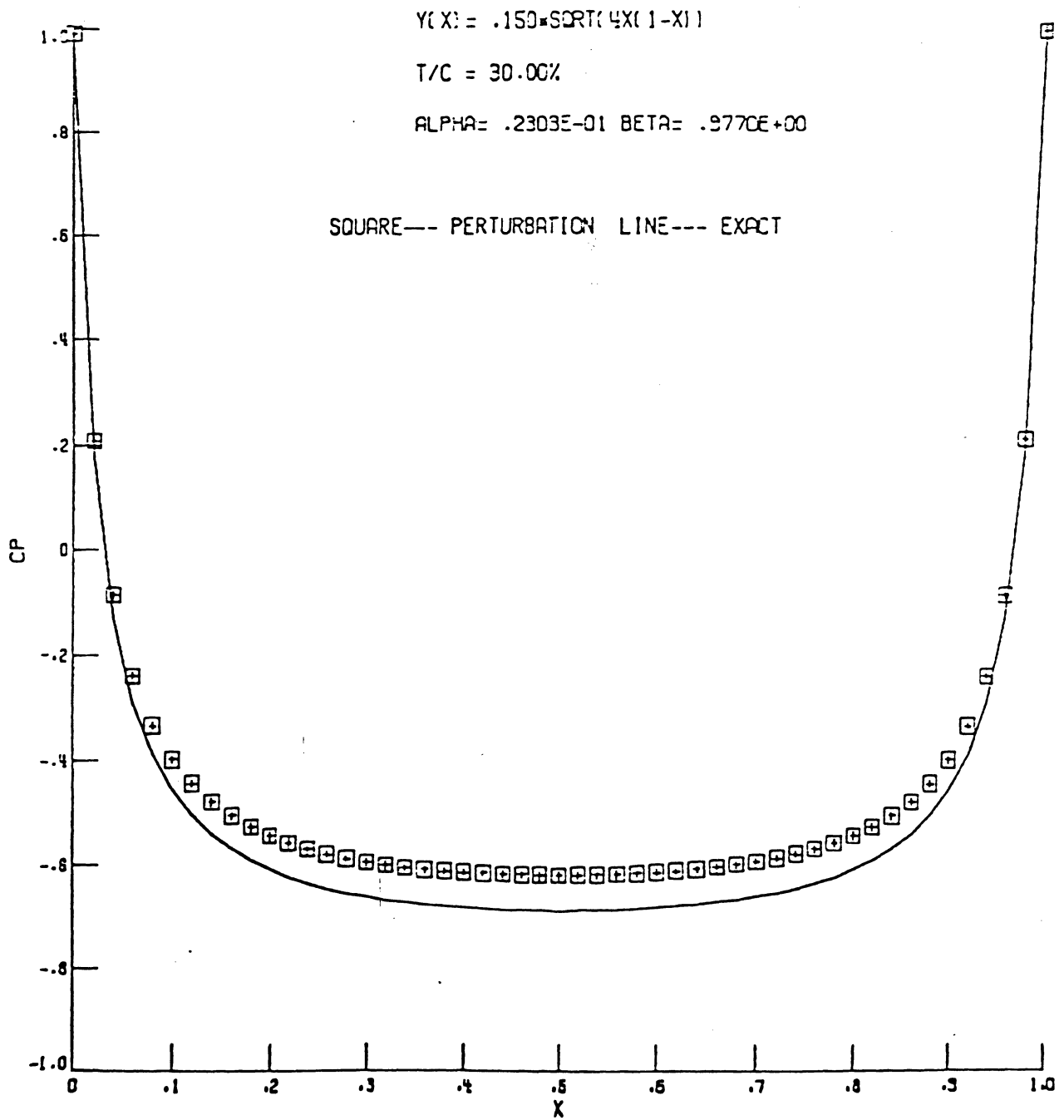
(a) $\epsilon = 0.1$; ϕ expanded up to ϵ^2 , $t/C = 20\%$.

Fig. 4.7 Comparison of pressure distributions from the perturbation analysis method with the exact solution for elliptic airfoil.



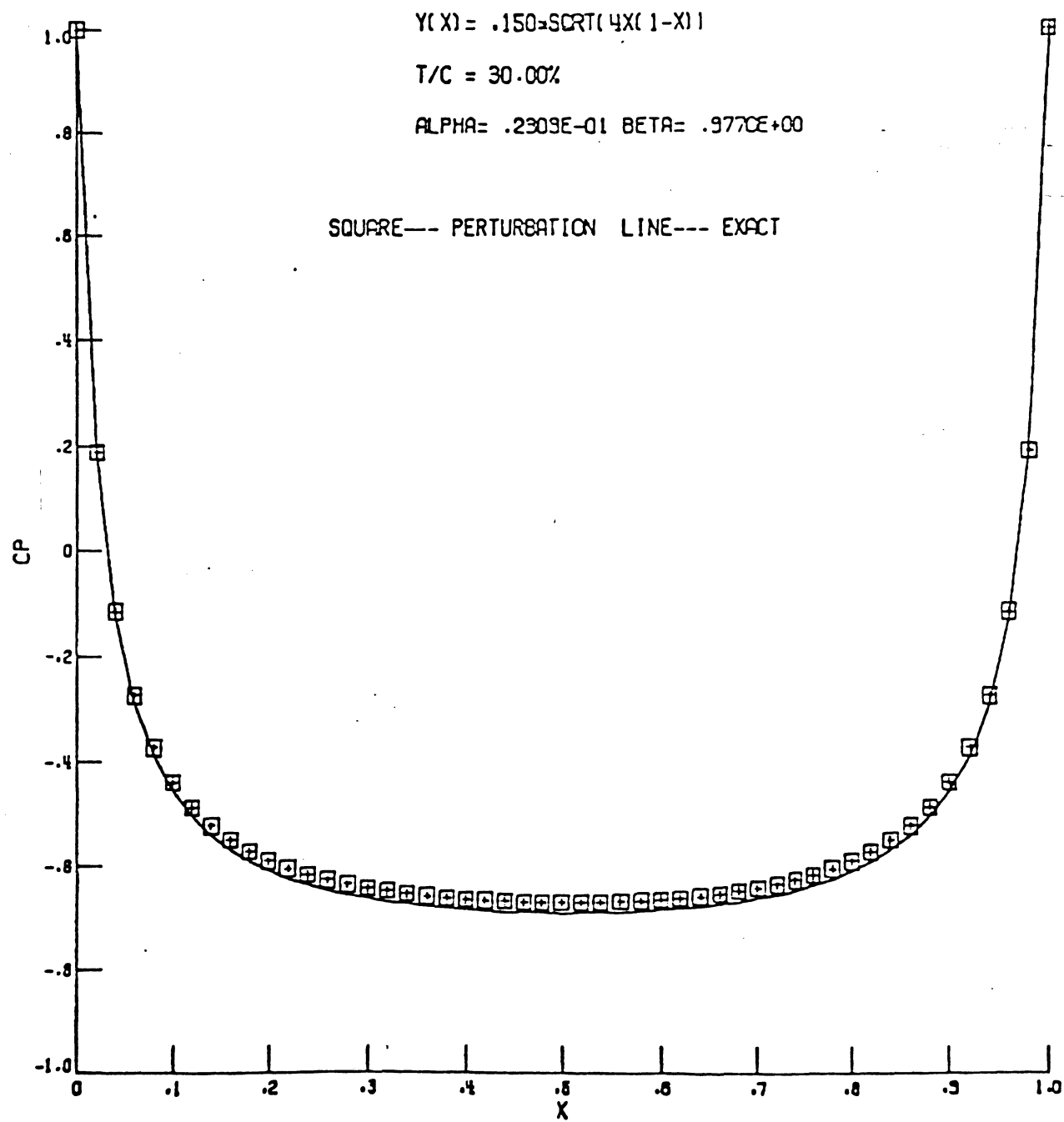
(b) $\epsilon = 0.1$; ϕ expanded up to ϵ^3 , $t/C = 20\%$

Fig. 4.7 Concluded.



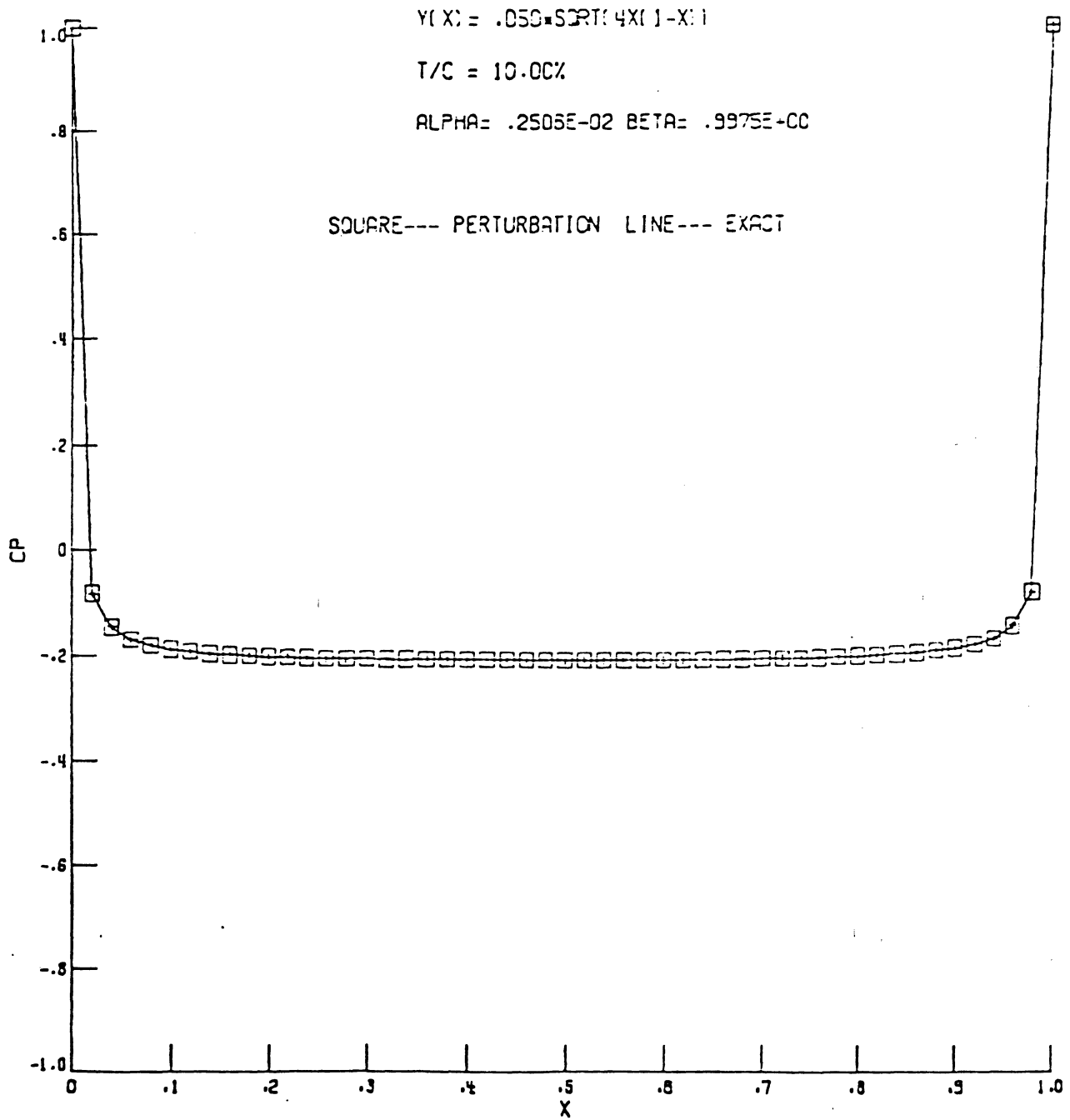
(a) $\epsilon = 0.15$; ϕ expanded up to ϵ^2 , $t/C = 30\%$.

Fig. 4.8 Comparison of pressure distributions from the perturbation analysis method with the exact solution for elliptic airfoil.



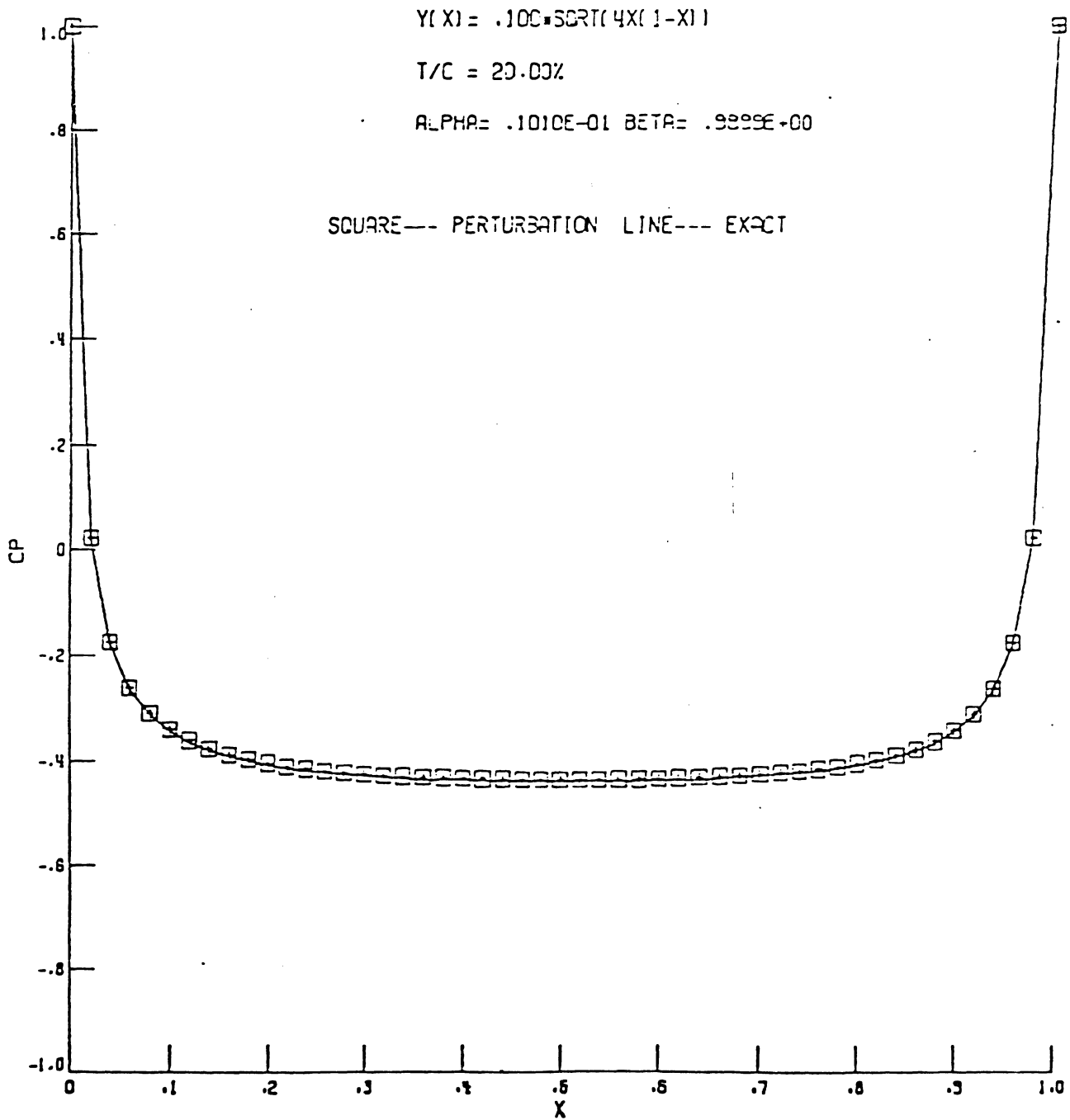
(b) $\epsilon = 0.15$; ϕ expanded up to ϵ^3 , $t/C = 30\%$.

Fig. 4.8 Concluded.



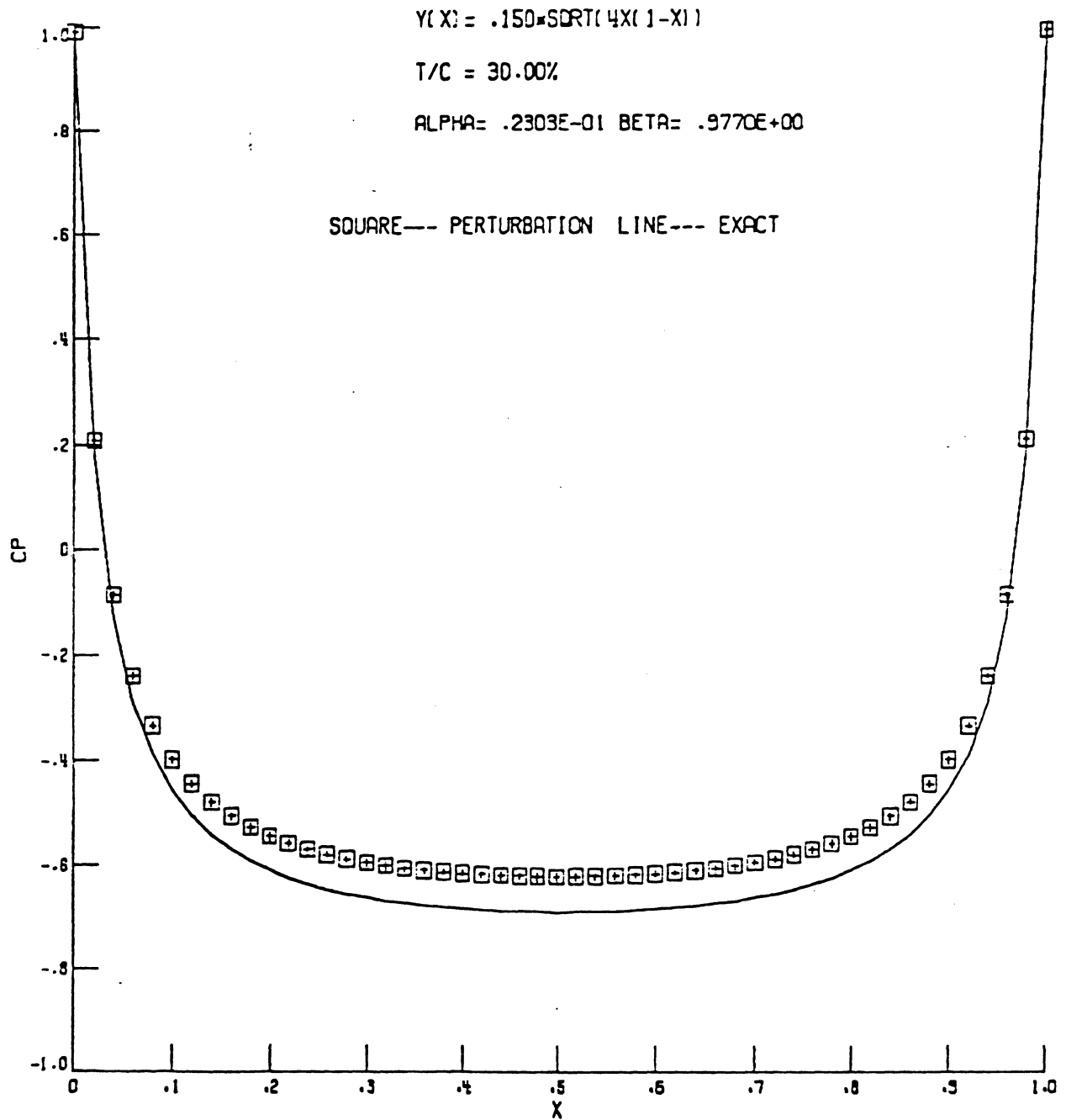
(a) $\epsilon = 0.05$; ϕ expanded up to ϵ^3 ; $t/C = 10\%$.

Fig. 4.9 Comparison of pressure distributions from the perturbation analysis method with the exact solution for elliptic airfoil.



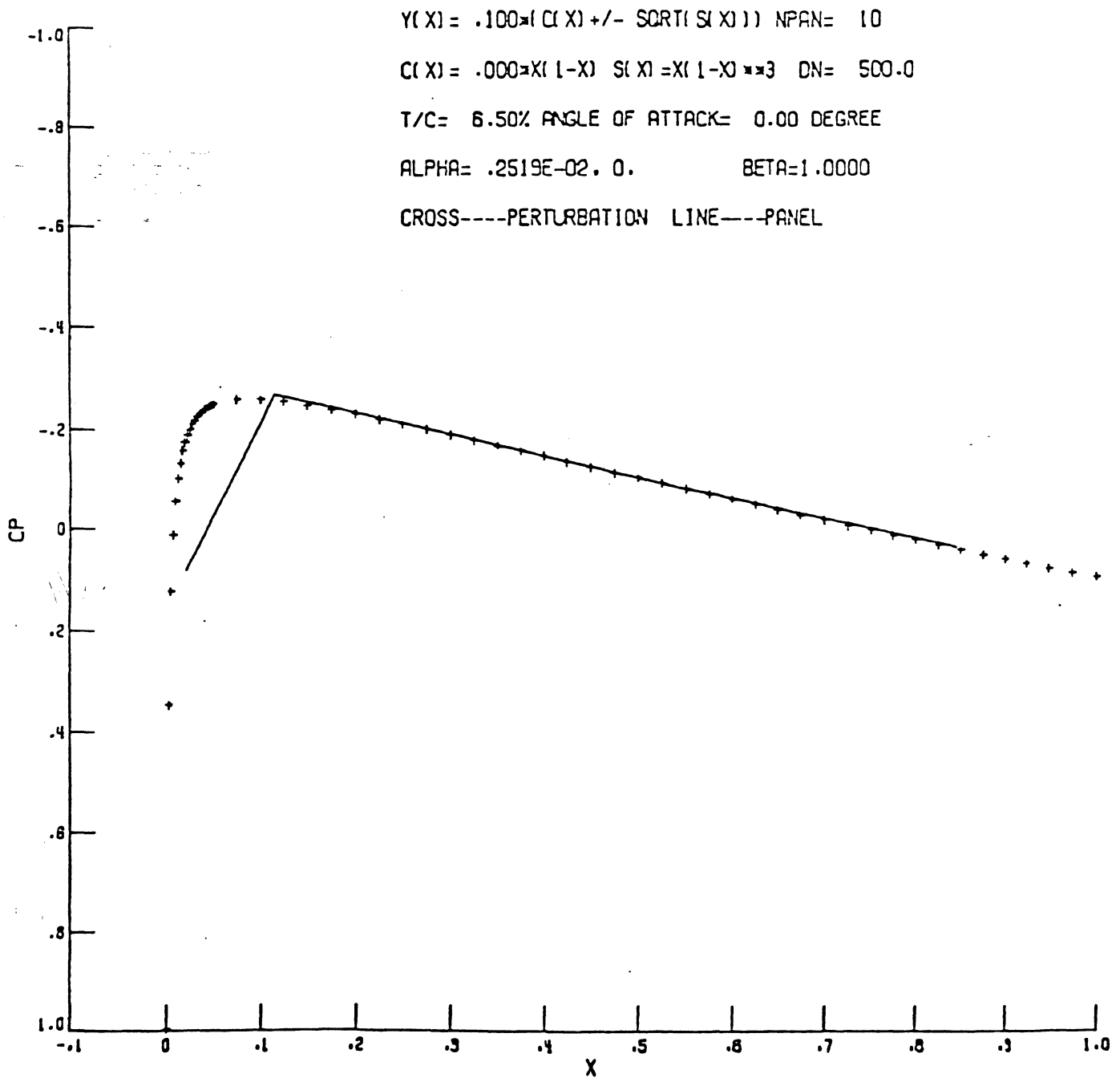
(b) $\epsilon = 0.10$; ϕ expanded up to ϵ^3 ; $t/C = 20\%$.

Fig. 4.9 Continued.



(c) $\epsilon = 0.15$; ϕ expanded up to ϵ^3 ; $t/C = 30\%$.

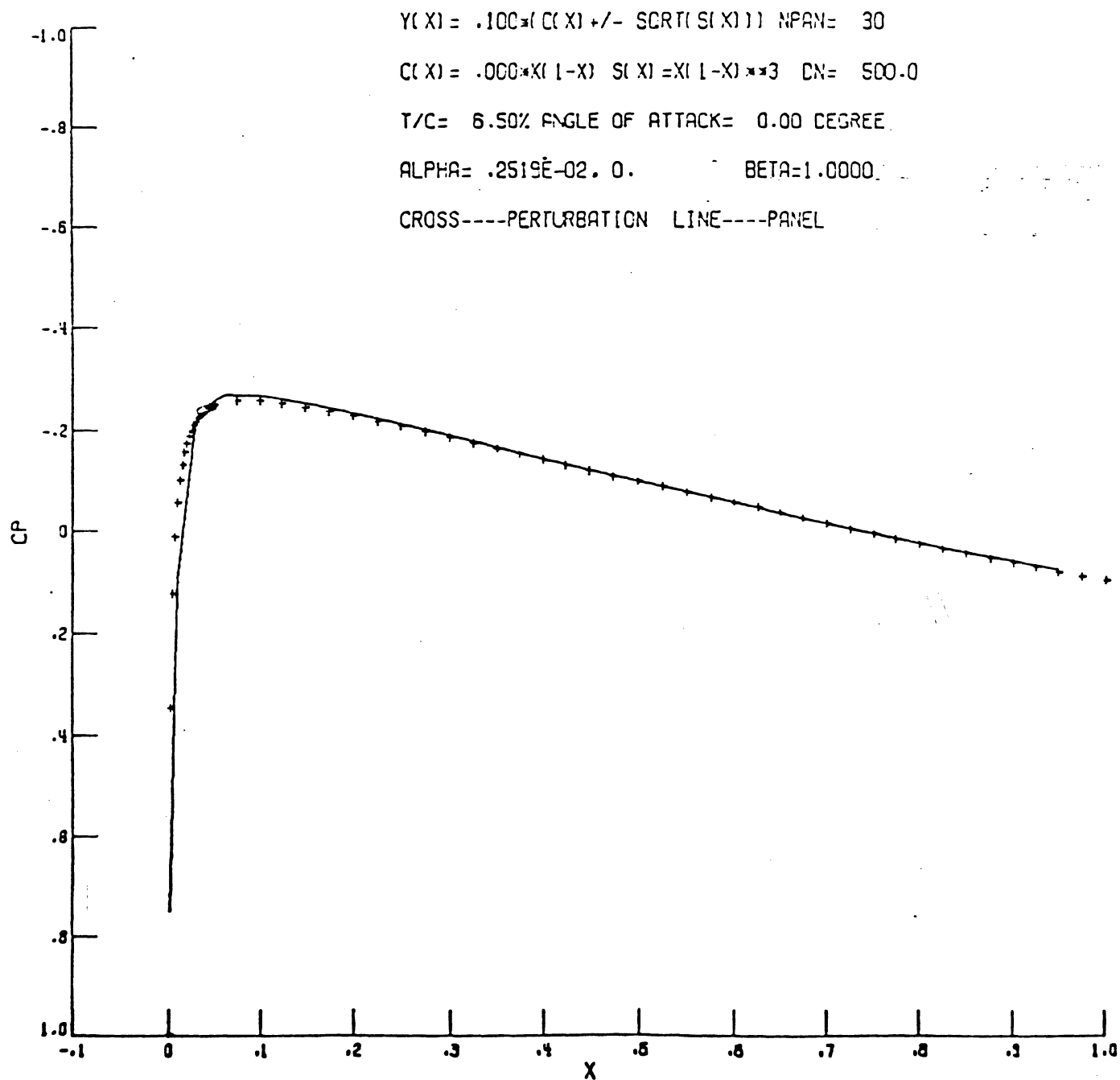
Figure 4.9 - Concluded.



(a) $\epsilon = 0.03248$; $\gamma = 0^0$; ϕ expanded up to ϵ^2 ; $t/C = 6.5\%$;

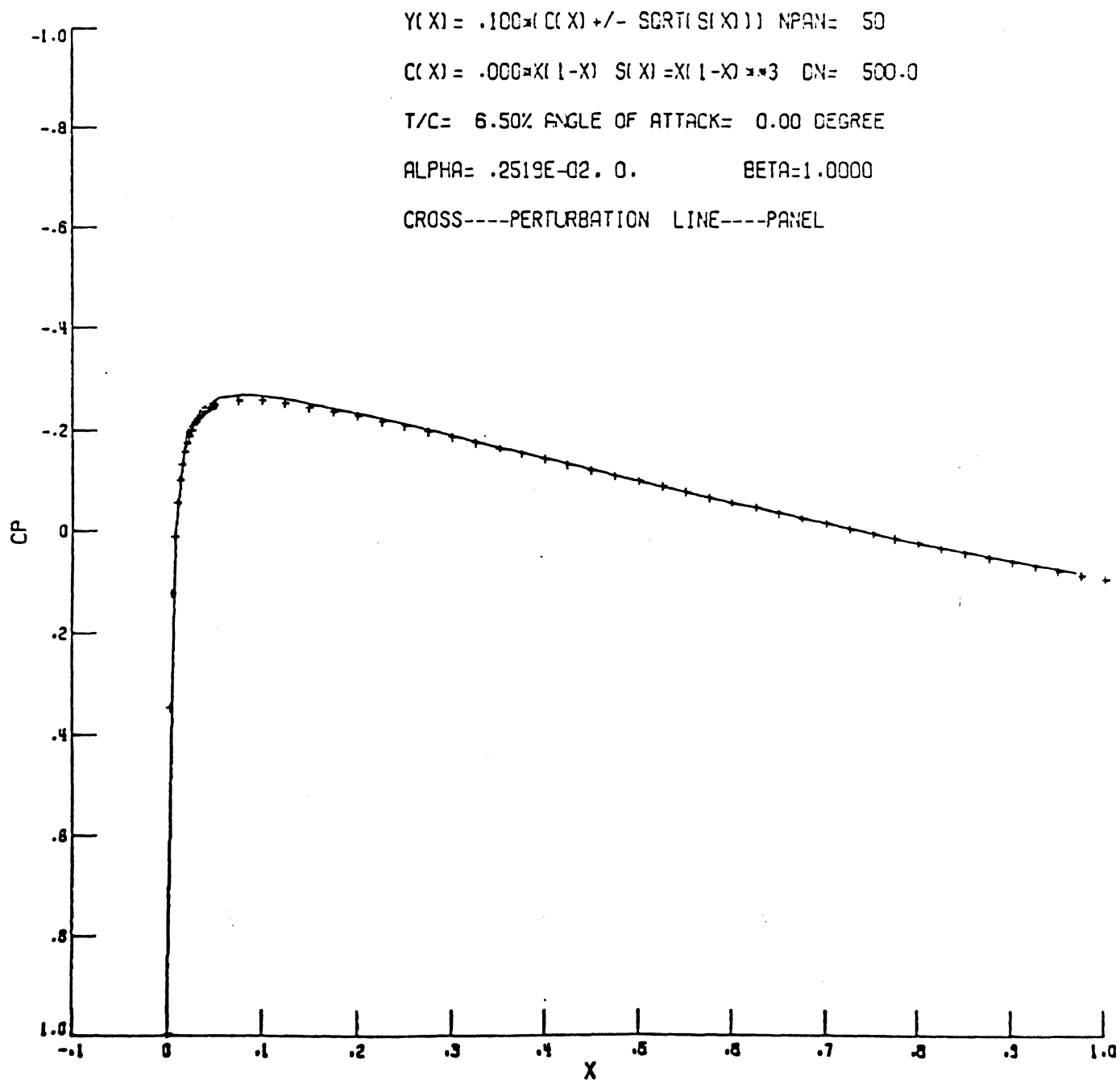
10 panels with cosine spacing.

Fig. 4.10 Comparison of pressure distributions from the perturbation analysis method with the panel method for symmetrical Joukowski airfoil.



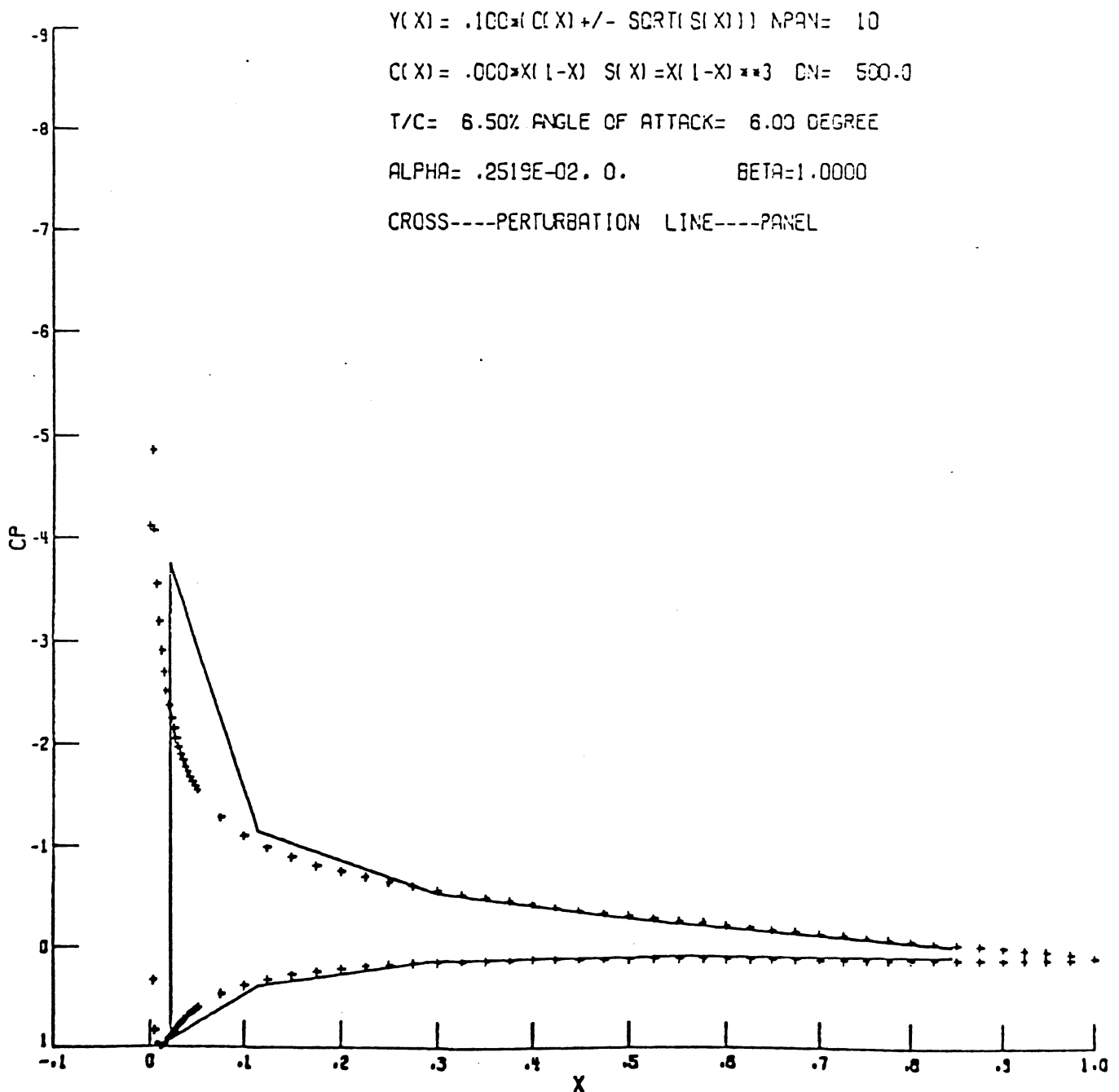
(b) $\epsilon = 0.03248$; $\gamma = 0^0$; ϕ expanded up to ϵ^2 ; $t/C = 6.5\%$;
 30 panels with cosine spacing.

Fig. 4.10 Continued.



(c) $\epsilon = 0.03248$; $\gamma = 0^0$; ϕ expanded up to ϵ^2 ; $t/C = 6.5\%$;
 50 panels with cosine spacing.

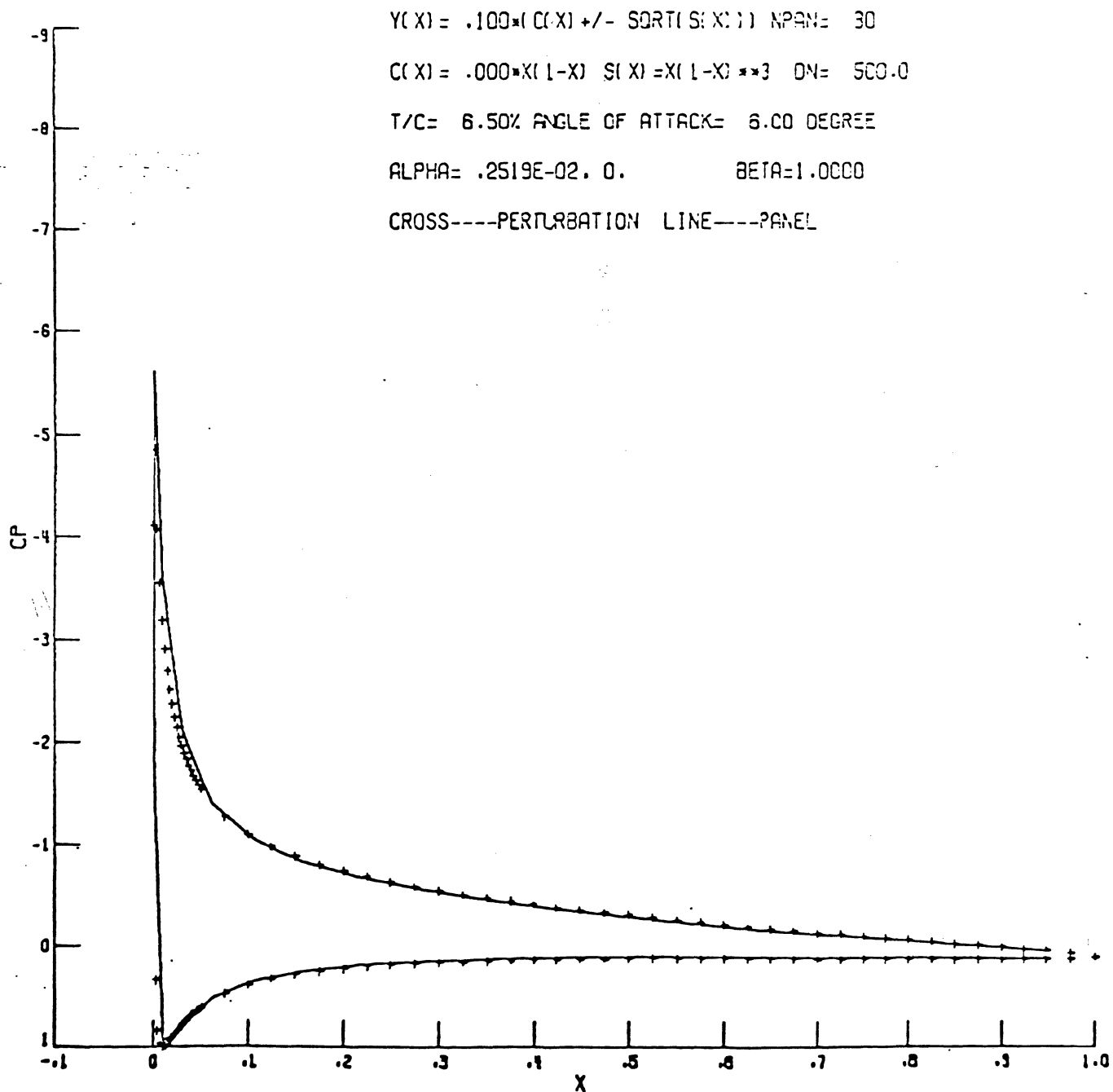
Fig. 4.10 Concluded.



(a) $\epsilon = 0.03248$; $\gamma = 6^0$; ϕ expanded up to ϵ^2 ; $t/C = 6.5\%$;

10 panels with cosine spacing.

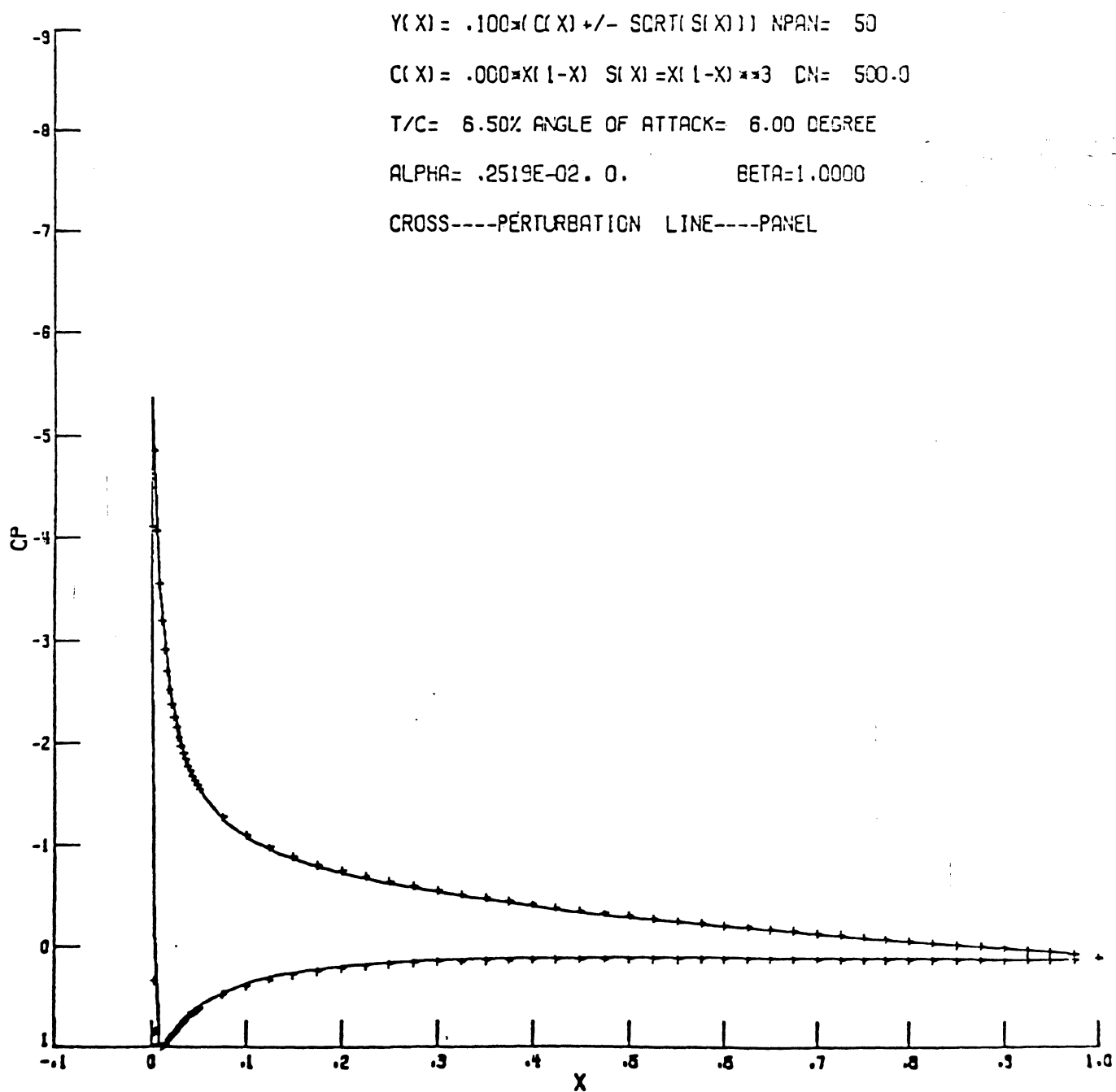
Fig. 4.11 Comparison of pressure distributions from the perturbation analysis method with the panel method for symmetrical Joukowski airfoil.



(b) $\epsilon = 0.03248$; $\gamma = 6^0$; ϕ expanded up to ϵ^2 ; $t/C = 6.5\%$;

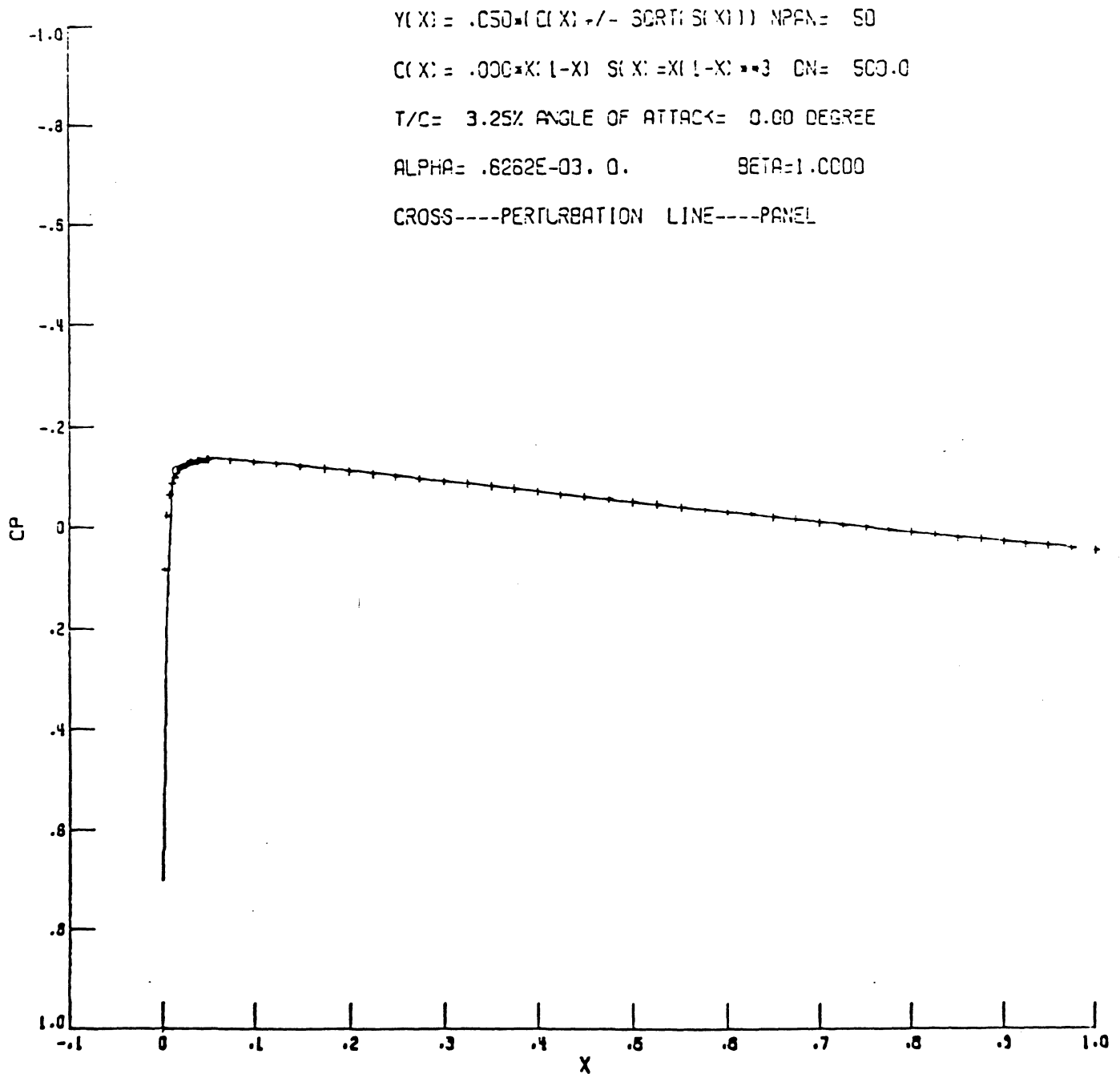
30 panels with cosine spacing.

Fig. 4.11 Continued.



(c) $\epsilon = 0.03248$; $\gamma = 6^\circ$; ϕ expanded up to ϵ^2 ; $t/C = 6.5\%$;
 50 panels with cosine spacing.

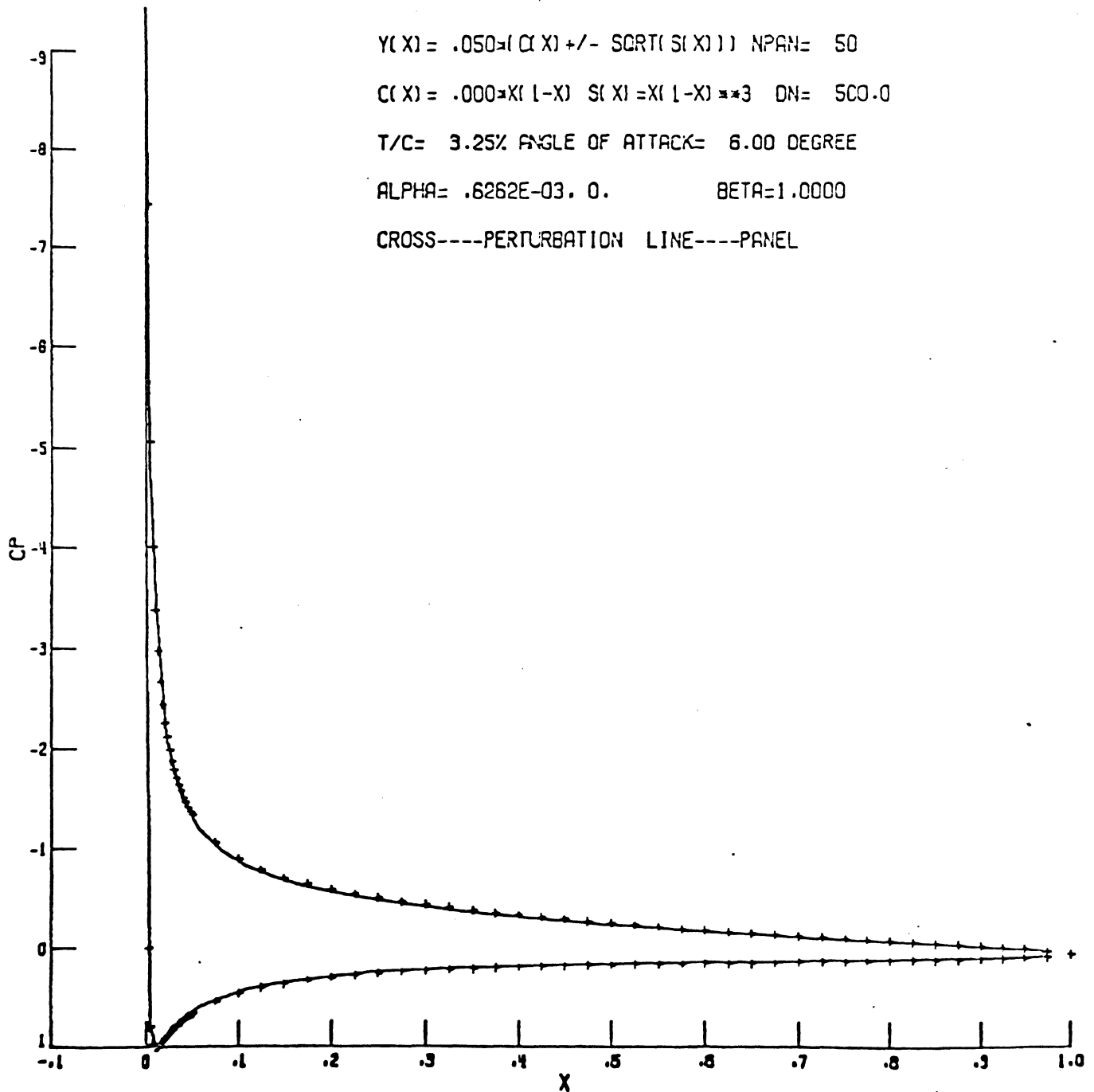
Fig. 4.11 Concluded.



(a) $\epsilon = 0.01624$; $\gamma = 0^0$; ϕ expanded up to ϵ^2 ; $t/C = 3.25\%$;

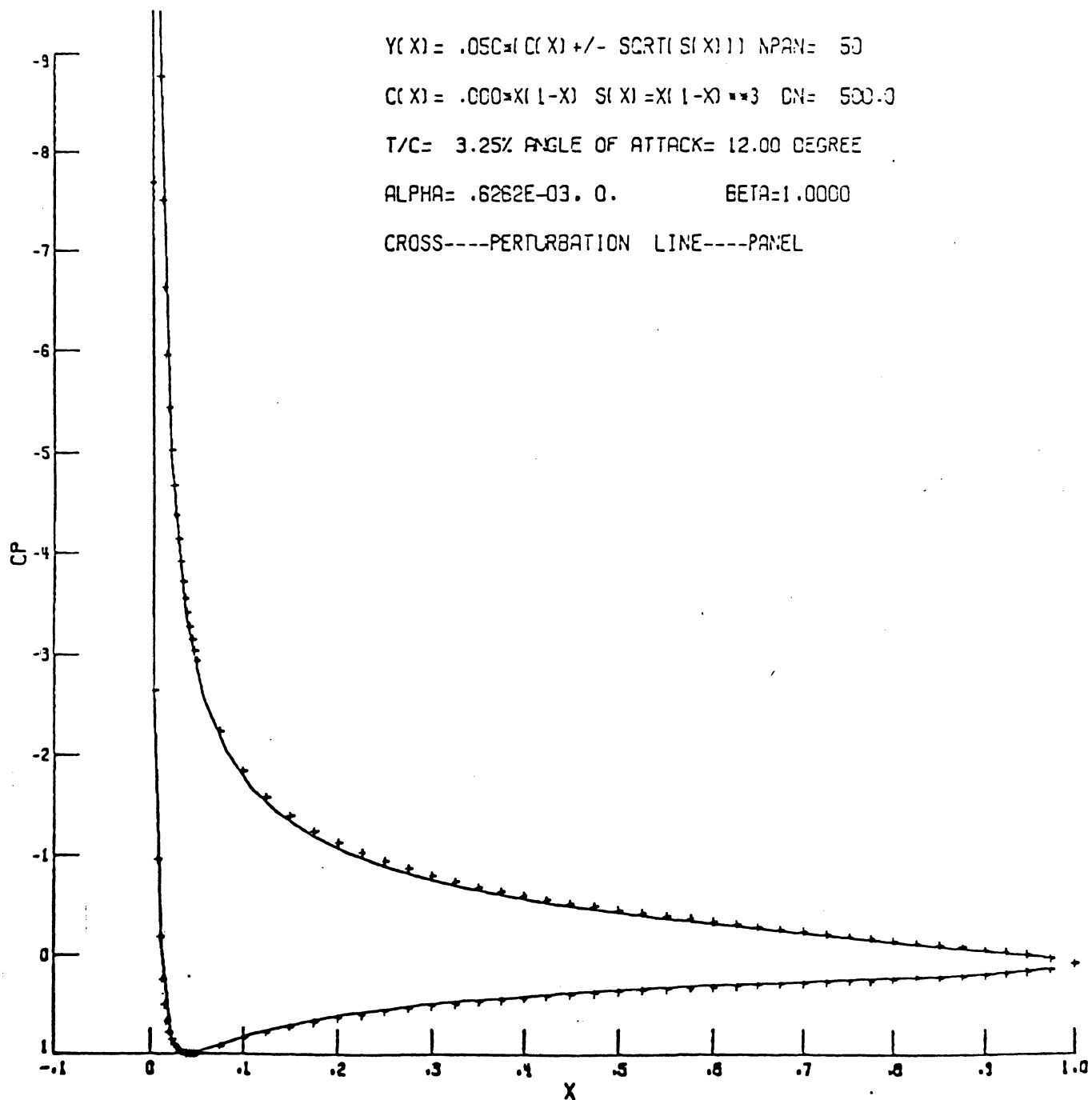
50 panels with cosine spacing.

Fig. 4.12 Comparison of pressure distributions from the perturbation analysis method with the panel method for symmetrical Joukowski airfoil.



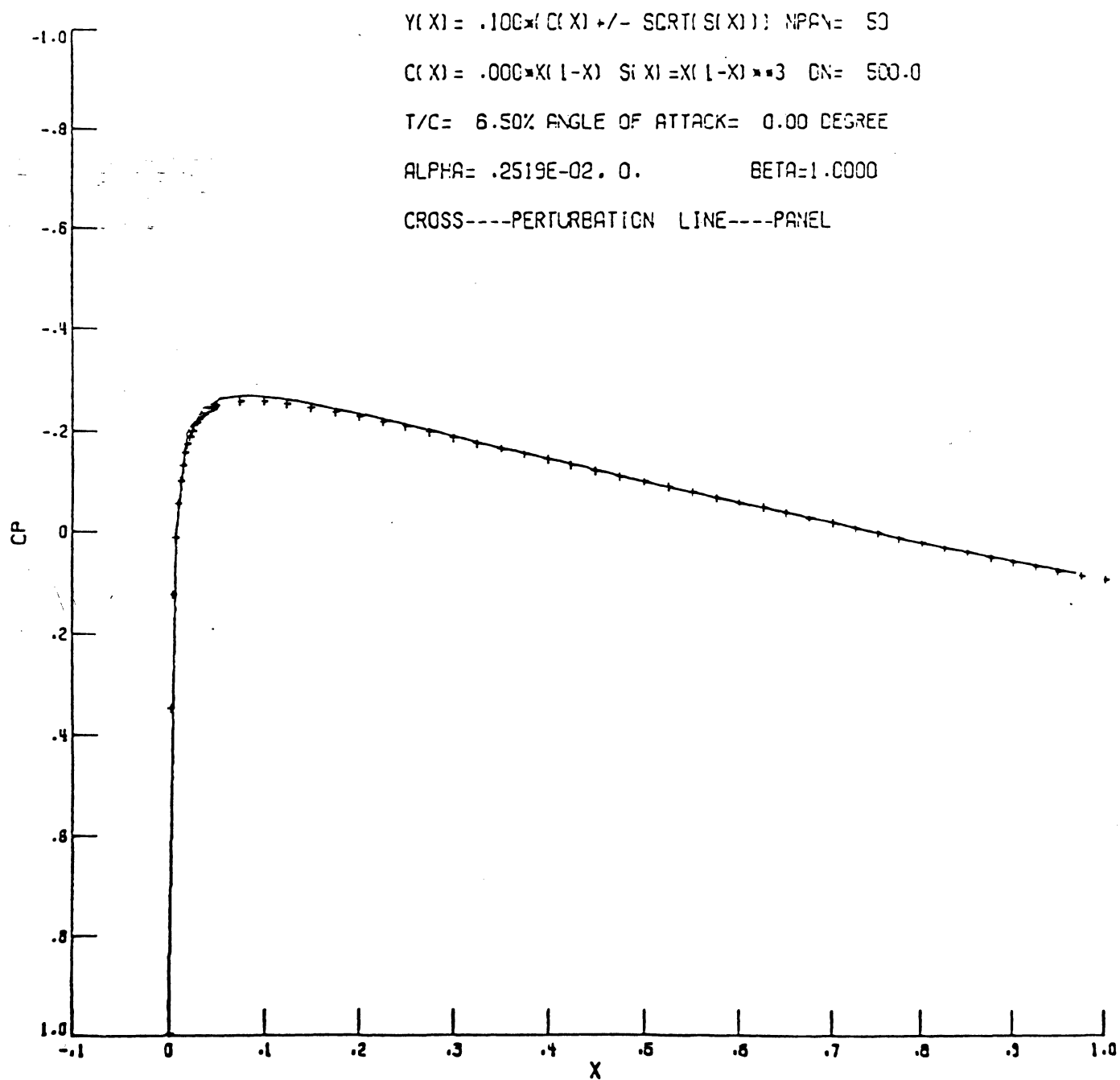
(b) $\epsilon = 0.01624$; $\gamma = 6^\circ$; ϕ expanded up to ϵ^2 ; $t/C = 3.25\%$;
 50 panels with cosine spacing.

Fig. 4.12 Continued.



(c) $\epsilon = 0.01624$; $\gamma = 12^\circ$; ϕ expanded up to ϵ^2 ; $t/C = 3.25\%$;
 50 panels with cosine spacing.

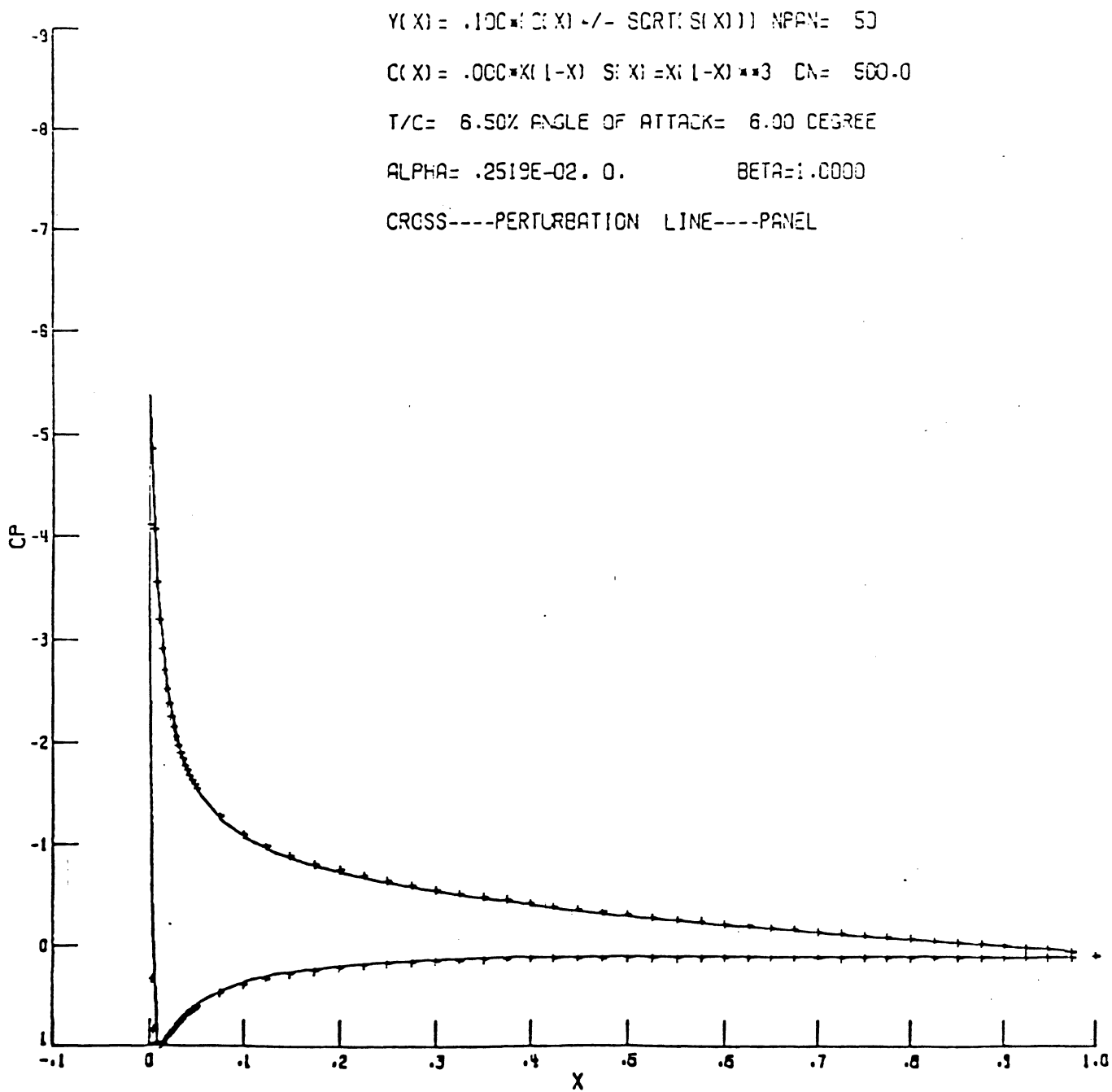
Fig. 4.12 Concluded.



(a) $\epsilon = 0.03248$; $\gamma = 0^\circ$; ϕ expanded up to ϵ^2 ; $t/C = 6.5\%$;

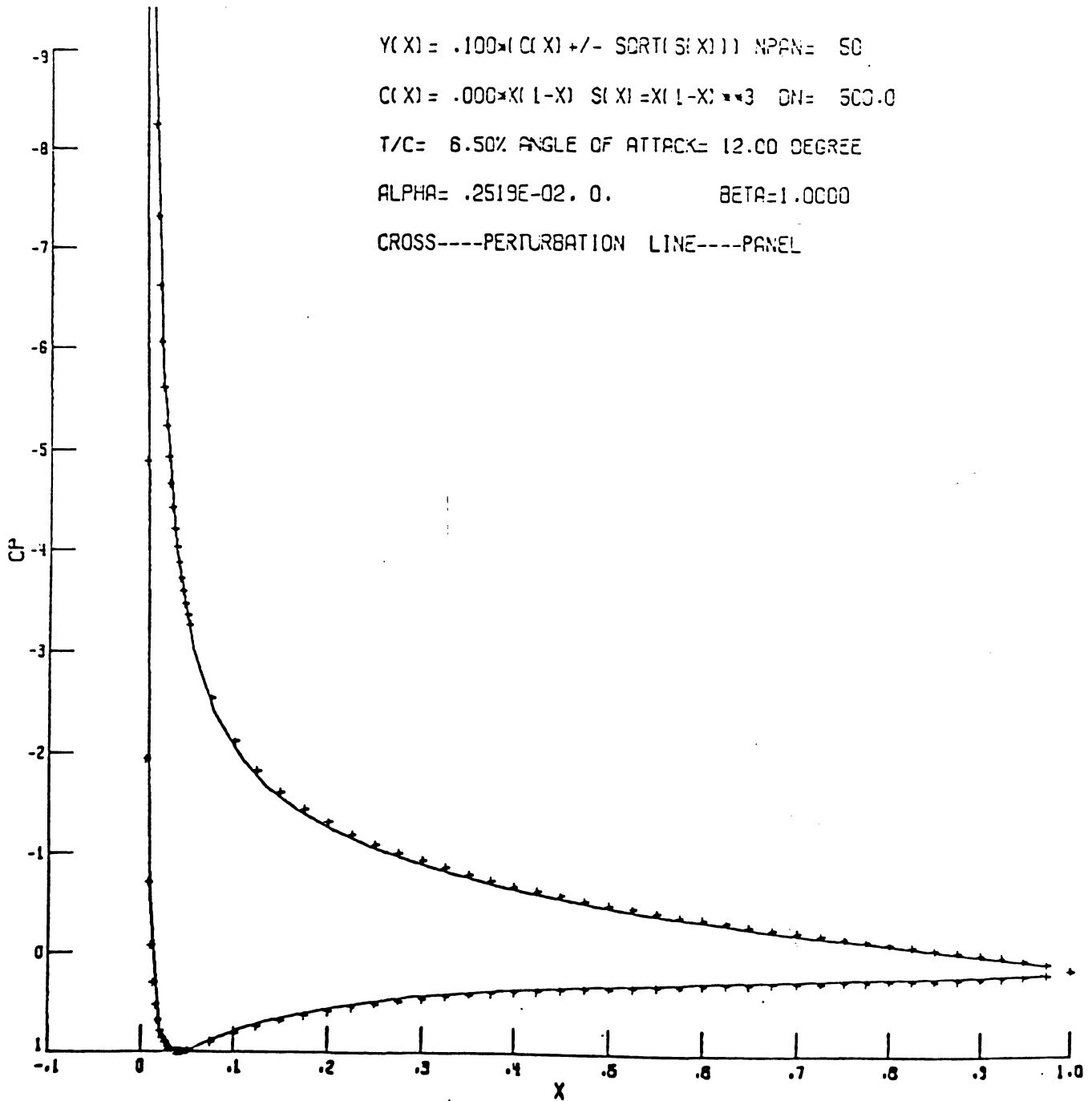
50 panels with cosine spacing.

Fig. 4.13 Comparison of pressure distributions from the perturbation analysis method with the panel method for symmetrical Joukowski airfoil.



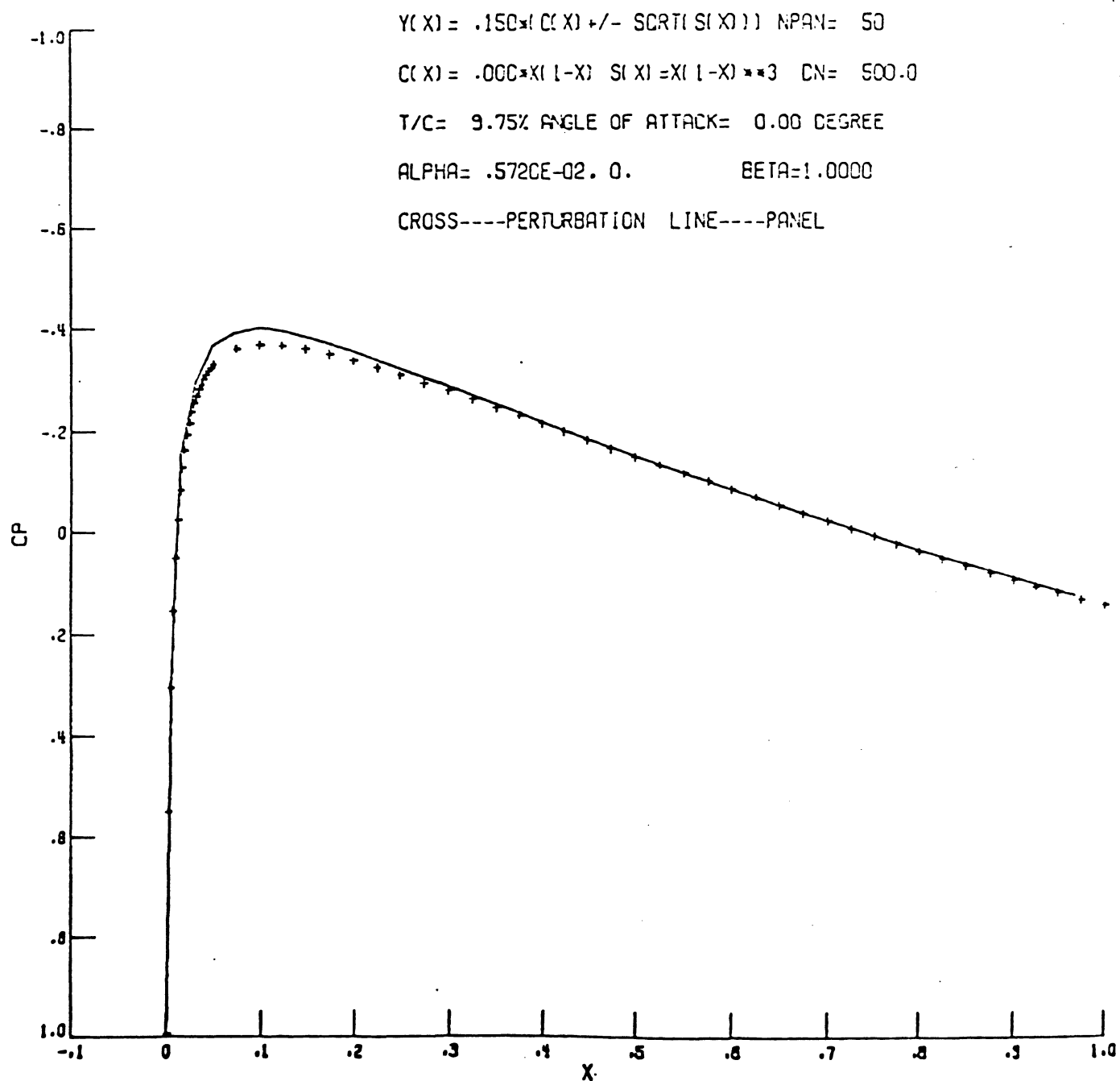
(b) $\epsilon = 0.03248$; $\gamma = 6^\circ$; ϕ expanded up to ϵ^2 ; $t/C = 6.5\%$;
 50 panels with cosine spacing.

Fig. 4.13 Continued.



(c) $\varepsilon = 0.03248$; $\gamma = 12^\circ$; ϕ expanded up to ε^2 ; $t/C = 6.5\%$;
 50 panels with cosine spacing.

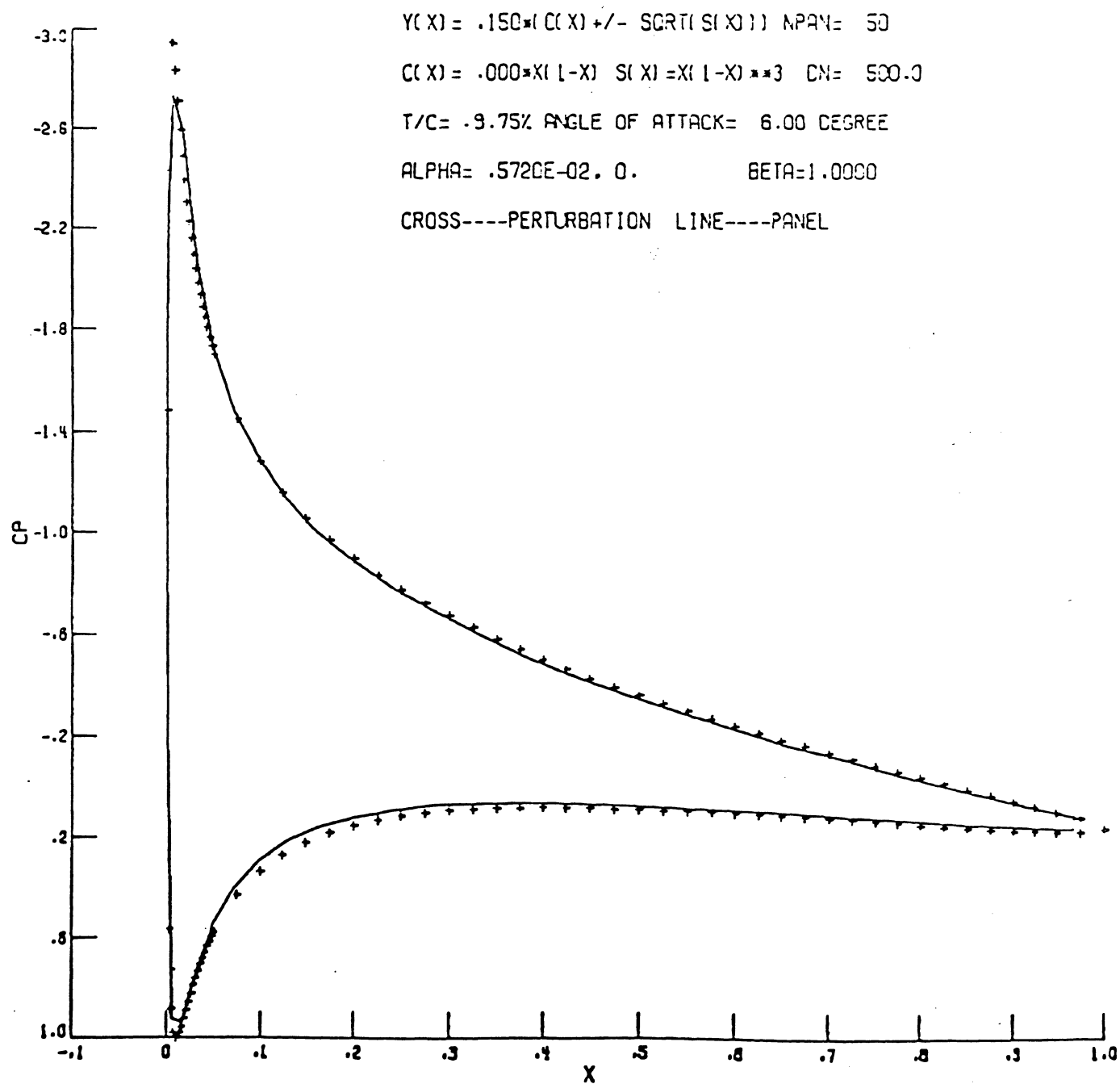
Fig. 4.13 Concluded.



(a) $\epsilon = 0.04872$; $\gamma = 0^0$; ϕ expanded up to ϵ^2 ; $t/C = 9.75\%$;

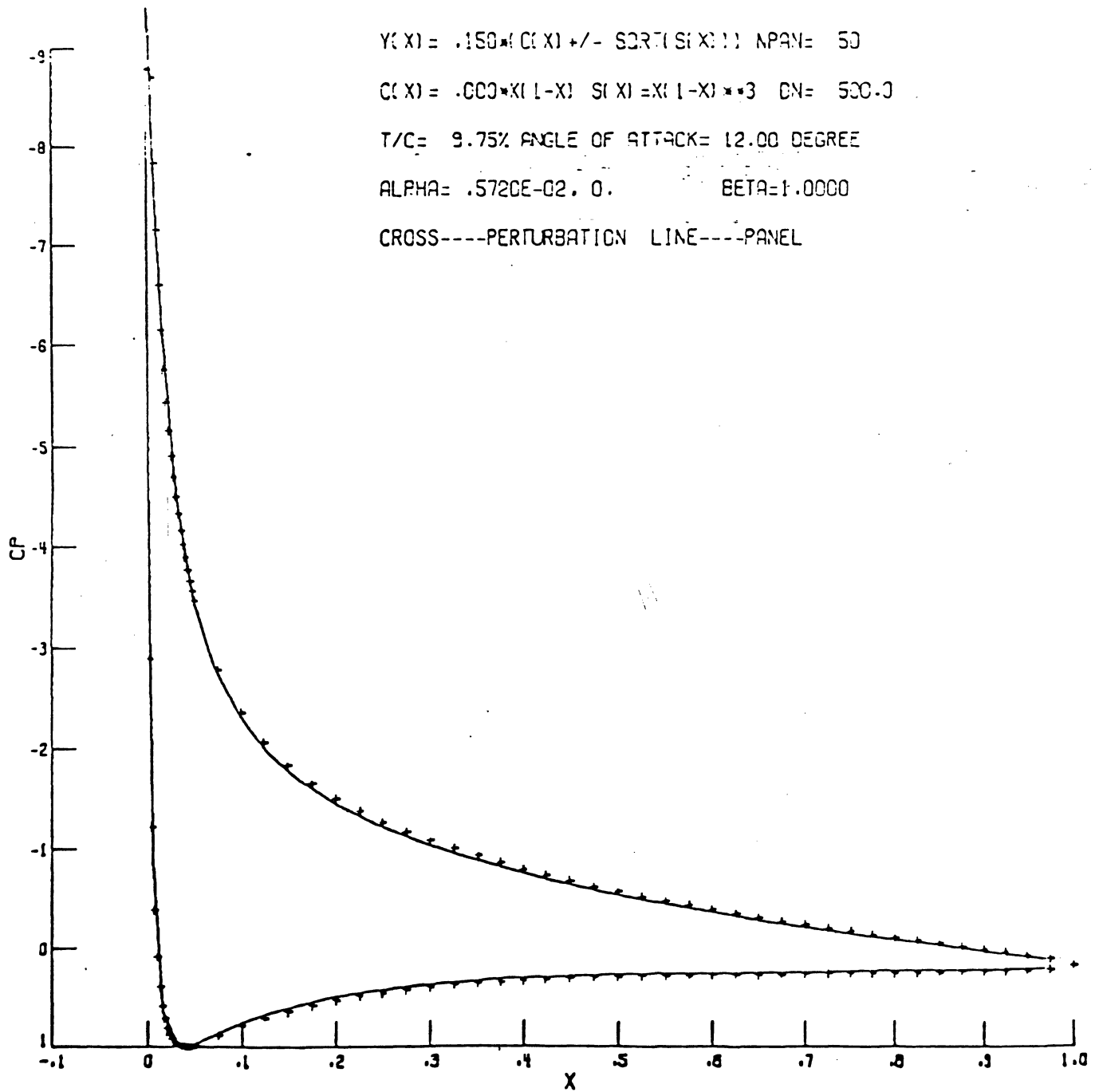
50 panels with cosine spacing.

Fig. 4.14 Comparison of pressure distributions from the perturbation analysis method with the panel method for symmetrical Joukowski airfoil.



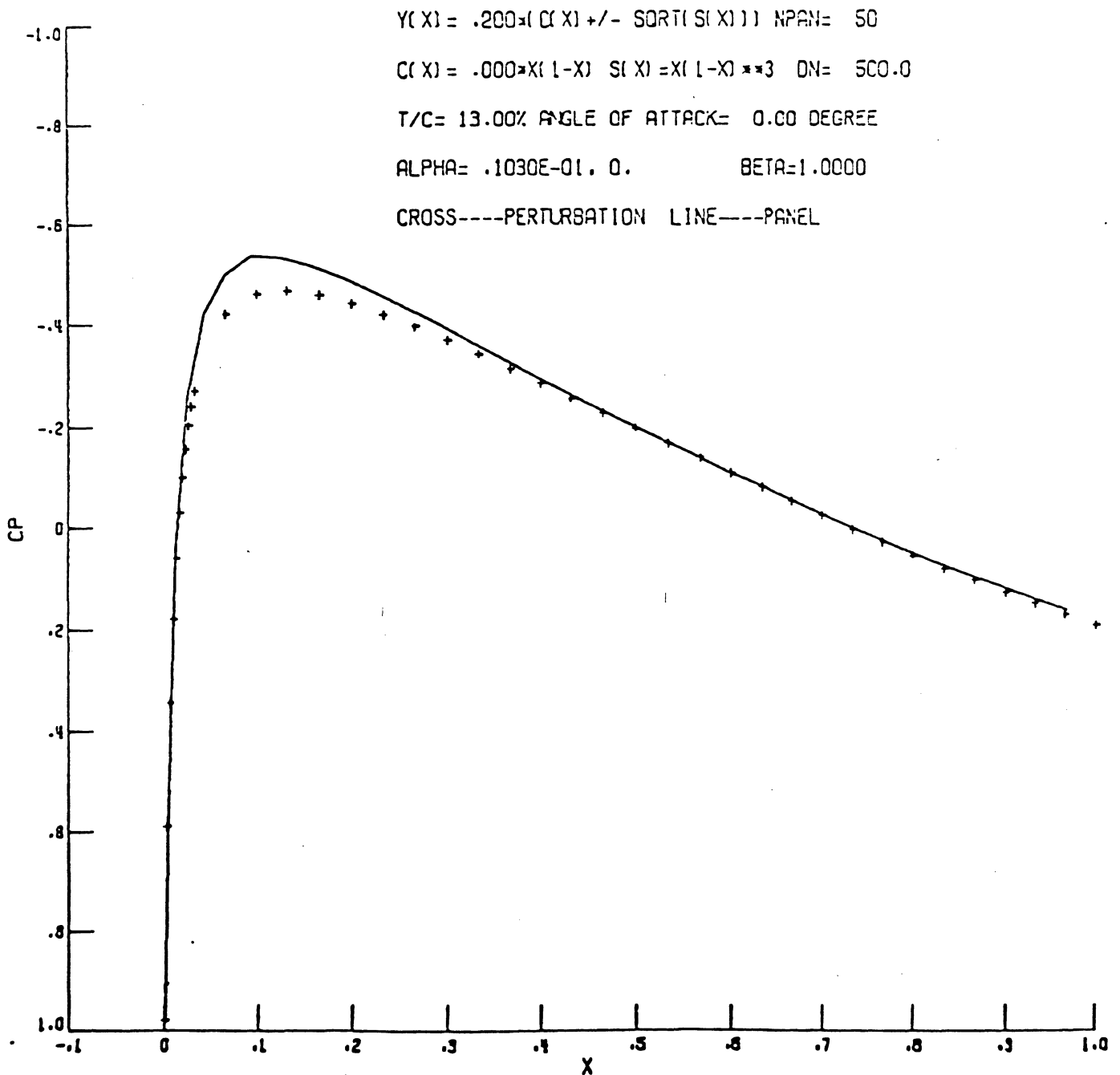
(b) $\epsilon = 0.04872$; $\gamma = 6^\circ$; ϕ expanded up to ϵ^2 ; $t/C = 9.75\%$;
 50 panels with cosine spacing.

Fig. 4.14 Continued.



(c) $\epsilon = 0.04872$; $\gamma = 12^\circ$; ϕ expanded up to ϵ^2 ; $t/C = 9.75\%$;
 50 panels with cosine spacing.

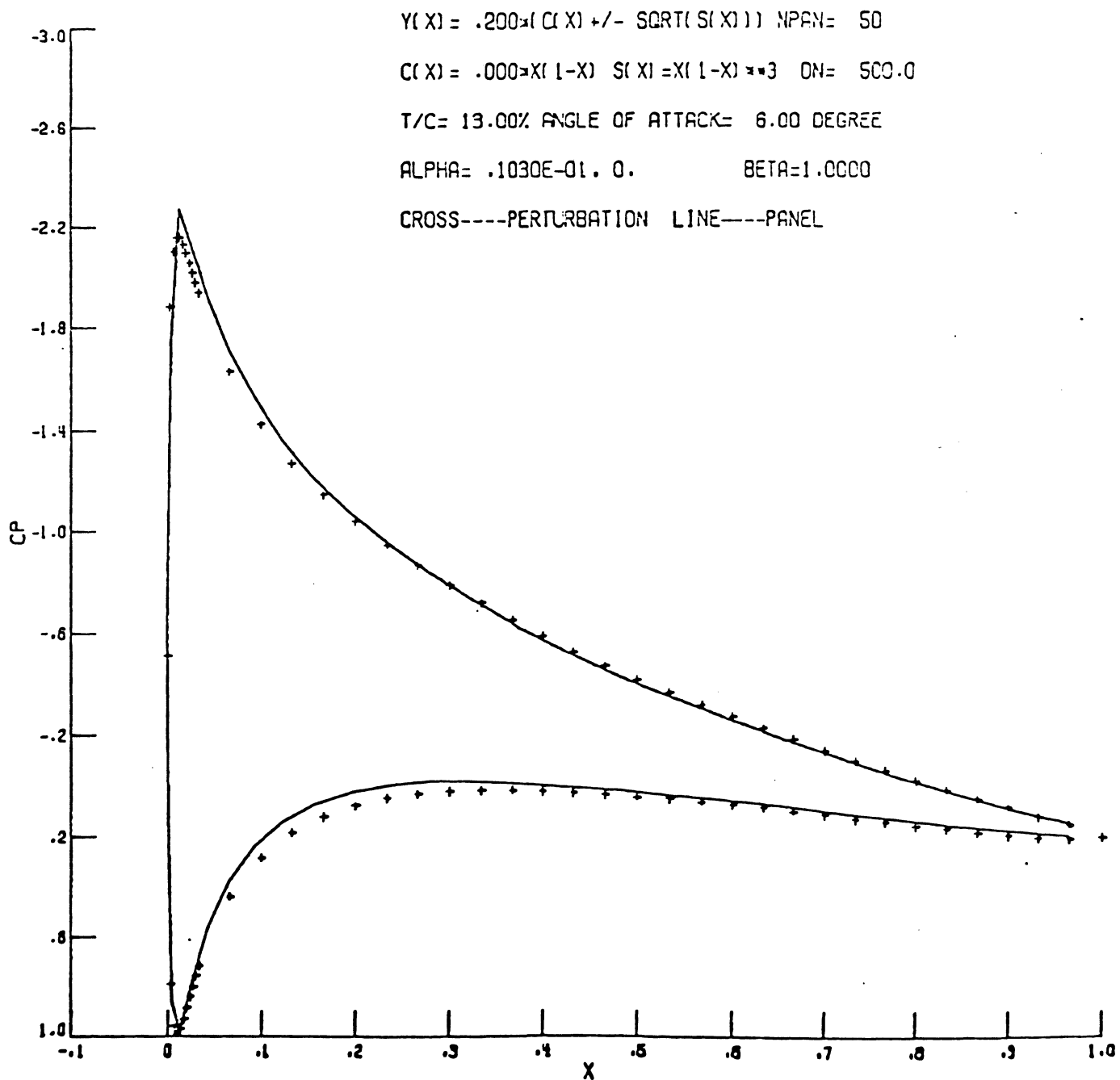
Fig. 4.14 Concluded.



(a) $\epsilon = 0.06496$; $\gamma = 0^\circ$; ϕ expanded up to ϵ^2 ; $t/c = 13\%$;

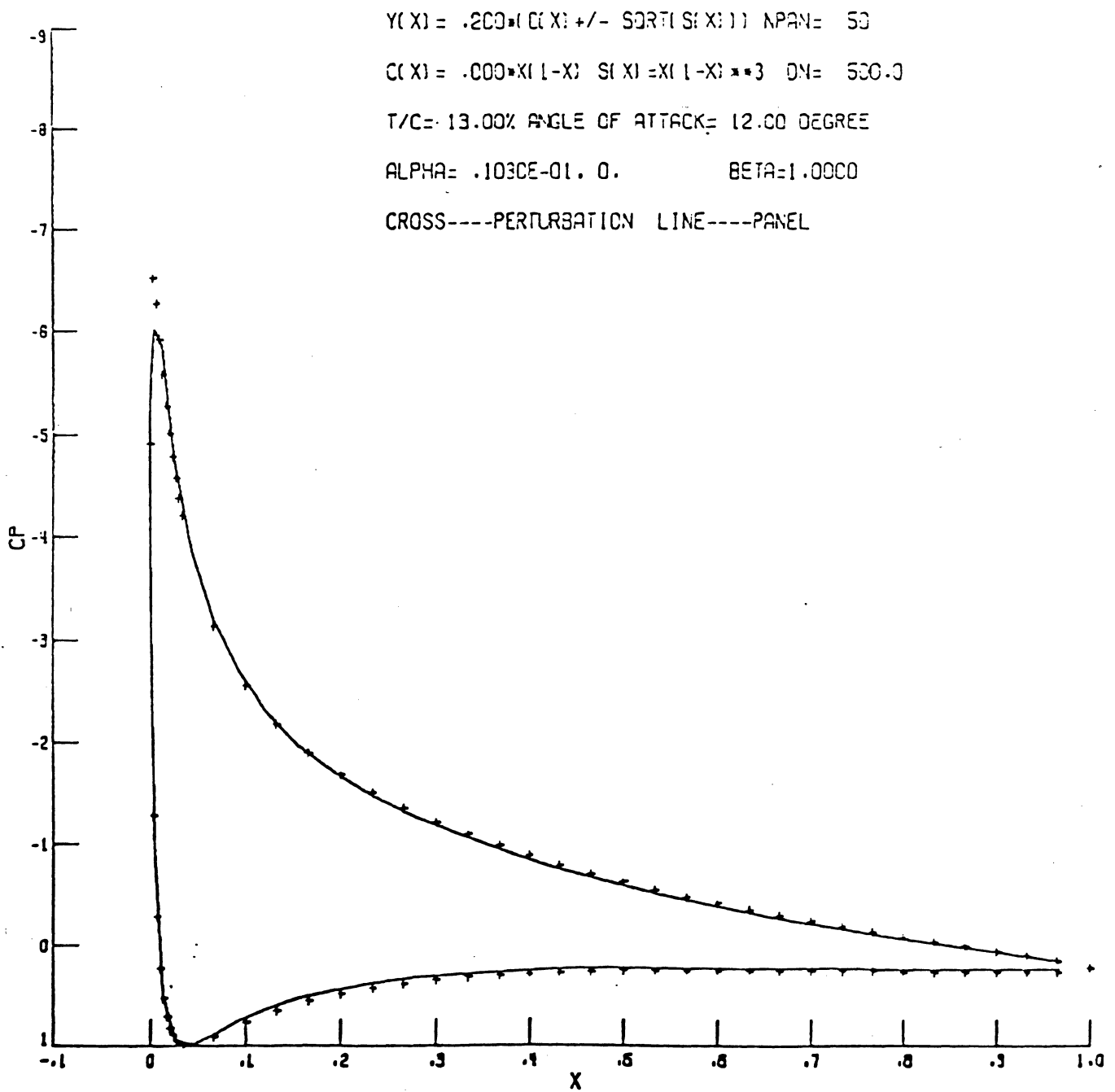
50 panels with cosine spacing.

Fig. 4.15 Comparison of pressure distributions from the perturbation analysis method with the panel method for symmetrical Joukowski airfoil.



(b) $\epsilon = 0.06496$; $\gamma = 6^\circ$; ϕ expanded up to ϵ^2 ; $t/C = 13\%$;
 50 panels with cosine spacing.

Fig. 4.15 Continued.

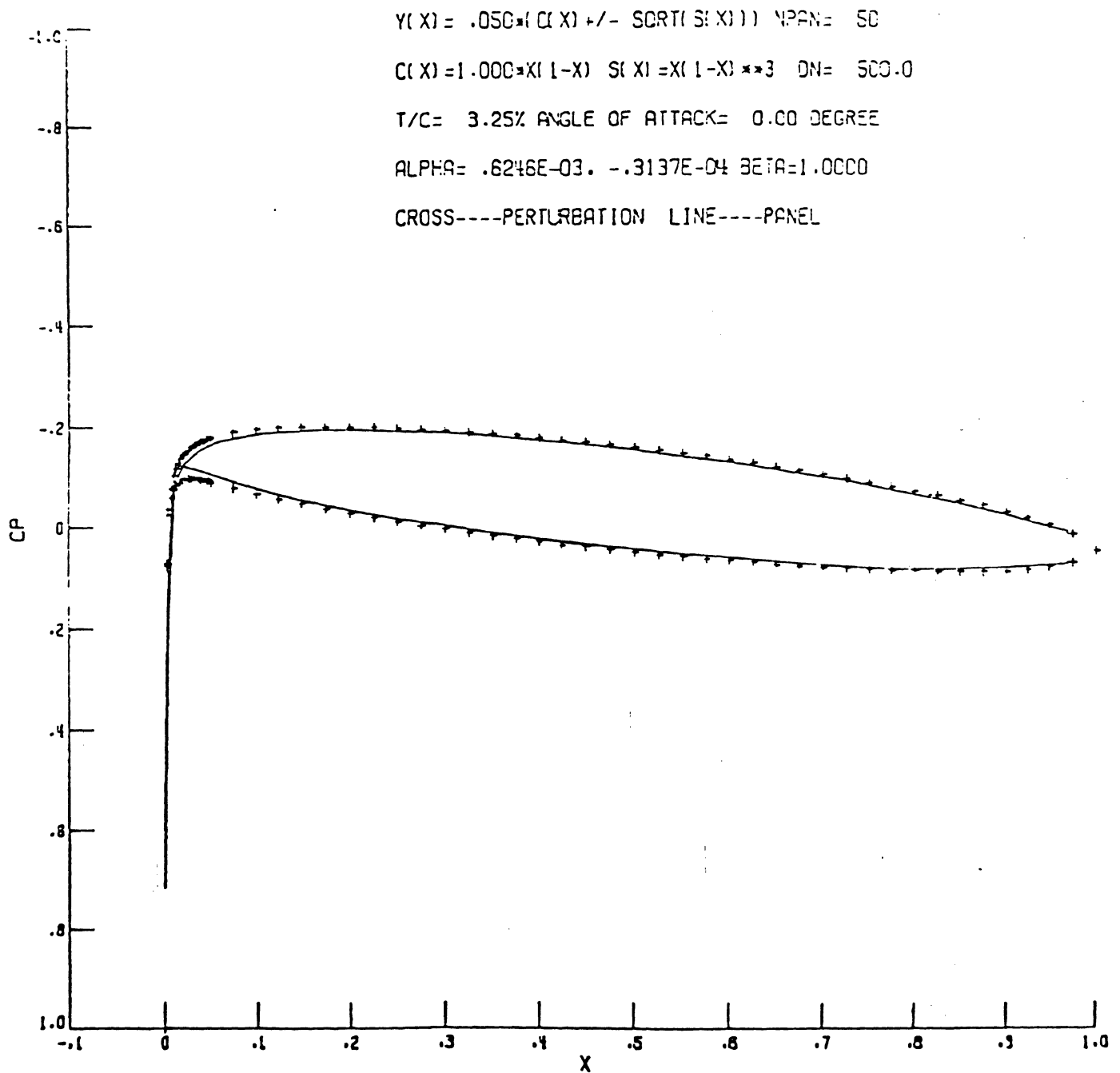


(c) $\epsilon = 0.06496$; $\gamma = 12^\circ$; ϕ expanded up to ϵ^2 ; $t/C = 13\%$;
 50 panels with cosine spacing.

Fig. 4.15 Concluded.

Table 4.1 Comparison of lift coefficients of the perturbation, panel and exact solutions for the symmetrical Joukowski airfoils

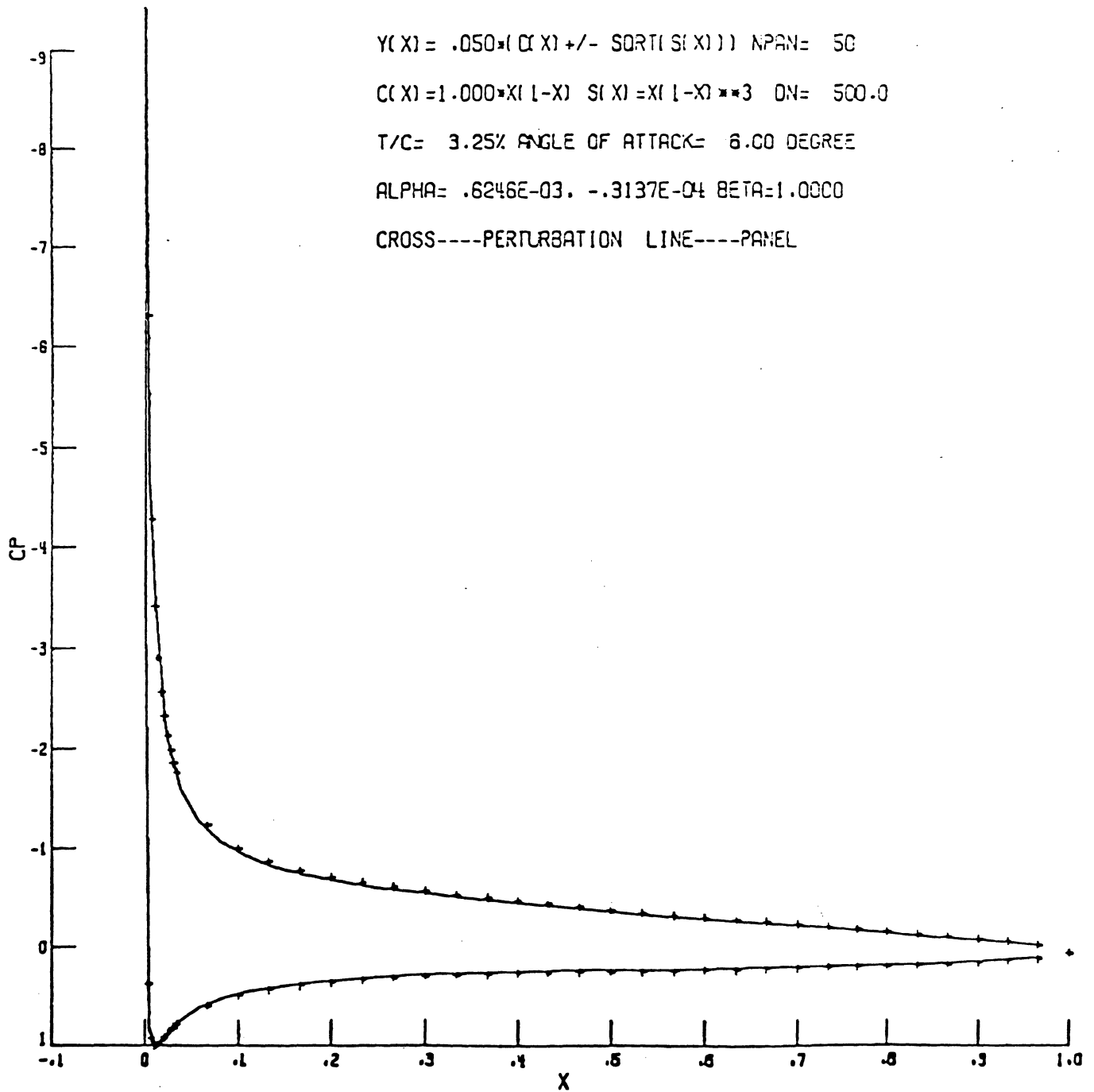
Slenderness ratio ϵ	Exact $C_{l,ex}$	Perturbation $C_{l,pt}$	Panel $C_{l,pn}$	$\frac{C_{l,pt} - C_{l,ex}}{C_{l,ex}} \times 100\%$	$\frac{C_{l,pn} - C_{l,ex}}{C_{l,ex}} \times 100\%$
$\gamma = 6^\circ$					
0.06496	0.71588	0.72245	0.67684	0.92	-5.45
0.04872	0.70234	0.70603	0.66472	0.53	-5.36
0.03248	0.68797	0.68961	0.65377	0.24	-4.97
0.01624	0.67278	0.67319	0.63080	0.06	-6.24
$\gamma = 12^\circ$					
0.06496	1.42391	1.43698	1.34485	0.92	-5.55
0.04872	1.39698	1.40432	1.32128	0.53	-5.42
0.03248	1.36840	0.37167	1.29823	0.24	-5.13
0.01624	1.33819	1.33901	1.23750	0.06	-7.52



(a) $\epsilon = 0.02688$; $\gamma = 0^0$; ϕ expanded up to ϵ^2 ; $t/C = 3.25\%$;

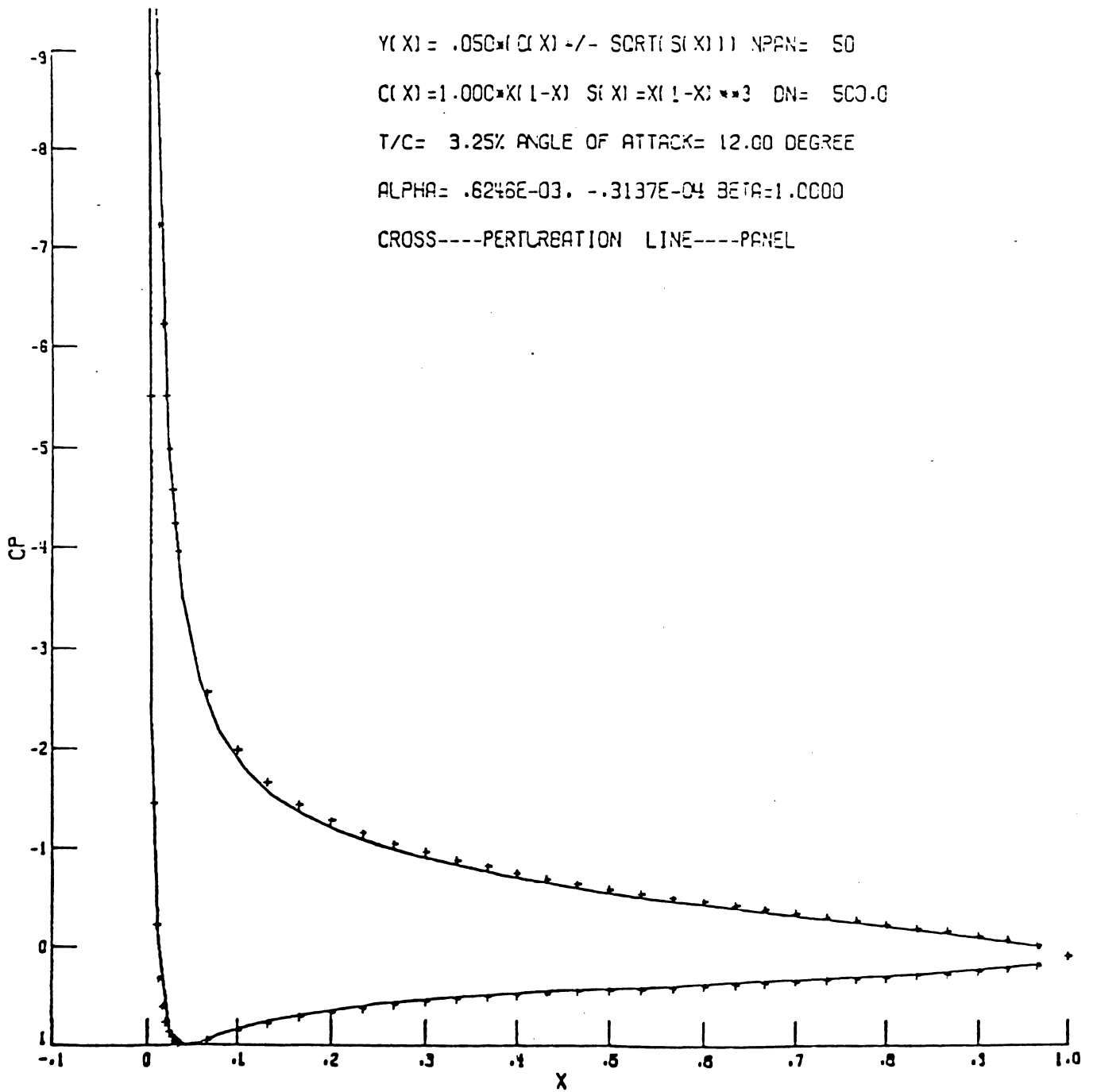
50 panels with cosine spacing.

Fig. 4.16 Comparison of pressure distributions from the perturbation analysis method with the panel method for cambered Joukowski airfoil.



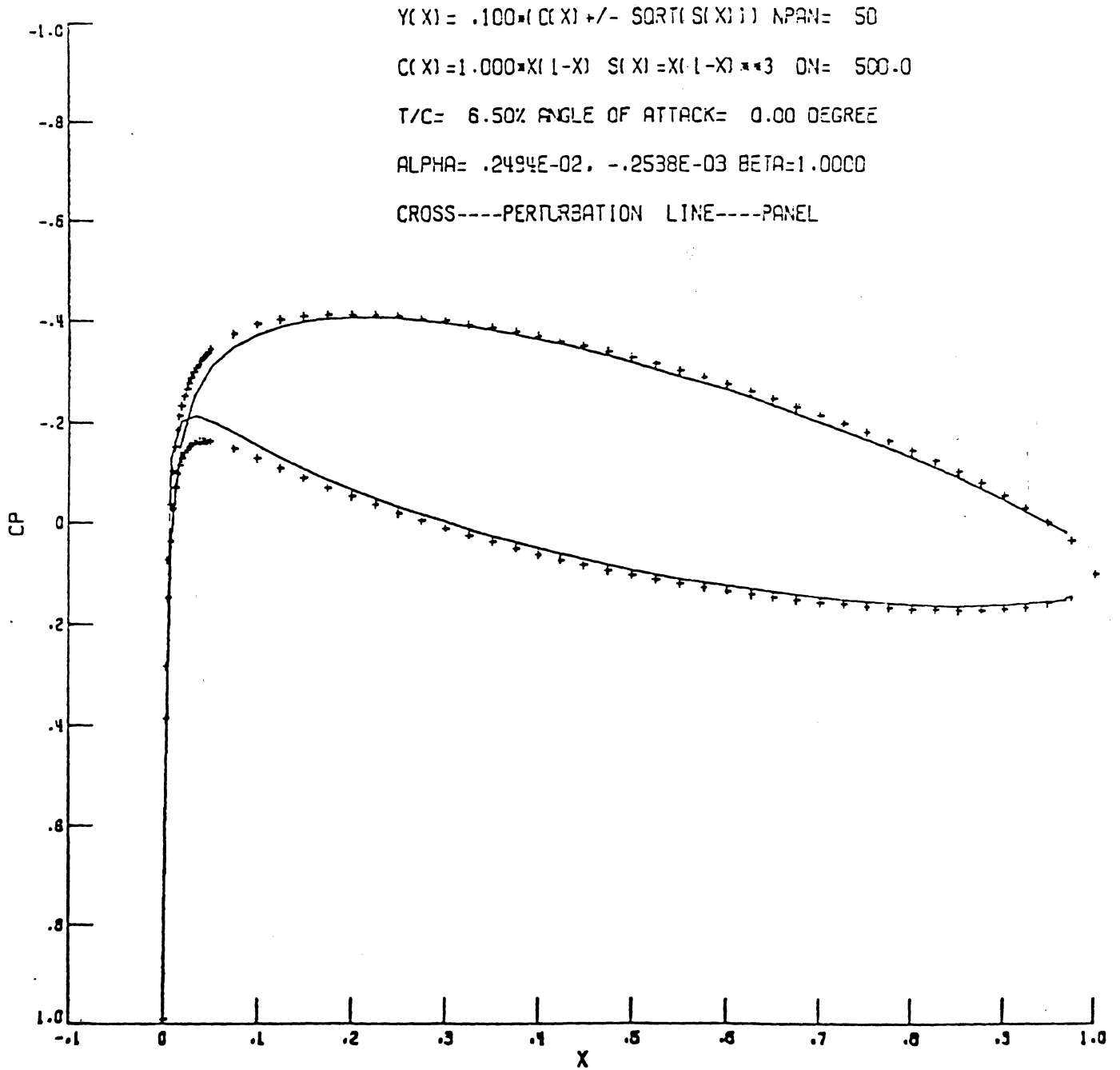
(b) $\epsilon = 0.02688$; $\gamma = 6^\circ$; ϕ expanded up to ϵ^2 ; $t/C = 3.25\%$;
 50 panels with cosine spacing.

Fig. 4.16 Continued.



(c) $\epsilon = 0.02688$; $\gamma = 12^\circ$; ϕ expanded up to ϵ^2 ; $t/C = 3.25\%$;
 50 panels with cosine spacing.

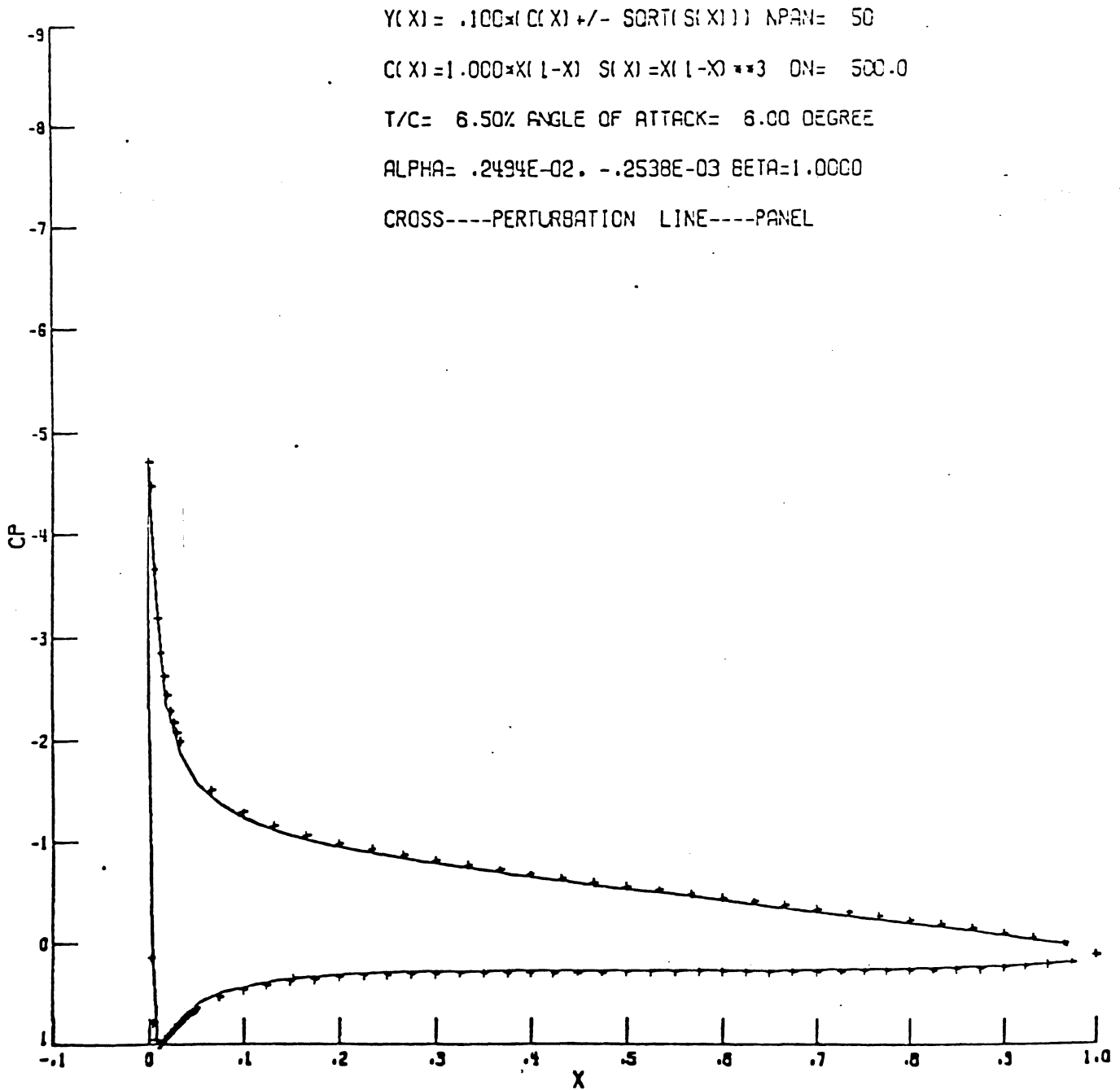
Fig. 4.16 Concluded.



(a) $\epsilon = 0.05376$; $\gamma = 0^0$; ϕ expanded up to ϵ^2 ; $t/C = 6.5\%$;

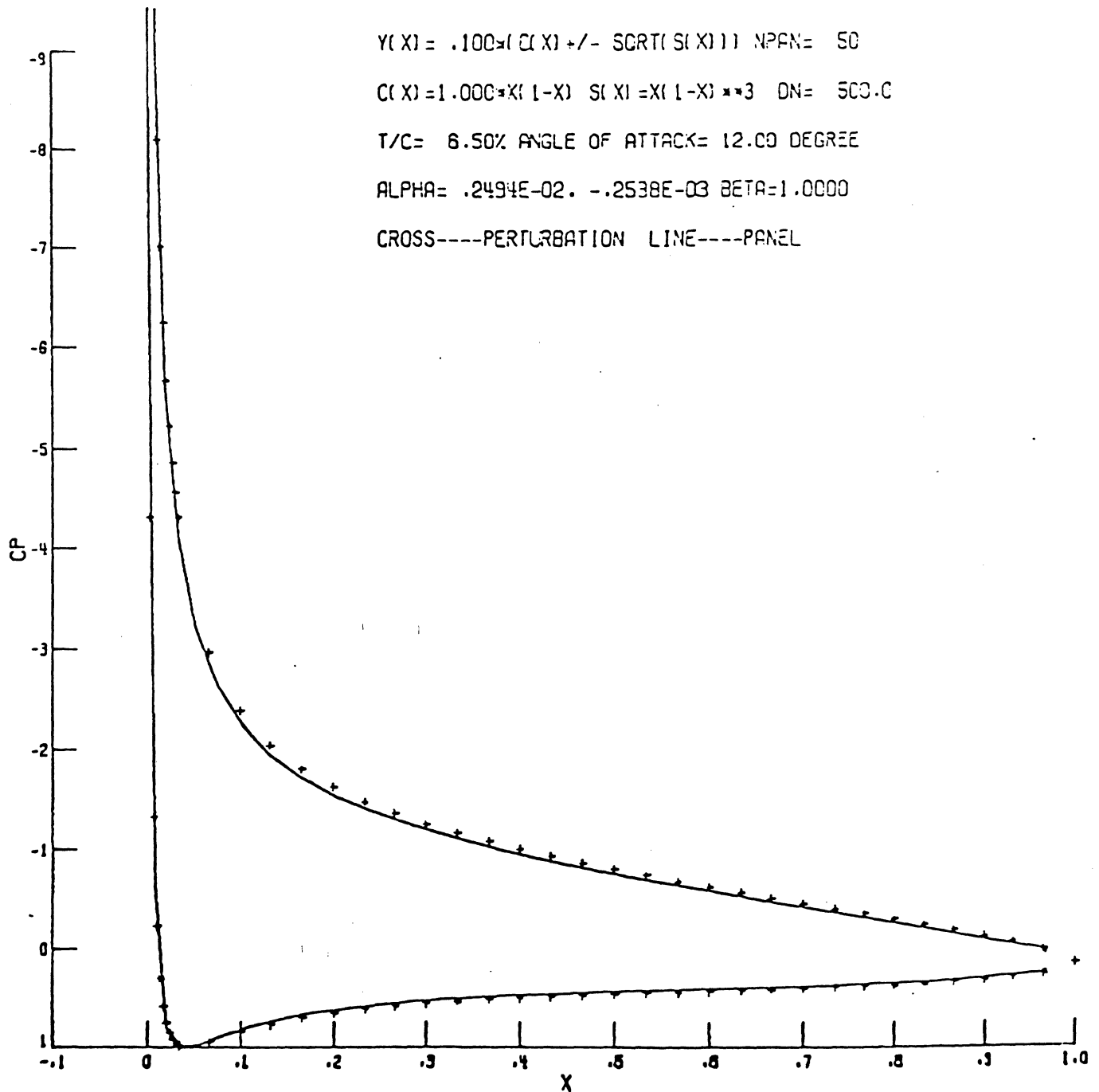
50 panels with cosine spacing.

Fig. 4.17 Comparison of pressure distributions from the perturbation analysis method with the panel method for cambered Joukowski airfoil.



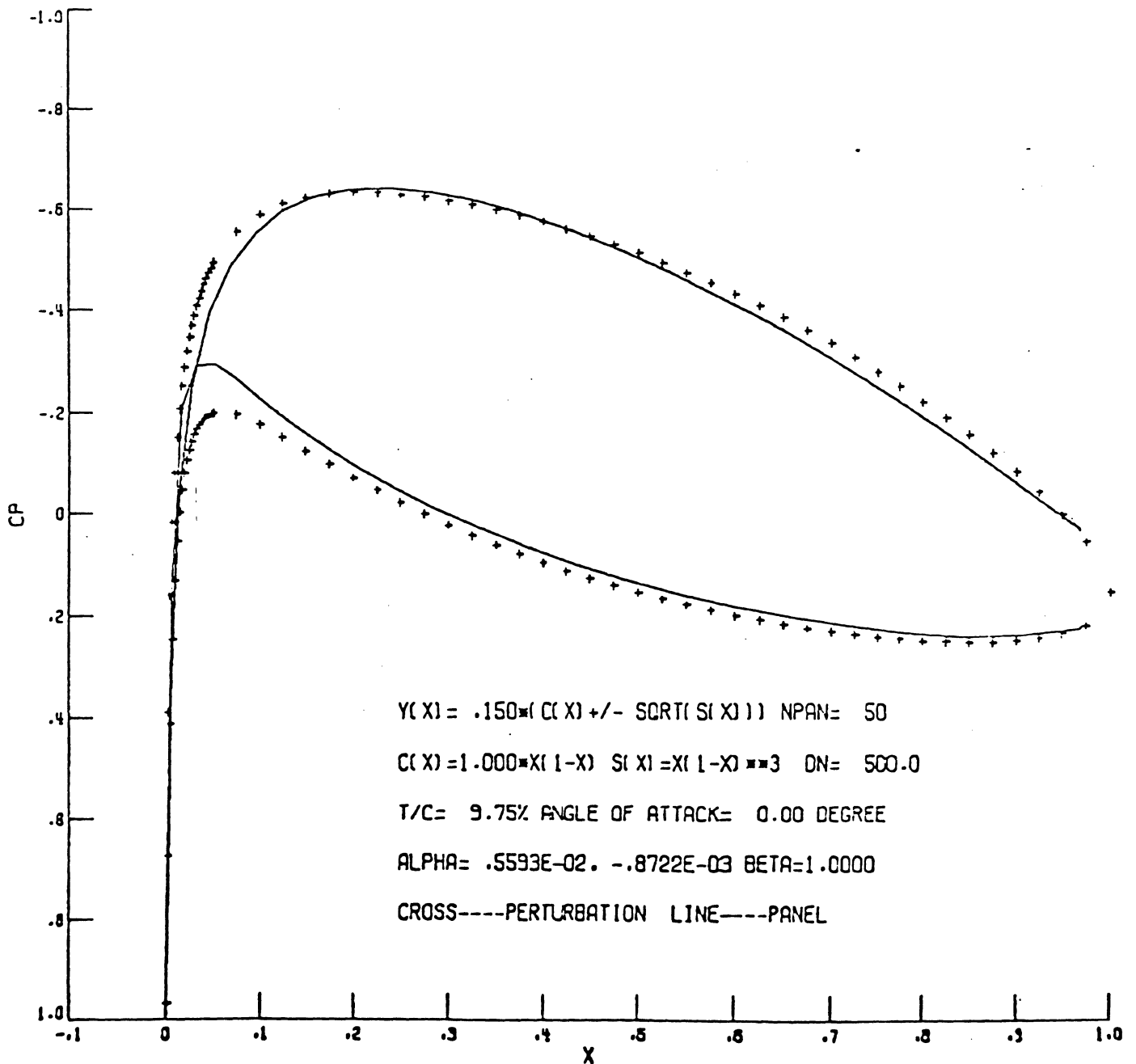
(b) $\epsilon = 0.05376$; $\gamma = 6^\circ$; ϕ expanded up to ϵ^2 ; $t/C = 6.5\%$;
 50 panels with cosine spacing.

Fig. 4.17 Continued.



(c) $\epsilon = 0.05376$; $\gamma = 12^\circ$; ϕ expanded up to ϵ^2 ; $t/C = 6.5\%$;
 50 panels with cosine spacing.

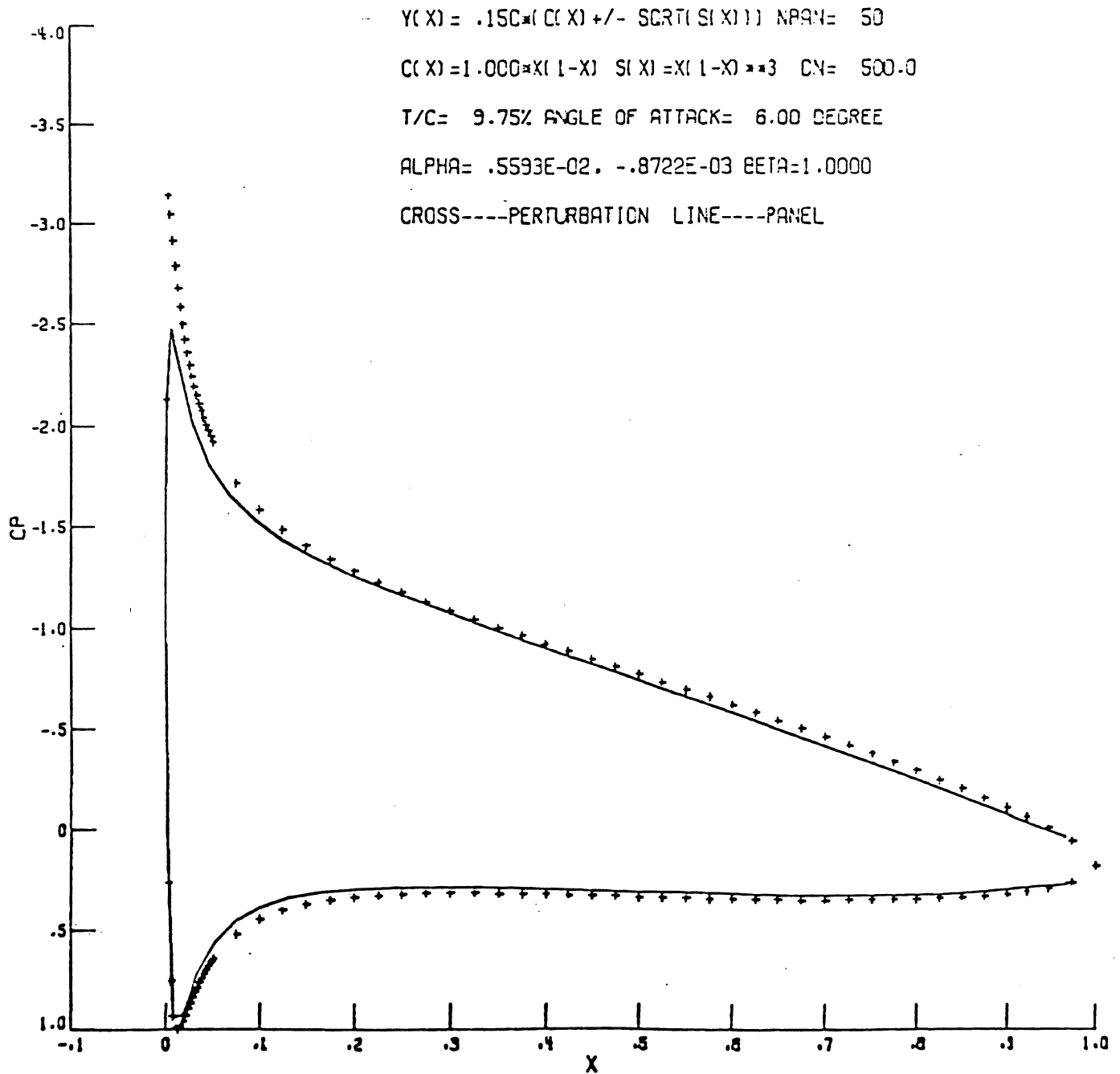
Fig. 4.17 Concluded.



(a) $\epsilon = 0.08064$; $\gamma = 0^0$; ϕ expanded up to ϵ^2 ; $t/C = 9.75\%$;

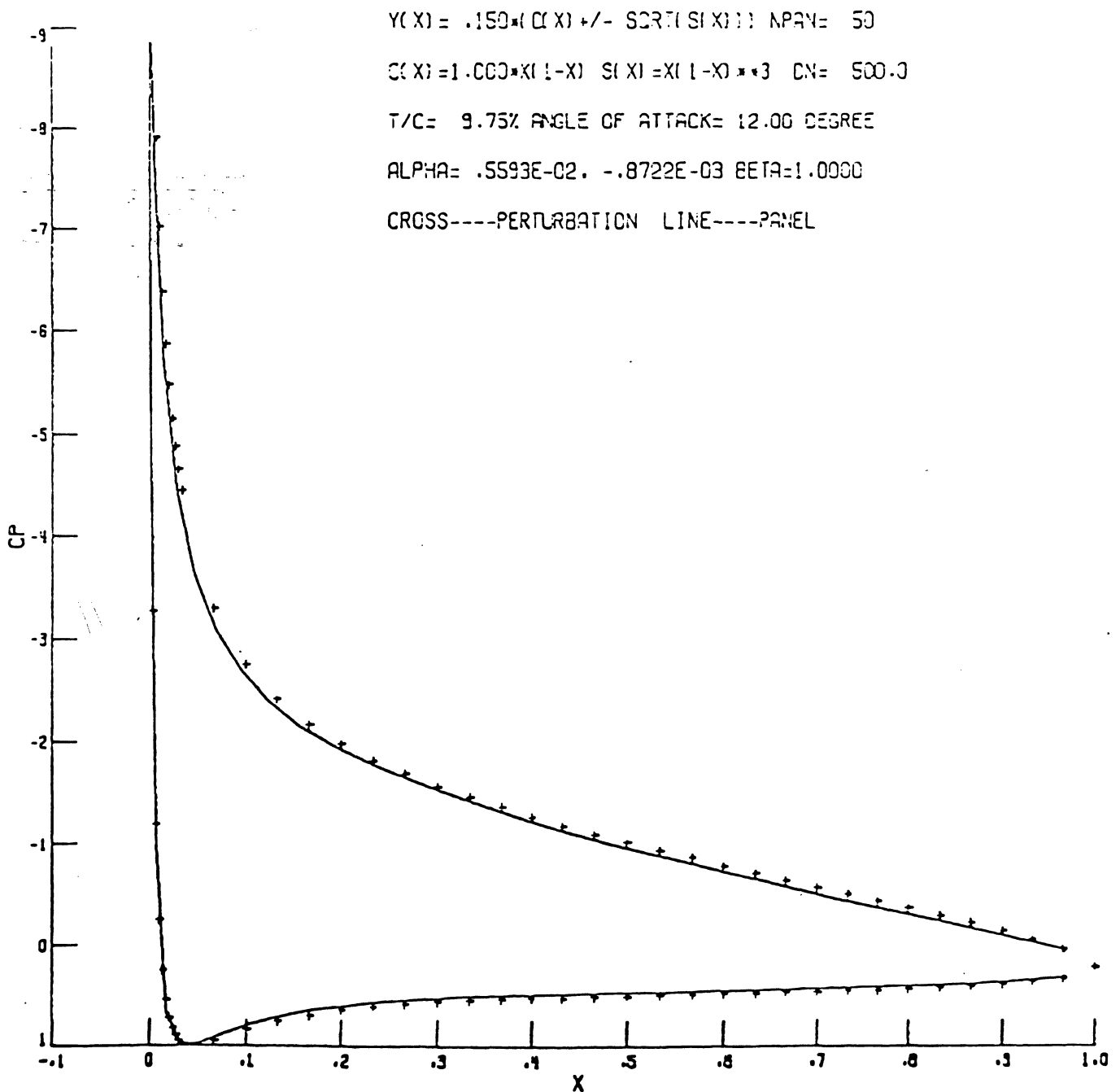
50 panels with cosine spacing.

Fig. 4.18 Comparison of pressure distributions from the perturbation analysis method with the panel method for cambered Joukowski airfoil.



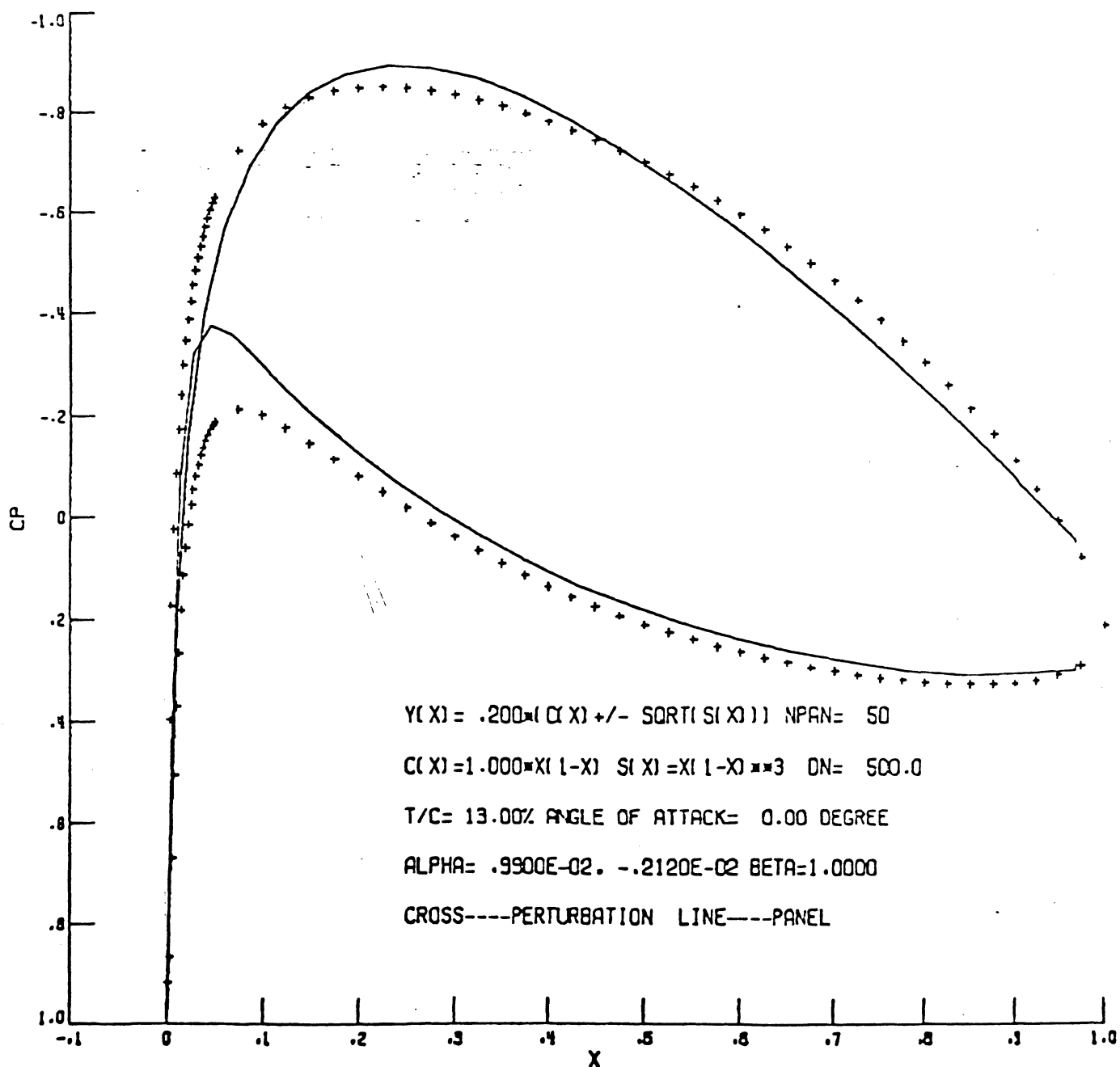
(b) $\epsilon = 0.08064$; $\gamma = 6^\circ$; ϕ expanded up to ϵ^2 ; $t/C = 9.75\%$;
 50 panels with cosine spacing.

Fig. 4.18 Continued.



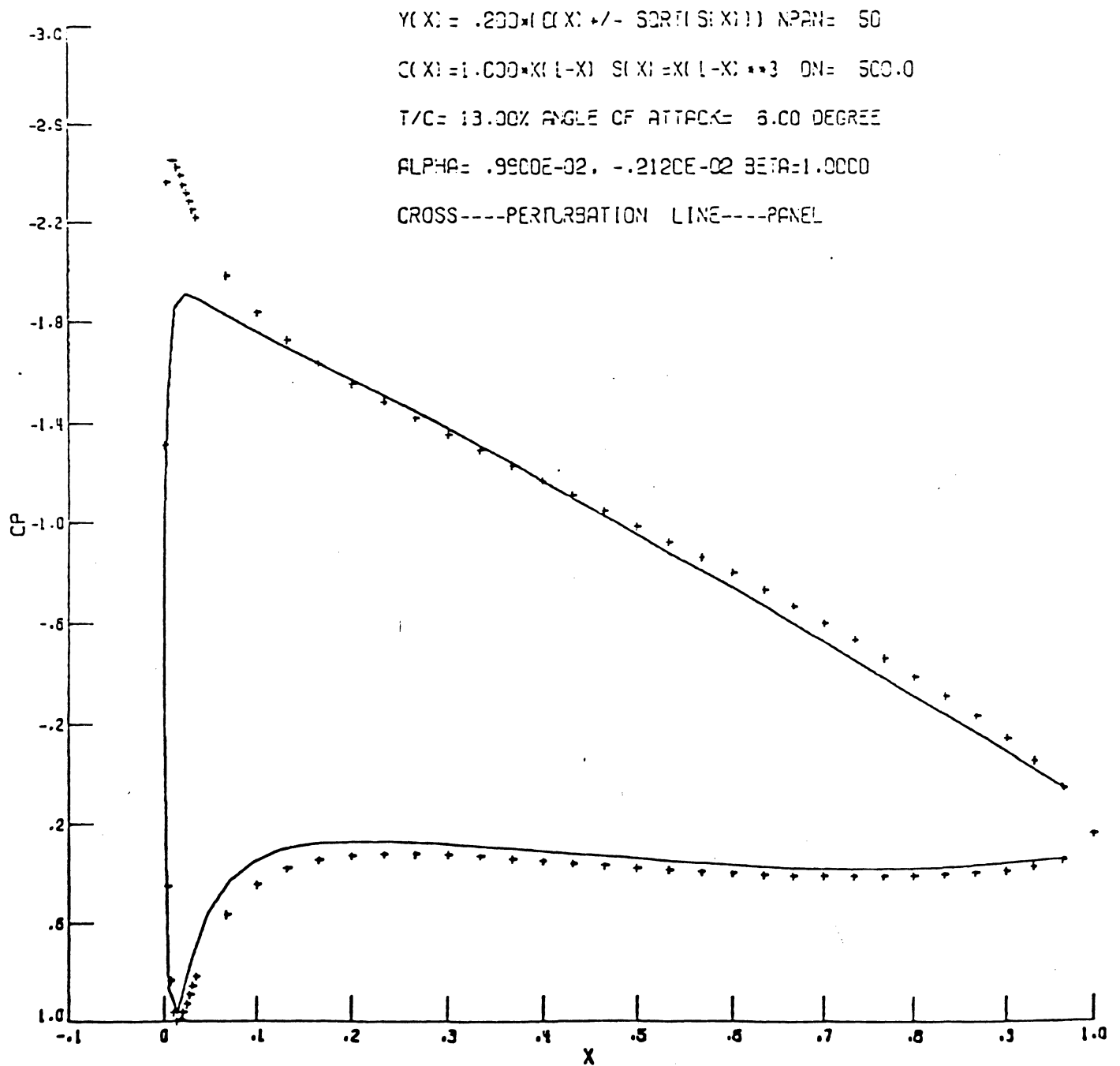
(c) $\epsilon = 0.08064$; $\gamma = 12^\circ$; ϕ expanded up to ϵ^2 ; $t/C = 9.75\%$;
 50 panels with cosine spacing.

Fig. 4.18 Concluded.



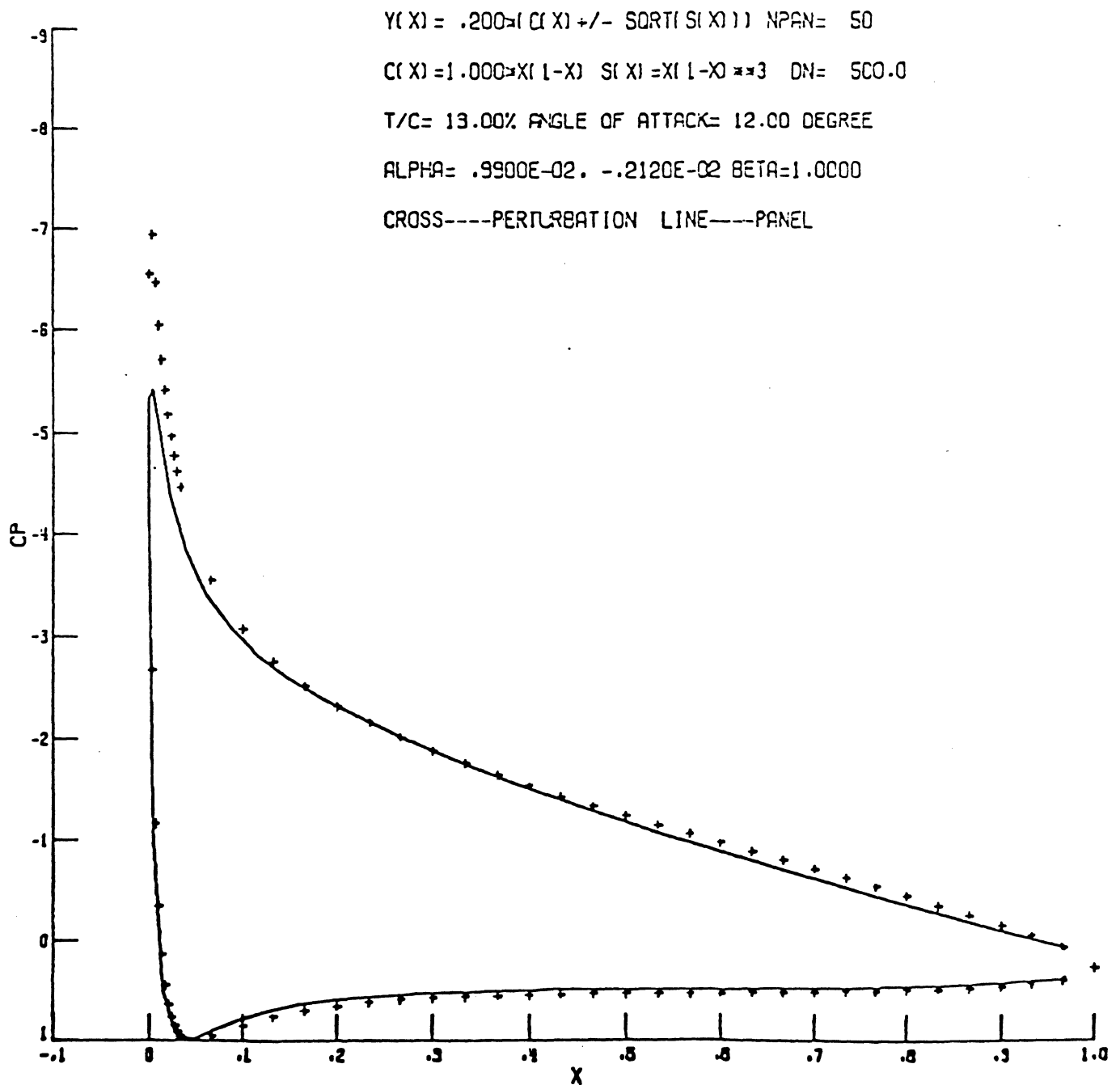
(a) $\epsilon = 0.10752$; $\gamma = 0^0$; ϕ expanded up to ϵ^2 ; $t/C = 13\%$;
 50 panels with cosine spacing.

Fig. 4.19 Comparison of pressure distributions from the perturbation analysis method with the panel method for cambered Joukowski airfoil.



(b) $\epsilon = 0.10752$; $\gamma = 6^\circ$; ϕ expanded up to ϵ^2 ; $t/C = 13\%$;
 50 panels with cosine spacing.

Fig. 4.19 Continued.



(c) $\epsilon = 0.10752$; $\gamma = 12^\circ$; ϕ expanded up to ϵ^2 ; $t/C = 13\%$;

50 panels with cosine spacing.

Fig. 4.19 Concluded.

Table 4.2 Comparison of lift coefficients of the perturbation, panel and exact solutions for the cambered Joukowski airfoils

Slenderness ratio ϵ	Exact $C_{l,ex}$	Perturbation $C_{l,pt}$	Panel $C_{l,pn}$	$\frac{C_{l,pt} - C_{l,ex}}{C_{l,ex}} \times 100\%$	$\frac{C_{l,pn} - C_{l,ex}}{C_{l,ex}} \times 100\%$
			$\gamma = 0^\circ$		
0.10752	0.61721	0.69115	0.63346	11.98	2.63
0.08064	0.46641	0.50658	0.46610	8.61	-0.07
0.05376	0.31268	0.32987	0.30390	5.50	-2.81
0.02688	0.15689	0.16101	0.14812	2.62	-5.59
			$\gamma = 6^\circ$		
0.10752	1.32350	1.40981	1.29947	6.52	-1.82
0.08064	1.16264	1.20984	1.12378	4.06	-3.34
0.05376	1.99734	1.01767	0.95359	2.04	-4.39
0.02688	1.82841	0.83332	0.77878	0.59	-5.99
			$\gamma = 12^\circ$		
0.10752	2.01528	2.11303	1.94816	4.85	-3.33
0.08064	1.84614	1.89984	1.76670	2.91	-4.30
0.05376	1.67107	1.69432	1.58984	1.39	-4.86
0.02688	1.49084	1.49649	1.38619	0.38	-7.02

Chapter 5

CONCLUDING REMARKS

The perturbation analysis method has been used to analyze the potential flow, due to a uniform stream, past an axisymmetric body or a two-dimensional airfoil. The theoretical formulations have been described in Chap. 2. Results obtained from the above method for certain classes of either axisymmetric slender bodies or two-dimensional thin airfoils have been compared with those generated by the panel method, as well as with exact solutions whenever available.

Numerical experiments for ellipsoidal bodies and elliptic airfoils have shown that the higher order expansion of ϕ in ϵ gives better results, as compared with exact solutions than lower order representations. The perturbation analysis method for axisymmetric slender bodies give pressure distributions which compare well with the panel and exact solutions for small slenderness ratio up to $\epsilon = 0.1$, corresponding to a L/d ratio of 5. The perturbation analysis method is quite inexpensive, because little computer memory is required; but it is only applicable to slender bodies. It is suggested to be an applicable method as a preliminary step in modelling some simple fuselages as part of the analysis of a wing mounted on a slender axisymmetric fuselage.

The utility of the perturbation analysis method for the two-dimensional airfoils is also confined to the thin airfoils with small slenderness ratios up to $\epsilon = 0.03248$, corresponding to $t/C = 6.5\%$. The

perturbation analysis method seems to relieve the numerical instability of the panel method at some regions near the leading edge of the airfoil surface. The perturbation analysis method can also provide more accurate results for thin airfoils (i.e., ϵ tends to a small value) as compared with the panel method. Moreover, the computing time and computer memory required are relatively small as compared with an existing panel method. The perturbation analysis method is recommended as a method which will provide reliable solutions for thin airfoils at low cost. Using the thin airfoil analysis as an illustrative example, the perturbation analysis method can be extended to analyze the three-dimensional wing as the next task. If the extension to the three-dimensional wing can be completed, the next step will be the development of a program for the wing design problem with the axisymmetric fuselage effects on a pair of wings. This study has been only a preliminary step for the wing-fuselage design problem.

In addition, the perturbation analysis method can be applied to solve the electrostatic and magnetostatic potentials around a slender conducting body in a similar manner.

REFERENCES

1. Van Dyke, M., Perturbation Methods in Fluid Mechanics, The Parabolic Press, 1975.
2. von Karman, T., "Calculation of the Flowfield Around Airships," NASA TM 574, July 1930.
3. Zedan, M. F. and Dalton, C., "Potential Flow Around Axisymmetric Bodies: Direct and Inverse Problems," AIAA Journal, Vol. 16, No. 3, March 1978, pp. 242-250.
4. Zedan, M. F. and Dalton, C., "Higher-Order Axial Singularity Distributions for Potential Flow About Bodies of Revolution," Computer Methods in Applied Mechanics and Engineering, Vol. 21, No. 3, March 1980, pp. 295-314.
5. Shu, J.-Y. and Kuhlman, J. M., "Calculation of Potential Flow Past Non-Lifting Bodies at Angle of Attack Using Axial and Surface Singularity Method," NASA CR-166058, February 1983.
6. Kuhlman, J. M. and Shu, J.-Y., "Potential Flow Past Axisymmetric Bodies at Angle of Attack," Journal of Aircraft, Vol. 21, No. 3, March 1984, pp. 218-220.
7. Handelsman, R. A. and Keller, J. B., "Axially Symmetric Potential Flow Around a Slender Body," Journal of Fluid Mechanics, Vol. 28, part I, April 1967, pp. 131-147.
8. Lighthill, M. J., "A New Approach to Thin Airfoil Theory," The Aeronautical Quarterly, Vol. 13, November 1951, pp. 193-210.
9. Hoogstraten, H. W., "Uniform Valid Approximations in Two-dimensional Subsonic Thin Airfoil Theory," Journal of Engineering Mathematics, Vol. 1, No. 1, January 1967, pp. 51-66.
10. Geer, J. F. and Keller, J. B., "Uniform Asymptotic Solutions for Potential Flow Around a Thin Airfoil and the Electrostatic Potential About a Thin Conductor," SIAM Journal on Applied Mathematics, Vol 16, No. 1, January 1968, pp. 75-101.
11. Geer, J. F., "Uniform Asymptotic Solutions for the Two-dimensional Potential Field About a Slender Body," SIAM Journal on Applied Mathematics, Vol 26, No. 3, May 1974, pp. 539-553.
12. Handelsman, R. A. and Keller, J. B., "The Electrostatic Field Around a Slender Conducting Body of Revolution," SIAM Journal on

- Applied Mathematics, Vol. 15, No. 4, July 1967, pp. 824-841.
13. Homencovschi, D., "Uniform Asymptotic Solutions for the Two-dimensional Potential Field Problem with Joining Relations on the Surface of a Slender Body," International Journal of Engineering Science, Vol. 20, No. 6, 1982, pp. 753-767.
 14. Homencovschi, D., "Uniform Asymptotic Solutions of Two-dimensional Problems of Elasticity for the Domain Exterior to a Thin Region," SIAM Journal on Applied Mathematics, Vol. 44, No. 1, February 1984, pp. 1-10.
 15. Karamcheti, K., Principles of Ideal-Fluid Aerodynamics, Wiley, August 1966.
 16. Thomas, J. L., Luckring, J. M., and Sellers, W. L., III, "Evaluation of Factors Determining the Accuracy of Linearized Subsonic Panel Methods," Presented at the 1st AIAA Applied Aerodynamics Conference, Paper No. AIAA-83-1826, July 1983.
 17. Bristow, D. R. and Grose, G. G., "Modification of the Douglas Neumann Program to Improve the Efficiency of Predicting Component Interference and High Lift Characteristics," NASA CR 3020, August 1978.
 18. Maskew, B., "Predicting of Subsonic Aerodynamic Characteristics--a Case for Low-order Panel Methods," Presented at the AIAA 19th Aerospace Sciences Meeting, Paper No. AIAA 81-0252, January 1981.
 19. Bristow, D. R. and Hawk, J. D., "Subsonic Panel Method for the Efficient Analysis of Multiple Geometry Perturbations," NASA CR 3528, March 1982.
 20. Maskew, B., Rao, B. M., and Dvorak, F. A., "Prediction of Aerodynamic Characteristics for Wings with Extensive Separations," Paper No. 31 in Computation of Viscous-inviscid Interactions, AGARD-CPP-291, September 1980.
 21. Maskew, B., "Predicting Aerodynamics of Vortical Flows on Three-dimensional Configurations Using a Surface-Singularity-Panel Method," Paper No. 13 in Aerodynamics of Vortical Type Flows in Three Dimensions, AGARD-CP-342, April 1983.
 22. Glauert, H., "A Generalized Type of Joukowski Aerofoil," Reports and Memoranda of the Aeronautical Research Committee No. 911, January 1924.
 23. Currie, I. G., Fundamental Mechanics of Fluids, McGraw-Hill Book Company, February 1979.

APPENDICES

APPENDIX A

DETERMINATION OF THE COEFFICIENTS OF $\alpha(\epsilon)$ and $\beta(\epsilon)$ FOR
AXISYMMETRIC BODIES

Appropriate constants α_k need to be determined such that $g_k(x)$ is regular at $x=0$. One can proceed in the following way. The functions $g_k(x)$ are defined by

$$g(x, \epsilon) = \sum_{k=0}^{\infty} g_k(x) \epsilon^{2k} = \{[x - \alpha(\epsilon)]^2 + \epsilon^2 S(x)\}^{1/2} \quad (A1)$$

where $\alpha(\epsilon) = \sum_{n=1}^{\infty} \alpha_n \epsilon^{2n}$. Since $S(0) = 0$ is assumed, as x is set equal to zero in Eq. (A1), one obtains

$$g_k(0) = \alpha_k, \quad k > 1 \quad (A2)$$

To determine α_k explicitly, one squares both sides of Eq. (A1) and has

$$[x - \alpha(\epsilon)]^2 + \epsilon^2 S(x) = \sum_{k=0}^{\infty} \left[\sum_{j=0}^k g_j(x) g_{k-j}(x) \right] \epsilon^{2k} \quad (A3)$$

Here, $\alpha_0 = -x$ is defined, such that $\alpha(\epsilon)$ can be written as

$$\alpha(\epsilon) = \sum_{n=0}^{\infty} \alpha_n \epsilon^{2n} \quad (A4)$$

Using Eq. (A4) in Eq. (A3), the left side of Eq. (A3) becomes

$$\sum_{k=0}^{\infty} \left[\sum_{j=0}^k \alpha_j \alpha_{k-j} \right] \epsilon^{2k} + \epsilon^2 S(x)$$

Equating the coefficients of the same power of ϵ^2 on both sides of the above equation, one obtains

$$\sum_{j=0}^k \alpha_j \alpha_{k-j} + \delta_{k,1} S(x) = \sum_{j=0}^k g_j(x) g_{k-j}(x) \quad (\text{A5})$$

where δ_{mn} is the Kronecker delta, i.e., $\delta_{mn} = 1$ if $m=n$, $\delta_{mn} = 0$ if $m \neq n$.

$$\text{For } k = 0 \quad g_0(x) = x \quad (\text{A6})$$

$$\text{For } k = 1 \quad g_1(x) = -\alpha_1 + \frac{S(x)}{2x} \quad (\text{A7})$$

Using Eq. (A2) and with the Taylor series expansion of $S(x)$, Eq. (A7)

yields $\alpha_1 = S'(0)/4$.

For $k > 2$, Eq. (A5) becomes

$$g_k(x) = -\alpha_k + \frac{1}{2x} \sum_{j=1}^{k-1} [\alpha_j \alpha_{k-j} - g_j(x) g_{k-j}(x)] \quad (\text{A8a})$$

Using Eq. (A2) in Eq. (A8a), one has

$$\alpha_k = -\frac{1}{2} \sum_{j=1}^{k-1} \alpha_j g'_{k-j}(0) \quad (\text{A8b})$$

One can determine α_k recursively by using Eqs. (A8a) and (A8b) and has the result as follows:

$$\alpha(\epsilon) = \frac{S'(0)}{4} \epsilon^2 - \frac{S'(0)S''(0)}{32} \epsilon^4 + \frac{1}{64} \left[\frac{[S'(0)]^2 S'''(0)}{6} + \frac{S'(0)[S''(0)]^2}{2} \right] \epsilon^6 + O(\epsilon^8) \quad (\text{A9})$$

Similarly, $\tilde{g}_k(x)$ can be made regular at $x=1$ and the coefficients β_k are determined by following the same procedures as above. The resulting expressions are as follows:

$$\tilde{g}(x, \epsilon) = \sum_{k=0}^{\infty} \tilde{g}_k(x) \epsilon^{2k} = \{[x - \beta(\epsilon)]^2 + \epsilon^2 S(x)\}^{1/2} \quad (\text{A10})$$

where $\beta(\epsilon) = 1 - \sum_{n=1}^{\infty} \beta_n \epsilon^{2n}$ with $\beta_0 = 0$ and $\beta_1 = -S'(1)/4$.

$$\tilde{g}_k(1) = \beta_k \quad (\text{A11})$$

$$\sum_{j=0}^k \beta_j \beta_{k-j} + \delta_{k,1} S(x) = \sum_{j=0}^k \tilde{g}_j(x) \tilde{g}_{k-j}(x) \quad k > 0 \quad (\text{A12})$$

$$\tilde{g}_0(x) = 1 - x \quad (\text{A13})$$

$$\tilde{g}_1(x) = -\beta_1 + \frac{S(x)}{2(1-x)} \quad (\text{A14})$$

For $k > 2$

$$\tilde{g}_k(x) = -\beta_k + \frac{1}{2(1-x)} \sum_{j=1}^{k-1} [\beta_j \beta_{k-j} - \tilde{g}_j(x) \tilde{g}_{k-j}(x)] \quad (\text{A15})$$

$$\beta_k = \frac{1}{2} \sum_{j=1}^{k-1} \beta_j \tilde{g}'_{k-j}(1) \quad (\text{A16})$$

$$\begin{aligned} \beta(\epsilon) = & 1 + \frac{S'(1)}{4} \epsilon^2 - \frac{S'(1)S''(1)}{32} \epsilon^4 \\ & + \frac{1}{16} \left[\frac{[S'(1)]^2 S'''(1)}{6} + \frac{S'(1)[S''(1)]^2}{2} \right] \epsilon^6 + O(\epsilon^8) \end{aligned} \tag{A17}$$

By using the above resulting equations, $\alpha(\epsilon)$ and $\beta(\epsilon)$ can be evaluated.

APPENDIX B
BOUNDARY CONDITIONS IN COMPLEX PLANE

The complex potential $\phi(z)$ is defined in Eq. (2.35) as $\phi(z) = \phi(x,y) + i\psi(x,y)$ which is analytic in the z -plane outside G . The derivative of the complex potential with respect to z is denoted by $W(z)$ and is known as the complex velocity, i.e.,

$$\begin{aligned} W(z) &= \frac{d\phi}{dz} = \frac{\partial\phi}{\partial x} + i\frac{\partial\psi}{\partial x} \\ &= \frac{\partial\psi}{\partial y} - i\frac{\partial\phi}{\partial y} \\ &= u(x,y) - iv(x,y) \end{aligned} \tag{B1}$$

where u and v are the velocity components in x and y direction respectively.

From Fig. 2.2, on the surface of the airfoil, one finds that

$$\frac{dy}{dx} = \frac{v}{u} \tag{B2}$$

The equation of the profile G is given by

$$y = \epsilon [C(x) \pm \sqrt{S(x)}] \quad \text{on } 0 < x < 1$$

$$\frac{dy}{dx} = \epsilon \left[C'(x) \pm \frac{S'(x)}{2\sqrt{S(x)}} \right] \quad (\text{B3})$$

Equating Eqs. (B2) and (B3), yields

$$v - \epsilon u \left[C'(x) \pm \frac{S'(x)}{2\sqrt{S(x)}} \right] = 0 \quad (\text{B4})$$

Using Eq. (B1) in Eq. (2.39), and considering the real part of the resulting expression, one has the same expression as Eq. (B4).

To satisfy the boundary condition at infinity in Eq. (2.39), one needs

$$\operatorname{Re} \int_{\alpha}^{\beta} f(\xi, \epsilon) d\xi = 0 \quad \text{and} \quad \operatorname{Im} \int_{\alpha}^{\beta} f(\xi, \epsilon) d\xi = \Gamma$$

where Γ is the total circulation about the body. Physically, the first condition says that there is no fluid flow through the surface of the body.

APPENDIX C

EXPRESSIONS FOR TWO-DIMENSIONAL AIRFOILS

1. Linear Operators of the Integral Equation

Linear operators $L_q^p, p=0, 1$ in Eq. (2.50) are defined in Sec. 4 of [11], and some of the related operators are given by

$$b_n(x) = \delta_{n,0} - \sum_{j=1}^n a_j(x) b_{n-j}(x) \quad (C1)$$

$$g(x, \epsilon) = \sum_{n=0}^{\infty} g_n(x) \epsilon^n = \{[\alpha - x - i\epsilon C(x)]^2 + \epsilon^2 S(x)\}^{1/2} \quad (C2)$$

$$h(x, \epsilon) = \sum_{n=0}^{\infty} h_n(x) \epsilon^n = \{[\beta - x - i\epsilon C(x)]^2 + \epsilon^2 S(x)\}^{1/2} \quad (C3)$$

$$\begin{aligned} \tilde{h}_{n,j}(x, F) = \frac{2}{j!} \int_0^{\frac{\pi}{2}} \left\{ \left(\frac{d}{d\epsilon} \right)^j \left[(T-x-i\epsilon C)^{-(2k+1)} \left[F(T) \right. \right. \right. \\ \left. \left. \left. - \sum_{p=0}^{2k} \frac{F^{(p)}(x+i\epsilon C)}{p!} (T-x-i\epsilon C)^p \right] \right] \right\}_{\epsilon=0} d\theta \quad (C4) \end{aligned}$$

where $T = [\alpha(\epsilon) - \beta(\epsilon)] \cos^2 \theta + \beta(\epsilon)$ and $C = C(x)$.

In particular, with $n = j = 0$ in Eq. (C4), yields

$$\tilde{h}_{0,0}(x, F) = 2 \int_0^{\frac{\pi}{2}} (\sin^2 \theta - x)^{-1} [F(\sin^2 \theta) - F(x)] d\theta \quad (C5)$$

2. Determination of the Coefficients of $\alpha(\epsilon)$ and $\beta(\epsilon)$

The functions $g(x, \epsilon)$ and $h(x, \epsilon)$ are defined in Eqs. (C2) and (C3)

where $\alpha(\epsilon) = \sum_{m=2}^{\infty} \alpha_m \epsilon^m$ and $\beta(\epsilon) = 1 - \sum_{m=2}^{\infty} \alpha_m \epsilon^m$.

Following the similar procedures mentioned in Appendix A, the general expressions for the determination of $\alpha(\epsilon)$ and $\beta(\epsilon)$ can be found as below:

$$\alpha_0 = 0 = \alpha_1$$

$$g_m(0) = \alpha_m, \quad m > 2$$

$$g_0(x) = x$$

$$g_1(x) = iC(x)$$

$$g_2(x) = -\alpha_2 + \frac{S(x)}{2x}$$

For $m > 3$

$$\alpha_m = -iC'(0) \alpha_{m-1} - \frac{1}{2} \sum_{j=2}^{m-2} \alpha_j g'_{m-j}(0) \quad (C6)$$

$$g_m(x) = -\alpha_m - \frac{iC(x)}{x} [\alpha_{m-1} + g_{m-1}(x)] + \frac{1}{2x} \sum_{j=2}^{m-2} [\alpha_j \alpha_{m-j} - g_j(x)g_{m-j}(x)] \quad (C7)$$

Applying Eqs. (C6) and (C7) with $m=3$ and $m=4$, one obtains

$$g_3(x) = -\alpha_3 - i \frac{C(x)S(x)}{2x^2}$$

$$g_4(x) = -\alpha_4 + \alpha_2 \frac{S(x)}{2x^2} - \frac{[C(x)]^2 S(x)}{2x^3} - \frac{[S(x)]^2}{8x^3}$$

$$\beta_0 = 0 = \beta_1$$

$$h_0(x) = 1 - x$$

$$h_1(x) = -i C(x)$$

$$h_m(1) = \beta_m, \quad m > 2$$

$$h_2(x) = -\beta_2 + \frac{S(x)}{2(1-x)}$$

For $m > 3$

$$\beta_m = -i\beta_{m-1} C'(1) + \frac{1}{2} \sum_{j=2}^{m-2} \beta_j h'_{m-j}(1) \quad (C8)$$

$$h_m(x) = -\beta_m + \frac{i C(x)}{2(1-x)} [\beta_{m-1} + h_{m-1}(x)] \\ + \frac{1}{2(1-x)} \sum_{j=2}^{m-2} [\beta_j \beta_{m-j} - h_j(x) h_{m-j}(x)] \quad (C9)$$

Using Eqs. (C8) and (C9) with $m=3$ and $m=4$, this yields

$$h_3(x) = -\beta_3 + i \frac{C(x)S(x)}{2(1-x)^2}$$

$$h_4(x) = -\beta_4 + \beta_2 \frac{S(x)}{2(1-x)^2} - \frac{[C(x)]^2 S(x)}{2(1-x)^3} - \frac{[S(x)]^2}{8(1-x)^3}$$

By using the resulting expressions, $\alpha(\epsilon)$ and $\beta(\epsilon)$ can be determined.

APPENDIX D
ELLIPTICAL COORDINATE SYSTEM

Consider the equations

$$\begin{aligned}x &= A \cosh \xi \cos \eta \\y &= A \sinh \xi \sin \eta \cos \beta \\z &= A \sinh \xi \sin \eta \sin \beta\end{aligned}\tag{D1}$$

With appropriate combination of x, y, z in Eq. (D1), one has two families of elliptical (ξ is constant) and hyperbolic (η is constant) curves as shown in figure D. The fineness ratio is defined by

$$\coth \xi = \frac{\text{length of major axis}}{\text{length of minor axis}}\tag{D2}$$

The system of the reference unit vectors at point P are denoted by \bar{e}_ξ , \bar{e}_η , and \bar{e}_β , corresponding to the coordinate ξ , η , β . Making reference to [15], the scale factors can be determined

$$h_\xi = h_\eta = A(\cosh^2 \xi - \cos^2 \eta)^{1/2}\tag{D3a}$$

$$h_\beta = A \sinh \xi \sin \eta\tag{D3b}$$

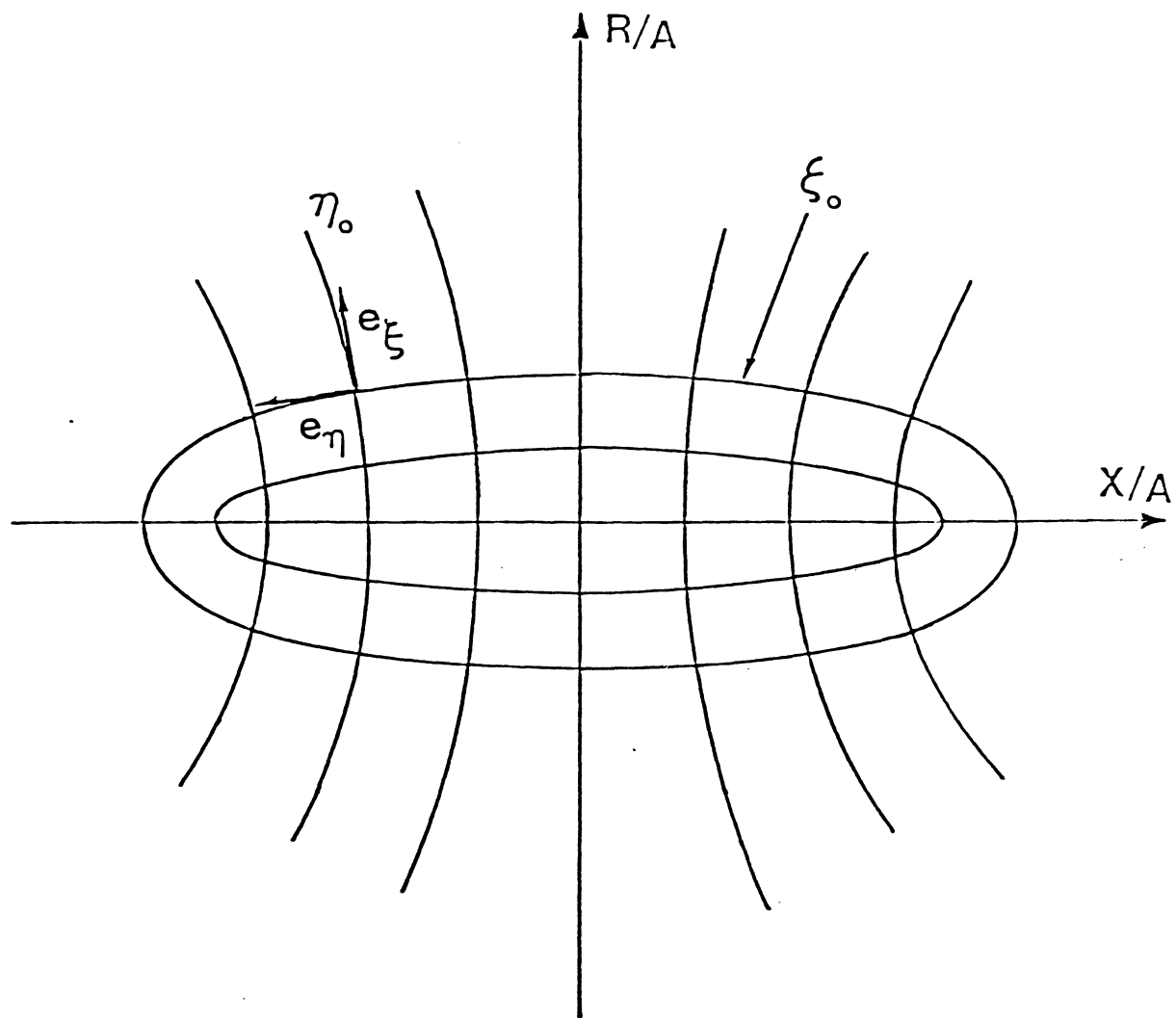


Fig. D Two families of elliptical and hyperbolic curves with different values of ξ and η .

The unit vectors of the desired coordinate system in terms of the Cartesian coordinate system are given by

$$\begin{aligned}\bar{e}_\xi &= \frac{A}{h_\xi} (\bar{i} \sinh\xi \cos\eta + \bar{j} \cosh\xi \sin\eta \cos\beta + \bar{k} \cosh\xi \sin\eta \sin\beta) \\ \bar{e}_\eta &= -\frac{A}{h_\eta} (\bar{i} \cosh\xi \sin\eta - \bar{j} \sinh\xi \cos\eta \cos\beta - \bar{k} \sinh\xi \cos\eta \sin\beta) \\ \bar{e}_\beta &= -\bar{j} \sin\beta + \bar{k} \cos\beta\end{aligned}\quad (D4)$$

Making reference to Chap. 2 of [15], one obtains

$$V = \frac{\bar{e}_\xi}{h_\xi h_\beta} \frac{\partial\psi}{\partial\eta} - \frac{\bar{e}_\eta}{h_\xi h_\beta} \frac{\partial\psi}{\partial\xi} \quad (D5a)$$

$$\nabla \times V = \frac{1}{h_\xi h_\eta h_\beta} \begin{vmatrix} h_\xi \bar{e}_\xi & h_\eta \bar{e}_\eta & h_\beta \bar{e}_\beta \\ \frac{\partial}{\partial\xi} & \frac{\partial}{\partial\eta} & \frac{\partial}{\partial\beta} \\ h_\xi V_\xi & h_\eta V_\eta & 0 \end{vmatrix} \quad (D5b)$$

Using Eqs. (D3a) and (D3b) in Eqs. (D5a) and (D5b), yields

$$\frac{\partial^2\psi}{\partial\xi^2} + \frac{\partial^2\psi}{\partial\eta^2} - \coth\xi \frac{\partial\psi}{\partial\xi} - \cot\eta \frac{\partial\psi}{\partial\eta} = 0 \quad (D6)$$

To find out the boundary conditions, one uses the requirements of no penetration and infinity conditions on Eq. (D5a), and has

$$\psi(\xi, \eta) = \text{constant} = C' \quad \text{on} \quad \xi = \xi_0 \quad (D7)$$

$$\psi(\xi, \eta) \rightarrow \frac{U_{\infty} A^2}{2} \sinh^2 \xi \sin^2 \eta + C'' \quad \text{as } \xi \rightarrow \text{infinity} \quad (\text{D8})$$

By using Eqs. (D7) and (D8), Eq. (D6) can be solved by separation of variables method.

APPENDIX E

SIMPLIFIED EXPRESSIONS FOR AXISYMMETRIC BODIES AND
TWO-DIMENSIONAL AIRFOILS

1. AXISYMMETRIC BODIES

Using the Eqs. (3.3a)-(3.3f) with the specified $S(x)$, one can find out some leading terms of $f_{nm}(x)$, $\alpha(\epsilon)$ and $\beta(\epsilon)$ as follows:

1.1 Ellipsoidal Body

$$S(x) = 4x(1 - x)$$

$$f_{10}(x) = 4\pi U_{\infty}(1 - 2x)$$

$$f_{20}(x) = 8\pi U_{\infty}(1 - 2x)$$

$$f_{21}(x) = -8\pi U_{\infty}(1 - 2x)$$

$$f_{30}(x) = 0$$

$$f_{31}(x) = 32\pi U_{\infty}(1 - 2x)$$

$$f_{32}(x) = 16\pi U_{\infty}(1 - 2x)$$

$$\alpha(\epsilon) = \epsilon^2 + \epsilon^4 + 2\epsilon^6 + O(\epsilon^8)$$

$$\beta(\epsilon) = 1 - \epsilon^2 - \epsilon^4 - 2\epsilon^6 + O(\epsilon^8)$$

1.2 Dumbbell Shaped Body

$$S(x) = 4bx(1-x)[1-bx(1-x)] \quad , \quad b > 2$$

$$f_{10}(x) = 4b\pi U_{\infty}(2x-1)[2bx(1-x)-1]$$

$$f_{20}(x) = 4b^2\pi U_{\infty} \{ [2 \log(b^2x^2 - b^2x + b)] [b^2x(36x^4 - 90x^3 + 76x^2 - 24x + 2) \\ + b(28x^3 - 42x^2 + 16x - 1) + 2x - 1] + b^2x(168x^4 - 420x^3 + 356x^2 - 114x + 10) \\ + b(92x^3 - 138x^2 + 52x - 3) \}$$

$$f_{21}(x) = 8b^2\pi U_{\infty} [b^2x(36x^4 - 90x^3 + 76x^2 - 24x + 2) \\ + b(28x^3 - 42x^2 + 16x - 1) + 2x - 1]$$

$$\alpha(\epsilon) = b\epsilon^2 + b^2(1+b)\epsilon^4 + O(\epsilon^6)$$

$$\beta(\epsilon) = 1 - b\epsilon^2 - b^2(1+b)\epsilon^4 + O(\epsilon^6)$$

2. TWO-DIMENSIONAL AIRFOILS

2.1 Elliptic Airfoil

If the airfoil is symmetric and is set at zero angle of attack,

then $\gamma = 0$, $r_n = 0$ and $C(x) = 0$. Notice that the imaginary parts of the functions $f_n(x)$ all vanish, which simplifies the derivation. With all these assumptions, one can find out $f(x, \epsilon)$ up to $O(\epsilon^3)$ as shown below:

$$f_0(x) = 0$$

$$f_1(x) = -2(1 - 2x)$$

$$f_2(x) = -4(1 - 2x)$$

$$f_3(x) = -8(1 - 2x)$$

$$\alpha(\epsilon) = \epsilon^2 + \epsilon^4 + 2\epsilon^6 + O(\epsilon^8)$$

$$\beta(\epsilon) = 1 - \epsilon^2 - \epsilon^4 - 2\epsilon^6 + O(\epsilon^8)$$

2.2 General Joukowski Airfoil

With the specified $S(x)$ and $C(x)$, all the operators can be evaluated, through Eqs. (3.8a)-(3.10c) can be evaluated and the constants $\text{Im } f_n(0)$ can be computed from Eq. (2.71). With this information, the following three $f_n(x)$ are obtained as follows:

$$f_0(x) = i(2 \sin \gamma)(x - 1)$$

$$\text{Re } f_1(x) = (\cos \gamma + A \sin \gamma)(x - 1)(1 - 4x)$$

$$\text{Im } f_1(x) = 2(x - 1)[2(A \cos \gamma - \sin \gamma)x + \sin \gamma]$$

$$\operatorname{Re} f_2(x) = 0.5(x - 1)\{3(\cos\gamma + A\sin\gamma)(8x^2 + 8x + 1)$$

$$+ 2A[6(A\cos\gamma - \sin\gamma)x(1 - 2x) + \sin\gamma(1 - 4x)]\}$$

$$\operatorname{Im} f_2(x) = -i 0.5(x - 1)[A(\cos\gamma + A\sin\gamma)(24x^2 - 16x + 1)$$

$$+ (A\cos\gamma - \sin\gamma)(24x^2 - 20x + 1) + 4\sin\gamma(2x - 1)]$$

Notice that $f_n(x)$ are complex-valued functions, so each $f_n(x)$ is represented by

$$f_n(x) = \operatorname{Re} f_n(x) + i \operatorname{Im} f_n(x) \quad , \quad n = 0, 1, 2$$

Using the above results in Eq. (2.73), with the definition of lift coefficient $C_{l,pt}$ one obtains

$$C_{l,pt} = 2\pi [\sin\gamma + 0.5(A\cos\gamma + \sin\gamma)\varepsilon + 0.25A(\cos\gamma)\varepsilon^2] + O(\varepsilon^3)$$

The leading terms for $\alpha(\varepsilon)$ is given in Eq. (2.67). Since this airfoil has a sharp trailing edge, $\beta(\varepsilon)$ should be set to one. Thus, by using the resulting expressions, the asymptotic expansion for $\phi(z;\varepsilon)$ is given by

$$\phi(z;\varepsilon) = e^{-i\gamma} z - \frac{1}{2\pi} \sum_{k=0}^2 \varepsilon^k \int_{\alpha(\varepsilon)}^1 \frac{\ln(z-\zeta) f_k(\zeta) d\zeta}{[(1-\zeta)(\zeta-\alpha)]^{1/2}} + O(\varepsilon^3)$$

In particular, if $A = 0$ or $C(x) = 0$, the real part of the results are

suitable for the symmetrical Joukowski airfoil. For this case, the first two terms of $\phi(z;\epsilon)$ above agree exactly with Eq. (12.9) of [10], when his results are expanded up to $O(\epsilon^3)$.

The third order lift coefficient for the general Joukowski airfoil is formulated to compare with the results obtained from the perturbation analysis and the panel methods. Making reference to [15, 22, 23], the exact lift coefficient for the Joukowski airfoil is given by

$C_{l,ex} = 8\pi a \sin(\gamma+\beta)/\ell$, where γ represents the angle of attack and ℓ is the chord of the airfoil. The radius a , the angles β and δ are connected by the Eq. (2.76). By applying the similar technique in Sec. 2.1.3, a perturbation parameter ϵ_1 is chosen, then

$$a = C(1-\epsilon_1 \cos\delta)/(1-0.5 \epsilon_1^2 \sin^2\delta) \text{ and } \ell = 4C(1-\epsilon_1 \cos\delta)^2/(1-2\epsilon_1 \cos\delta).$$

By using the resulting expressions and retaining terms up to order of ϵ_1^2 , the lift coefficient can be expressed as

$$C_{l,ex} = 2\pi \sin(\gamma+\beta)(1 - \epsilon_1 \cos\delta - \epsilon_1^2 \cos^2\delta - 0.5 \epsilon_1^2 \sin^2\delta) + O(\epsilon_1^3)$$

where $\beta = \tan^{-1}(\epsilon_1 \sin\delta/(1-\epsilon_1 \cos\delta))$ and the lift coefficient for the Joukowski airfoil can be computed up to $O(\epsilon_1^3)$ if the angle of attack γ , the parameters δ and ϵ_1 are specified.

